Geo-modelling of paleokarst reservoirs - from cave-survey to geocellular paleokarst model

Master Thesis

Karina Ledsaak

Department of Earth Science

University of Bergen

November 2016

This thesis was written in cooperation with Uni Research

Centre for Integrated Petroleum Research

Contact info:

ledsaakkarina@gmail.com

+47 984 85 485

ABSTRACT

Hydrocarbon reservoirs exhibiting features inherited from former karst processes acting on the reservoir rocks are relatively common worldwide. However, on the Norwegian continental shelf, paleokarst plays have only recently been identified in the Barents Sea. The substantial resource potential of the new plays is balanced by the known inherent complexity of paleokarst, and highlights the need for improved understanding of these reservoirs. Paleokarst reservoir characteristics are the sum of complex depositional, erosional and diagenetic processes, which tend to produce reservoirs with extreme and highly localized contrasts in permeability. In order to study how different paleokarst reservoirs respond to production and injection it is necessary to employ reservoir models. These models can provide guidelines for production strategies and ensure safe and optimal recovery. As individual paleokarst features are generally below seismic resolution, the obvious way to construct models of likely paleokarst reservoirs is to employ maps of present day karst features as a starting point and forward model their likely collapse, diagenesis and infill. Such models provide analogues for subsurface reservoirs.

At present, industrial reservoir modelling software packages do not include dedicated tools or workflows for handling common paleokarst features such as cave networks. For this reason, work-arounds and a lot of "out-of-the box" thinking must be applied to create a realistic and natural looking paleokarst reservoir. Some work has previously been done with respect to modelling cave systems in a stochastic manner, but there has been limited work concentrating on deterministically modelling of cave systems based on existing caves. The present thesis is a contribution to this on-going effort.

The workflow employs the RMS™ 2013.1.2 reservoir modelling suite, and is based on a survey of the Setergrotta cave, located in the northern parts of Norway. It allows deterministic incorporation of the original cave geometry into a geo-cellular model. A "forward modelling" of the expected collapse and infill was carried out, and the model populated stochastically with likely petrophysical properties. Fracture modelling was performed for the host rock outside the collapsed cave passages and included as part of the petrophysical model. Due to time constraints, only very limited dynamic testing of the final model was carried out. Different upscaled versions of the reservoir model were tested to investigate the effect of upscaling on the fluid flow through the reservoir. Streamline simulations used for this exercise suggests that upscaling up to a certain level does not affect fluid patterns, and that preferential flow along collapsed passages will only occur if there is a strong contrast between permeability of the passages and the surrounding host rock. The streamline simulation results should be subjected to more detailed investigations using more advanced flow simulation tools.

ACKNOWLEDGEMENTS

This master thesis is a part of a master's degree in Geodynamics at the Department of Earth Science at the University of Bergen. The thesis was mainly supervised by Jan Tveranger at Uni CIPR, but invaluable assistant was also given to me by my co-supervisors Øystein Pettersen at Uni CIPR and Stein-Erik Lautrizen at the Department of Earth Science.

First and foremost I want to give my sincere gratitude to Jan Tveranger for all his guidance, motivation and inspirational discussions. Many hours were spent in his office discussing different challenges regarding RMS and other aspects of this thesis. Jan also provided excellent guidance regarding my writing and proofreading of this thesis. Stein-Erik provided the cave survey used in this thesis as well as answering all my questions regarding karst and caves in general. Øystein Pettersen contributed to this thesis with discussions regarding the fluid flow through the reservoir. I could not have done this without the help from them.

I would also like to thank fellow student Marte for proofreading and commenting on parts of this thesis.

I want to give a special thank you to my fellow geology students at the University of Bergen for five great years. All the fieldtrips and hours spent studying together has given me friends for life and I will forever be grateful for that. A special thanks to the wonderful people at "Midtrommet" for keeping my spirits up by spending an incredible amount of hours playing cards in the canteen and of course a big thank you to my roomie Kari.

Karina Ledsaak

Karina Ledsaak
Bergen, November 2016

TABLE OF CONTENTS

1 INTRODUCTION

Society continuously hunts for new energy supplies to keep up with the steadily rising demand and consumption. Non-renewable resources like oil, gas and coal have been important contributors to global energy supply for centuries and will probably continue to form a key component of future energy supply, although probably forming a smaller fraction of the total energy mix as renewable energy sources are increasingly phased in.

In Norway, the focus of petroleum E & P has been on siliciclastic reservoirs. As these plays are moving into a mature phase, the industry is considering other, less well-known play types. Carbonate reservoirs could potentially play a big role. In the Middle East, South East Asia and the US, for example, carbonate reservoirs are very common. In a global perspective, carbonate plays contain almost half of the known hydrocarbon reserves today (Halbouty et al., 1970), but apart from the well-known chalk plays in the southern North Sea, carbonate plays have so far not played a prominent role on the Norwegian Shelf. The exploration of the Barents Sea has shed new light on the potential offered by carbonate plays, especially after Lundins discovery in the Gotha (Well 7120/1-3) and Alta prospects on Loppa High.

Carbonate reservoirs are far more complex than siliciclastic reservoirs. Both the variety of processes active during deposition and subsequent alterations introduced through dissolution and diagenesis give rise to complex features and structures influencing reservoir properties. Although carbonate reservoirs have been studied extensively (e.g. (Brigaud et al., 2014, Brown, 1997)), many aspects are still difficult to address based on seismic and well data. This is mainly due to a combination of limited seismic resolution and inability of well data to render a comprehensive picture of the extreme spatial heterogeneity often encountered in these reservoirs. These shortcomings can partly be addressed using a combination of outcrop analogues and conceptional models, which can render a more detailed and complete picture of reservoir architecture and property distributions.

Using conceptional models of reservoirs enable workers to obtain a valuable understanding of the reservoir, its properties and the interaction between reservoir properties and dynamic response to production measures. The understanding gained from these models of how different carbonate reservoirs look and behave, can in turn be utilised to improve interpretation of available seismic-, well- and production data.

Many carbonate reservoirs display evidence of paleokarst, indicating that the rock was formerly subjected to dissolution processes caused by subaerial exposure, forming cavities and karst topography (Loucks, 1999). These features are commonly accompanied by collapse- and infill-structures that formed either contemporaneously with the karstification or during subsequent burial. Some caves can also be preserved down to several kilometres depth, as evidenced by drill-stem drops of several meters while drilling paleokarst reservoirs. This will be more thoroughly addressed in chapter 2.2.3.

Although karst processes and products in carbonate and evaporate rocks are well known from decades of speleological and ground water research, this knowledge has only to a limited extent been transferred to the realm of reservoir characterization. This is partly due to lack of communication between disciplines, but also due to the fact that few ready-to use analogue models of paleokarst reservoirs are being extant: Understanding karst and karst processes is only one step along the way. In order to utilize the information provided by speleology and karst research, conceptional models should be used to “forward model” karstified rocks into paleokarst reservoirs. The key question is then primarily to develop techniques for implementing paleokarst features and properties in reservoir models, and, secondly, map out the interplay between model input parameters and performance in order to understand the dynamics of the systems.

1.1 Aim of study

The complexity of paleokarst reservoirs presents a substantial challenge to reservoir modelling. Most standard software packages used by the industry (e.g. Petrel, RMS, Jewel Suite etc.) do not include specific modules dedicated to handle the very distinct paleokarst features. Considering the ubiquity of paleokarst reservoirs globally this may come as a surprise, but it reflects the lack of realization by the industry that paleokarst reservoirs require a very different approach to modelling than other reservoir types which depositional processes and diagenesis mainly govern. Developing the required set of modelling techniques is therefore an important first step. This will in turn enable the generation of models capturing paleokarst features in a realistic manner and subsequently studying their dynamic behaviour.

The primary aim of the present study is to contribute to the development of modelling techniques and workflows for modelling features and properties encountered in paleokarst reservoirs. Due to time constraints only an initial assessment of the impact of the modelled structures on fluid flow is carried out. This should be subject for a more comprehensive and focussed study. The present thesis provides the framework for carrying this out.

2 THEORETICAL BACKGROUND

2.1 Carbonates

2.1.1 Formation and composition

Carbonate rocks are a product of biological and chemical processes and form about 25 percent of the sedimentary rocks (Boggs Jr, 2012, p.308), providing important clues to Earth's past climates and evolutionary history. Carbonate sediments consist of biological fragments like skeletons, and carbonate grains originating from chemical precipitation.

Figure 2.1.1-1 illustrates the global distribution of carbonates. Areas where sedimentation is dominated by carbonate production are commonly labelled "carbonate factories" (Lucia, 2007). The most prolific carbonate factories are located in shallow, tropical to subtropical seas, like the Great Barrier Reef in western Australia. Carbonate sediments can also accumulate in higher latitudes on cool-water shelves, but will here predominantly consist of shell material, like the Ekofisk formation in the North Sea.

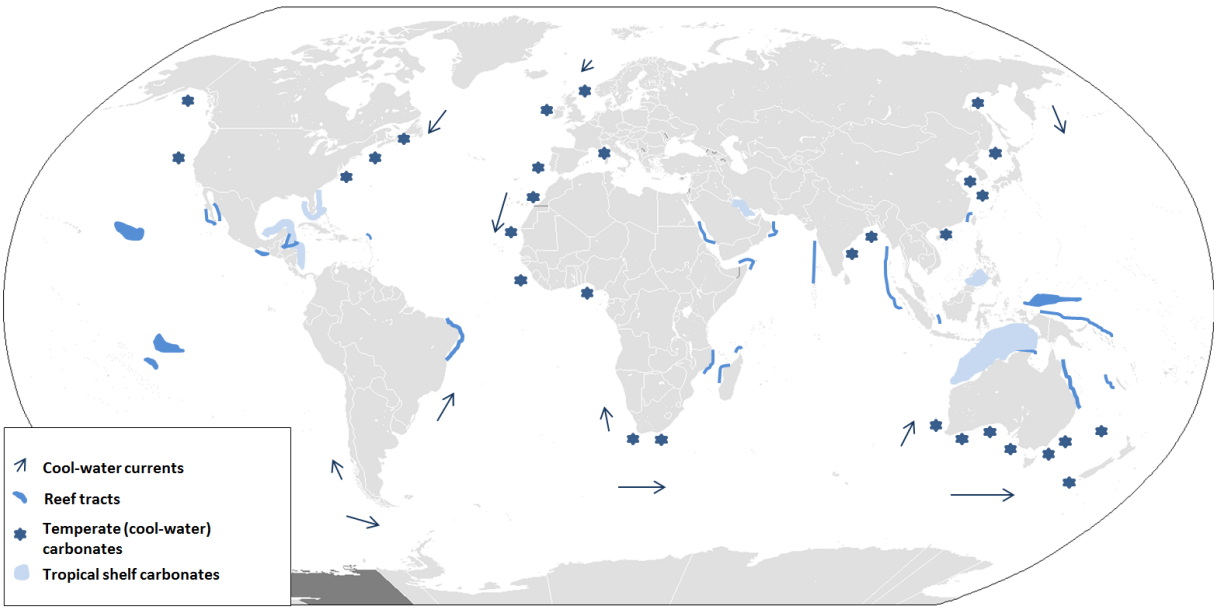

Figure 2.1.1-1: Distribution of carbonates around the world. Figure inspired by Boggs Jr.(2012) and based on Wilson (1975), Nelson (1988) and James (1997).

The composition of carbonate sediments is mainly controlled by the composition of seawater at the time of formation and the depositional environment. Carbonate sediments are mainly composed of calcium (Ca^{2+}), magnesium (Mg^{2+}) and carbonate ions (CO_3^{2-}). These elements form the three most common carbonate minerals; high-magnesium calcite ($(CaMg)CaCO_3$), low-magnesium calcite ($CaCO_3$) and aragonite ($CaCO_3$) (Boggs Jr, 2012, p. 135-137). Carbonate rocks are often divided into two groups, based on their mineralogy. Limestone contains 50 percent or more calcium carbonate ($CaCO_3$) and dolomite contains 50 percent or more calcium-magnesium carbonate ($CaMg(CO_3)_2$). Limestone can be found as aragonite, high-magnesium calcite and low-magnesium calcite. Dolomite typically forms where calcium carbonate is subjected to pore fluids rich in magnesium.

Formation of high-magnesium calcite and aragonite precipitation is favoured in modern waters, but changes have occurred over time due to variations in the relative content of magnesium and calcium in seawater (Boggs Jr, 2012, p. 135-137). During Mesozoic and early parts of Palaeozoic times, production of low-magnesium calcite were dominating. These periods were dominated by a generally warmer climate often referred to as greenhouse conditions, thus the production of low-magnesium calcite prevailed.

2.1.2 Diagenesis of carbonate rocks

Several diagenetic processes will change the porosity, permeability, mineralogy and chemistry of the carbonate sediments after deposition, influencing the transformation from carbonate sediments to carbonate rocks (Boggs Jr, 2012, p. 159). Consisting of soluble material, carbonate minerals are more susceptible to some diagenetic processes than siliciclastic minerals, making carbonate sediments more vulnerable to change.

Compaction, cementation, biogenic alteration and dissolution are some of the diagenetic processes affecting carbonates, and which may cause reduction or enhancement of secondary porosity and permeability values (Brown, 1997). These individual diagenetic processes tend to overlap in both time and space (Lucia, 2007). Dissolution of carbonate

grains will lead to unconnected vuggy porosity in the carbonate rock, yielding high degree of porosity, and low permeability (Murray, 1960).

We commonly distinguish between three different stages of diagenesis: Shallow burial (eogenesis), deep burial (mesogenesis), and uplift and unroofing (telogenesis)(Bathurst, 1976). Moore (1989) further distinguished three major diagenetic realms, the marine, meteoric and subsurface realms, as shown in figure 2.1.2-1.

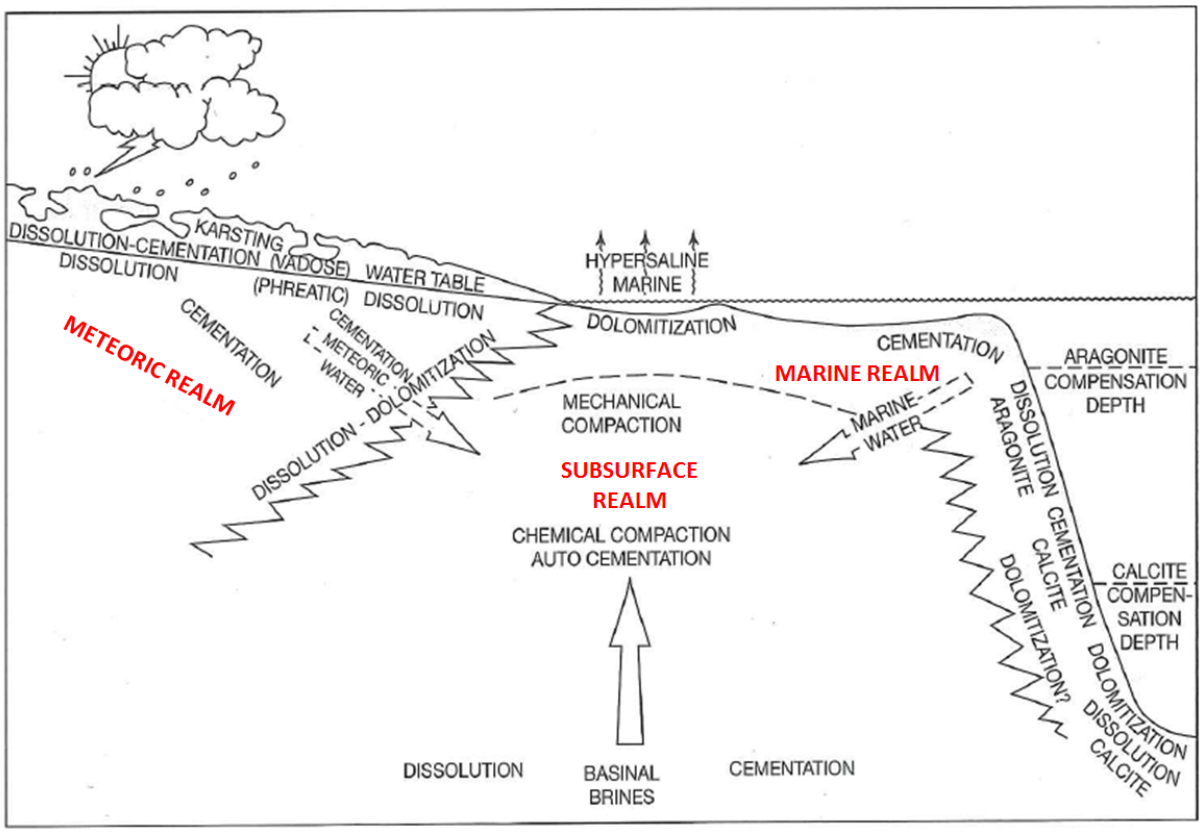

Figure 2.1.2-1: The three major realms where diagenesis of carbonate sediments typically occur; The marine realm, the Subsurface realm and the Meteoric realm. Modified from (Moore, 1989).

The marine realm comprises the shallow marine subsurface and the seafloor, and is characterized by seawater temperature and marine waters. In this environment, diagenetic processes like bioturbation, boring by organisms and cementation of grains in warm-water areas are the main diagenetic processes influencing the carbonate sediments.

The meteoric realm is characterized by the presence of fresh water, including both the vadose and the phreatic zone. This water is usually rich in CO_2, which may cause

dissolution of aragonite and high-magnesium calcite (Choquette and James, 1988). This process can lead to saturation of calcium carbonate in the water, and precipitation of calcite as cement in open pores. Calcite cementation, dissolution and alteration of aragonite and high-magnesium calcite are the main diagenetic processes in the meteoric regime.

The subsurface realm is located on the seafloor during burial of carbonate sediments. At this time, the sediments may have been subjected to one or more diagenetic processes in another realm. During burial, the sediments will be exposed to increasing temperature, pressure and change in pore fluids. The carbonate sediments may be subjected to both physical and chemical compaction, as well as several other diagenetic processes, depending on the specific conditions of the burial environment i.e. temperature, pH and pore-fluid composition (Boggs Jr, 2012, p.159-164).

The geological age of carbonates also plays a significant role as carbonates may be subjected to a range of contrasting processes during their lifetime, which in sum control the resultant porosity, and permeability of the rock.

As the carbonate sediments are subjected to alteration in the form of burial, the porosity and permeability will decrease (Lucia, 2007). Scholle and Scholle (2014) found that the main diagenetic processes negatively affecting porosity and permeability are cementation of open pore space, inversion of porosity, and formation of soil crust during exposure. On the other hand there are several diagenetic processes that enhance porosity and permeability (Boggs Jr, 2012, p.159-164). Solution of the carbonate rock can lead to enlargement of fractures and can possibly result in cave formation. Secondary porosity can be formed by dissolution of chemically unstable grains, if the calcium carbonate can be transported out of the system. Dissolution of carbonate rock is influenced and dependent on contact with acidic waters, and follows the equation below (Boggs Jr, 2012, Ford and Williams, 2013):

$CO_2 + H_2O \leftrightarrow H_2CO_3$

$H_2CO_3 + CaCO_3 \leftrightarrow Ca^{2+} + 2HCO_3^-$

The diagenetic processes that act on carbonate sediments will lead to changes in mineralogy, porosity and permeability.

Research on the resistance to chemical compaction in limestones and dolostone (Schmoker and Halley, 1982) found that dolostone has a higher resistance to compaction than limestone, and that the primary porosity may be preserved at greater burial depth in dolostone than in limestone. Dolomites are also more resistant to pressure solution (Glover, 1968), and will as a result of this more easily fracture in the subsurface (Schmoker et al., 1985).

2.1.3 Classification of carbonate rocks

There are several ways of classifying carbonates. Classification is rarely based on mineralogy due to the fact that carbonate rocks most often are monomineralic. Instead several attempts have been made to classify carbonates based on texture, depositional environment (Ham and Pray, 1962) and descriptive classification. The most widely used classification schemes today are those by Folk (1959) and Dunham (1962) shown in figure 2.1.3-1.

Folk's classification is based on the relative abundance of the three major end-members; carbonate grains or allochems, microcrystalline carbonate mud and sparry calcite cement (Folk, 1959).

Dunham's classification on the other hand is based on the original depositional texture where two aspects of texture are considered; grain packing and the relative abundance of grains to micrite, and the depositional binding of grains (Dunham, 1962). Dunham's classification may be best to use in combination with another classification method like Folk's since it does not consider the carbonate grains.

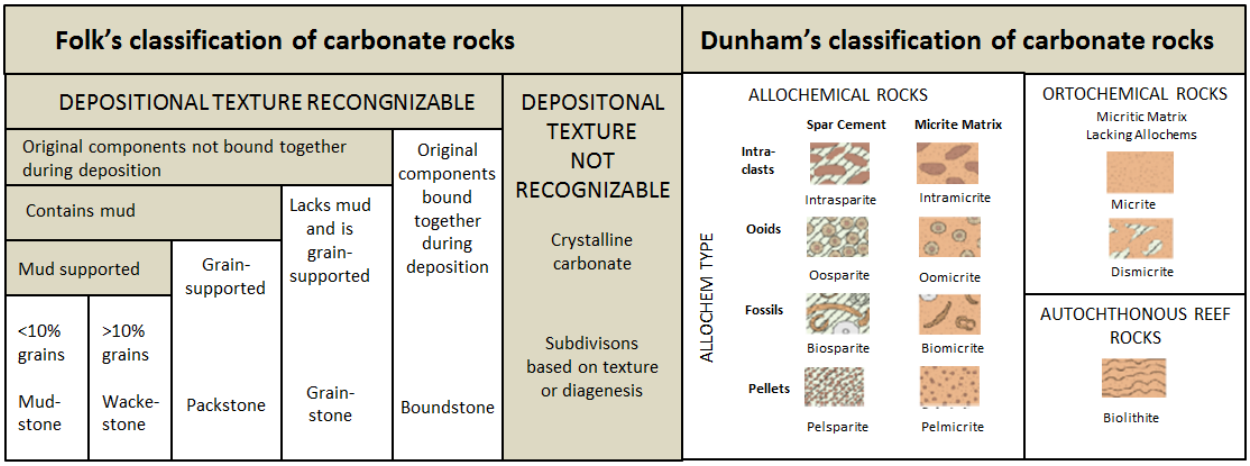

Figure 2.1.3-1: Folk's and Dunhams's classification of carbonate rocks, modified from (Scholle and Scholle, 2014), (Folk, 1959) and (Dunham,1962)

2.2 Karst

2.2.1 Formation

Choquette and James (1988) defined the term *karst* as all the diagenetic features that are produced in association with chemical dissolution and later modification of a carbonate sequence, both macro- and microscopic, and surface and subterranean terrain.

Karst landscapes occupy around 10-20 % of all the earths' continental area (Ford and Williams, 2013). Karstification occurs as carbonate rocks dissolve as a response to being exposed to corrosive fluids of meteoric or subsurface origin and is usually initiated along joints, fractures or bedding planes (Erzeybek Balan, 2012). According to Esteban (1993) the evolution of karst can be divided into four stages, as illustrated in figure 2.2.1-1.

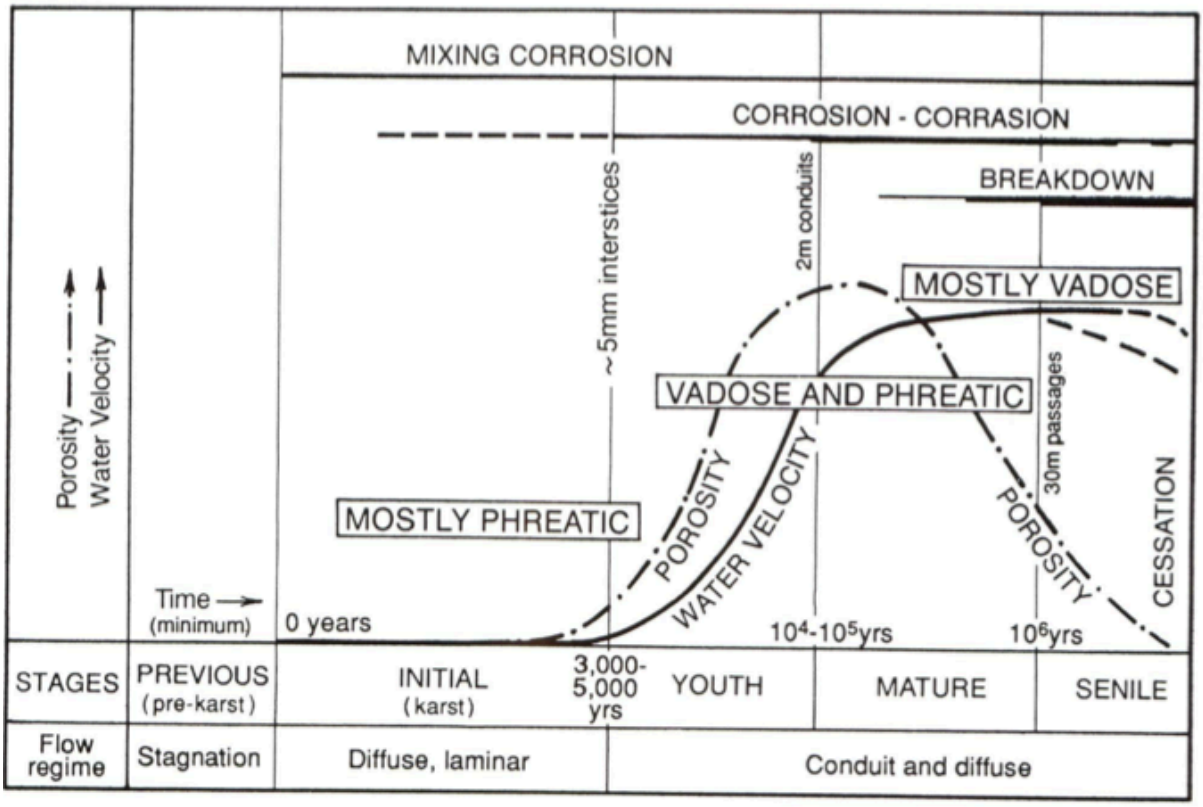

Figure 2.2.1-1: The 4 stages of karst evolution. Figure derived from Esteban (1993).

Figure 2.2.1-1 illustrates the theoretical evolution of a karstic system from initiation, involving gradual enhancement of pore space by dissolution and erosion, to a final stage of porosity destruction and collapse of passages.

There are several factors affecting the formation of karst. The length of subaerial exposure on a carbonate surface is one of the most important factors in the formation of karst and its degree of karstification. Choquette and James (1988) identified and divided the different factors into two groups; intrinsic and extrinsic factors.

Intrinsic factors are the "inherited" factors of the rock, mainly the general lithology, matrix permeability, availability of fractures or potential conduits and the maturity of the host rock. The stratal permeability and permeable flow paths such as faults and fractures within the host rock will control the extent of karstification. According to Choquette and James (1988) the intrinsic factors like the fabric and texture of the rocks, bedding thickness and bulk purity will have the greatest affect on the dissolution and the formation of karsts.

The extrinsic factors affecting karst and its formation are external factors like climate, base level elevation, vegetation and duration of exposure, which affect how and when the rock is exposed, process rates and the chemistry of corroding fluids.

Karst can be subdivided into two main groups according to where it forms; epigenic and hypogenic karsts. Palmer (1991) defined epigenic karst as karst formed where meteoritic waters causes dissolution in a near-surface environment. This can lead to collapse and formation of features that are typical for surface karst topography, like sinkholes and collapse dolines. Epigenic caves are most common, and are the likely ancestor to most of the paleocave reservoirs that are known today (Loucks, 1999).

Hypogenic karst on the other hand is less common. It is formed by processes occurring in association with hydrothermal fluids. Chemical processes and the movement of acidic water drive this dissolution, and there is no connection to the overlying surface (Palmer, 1991).

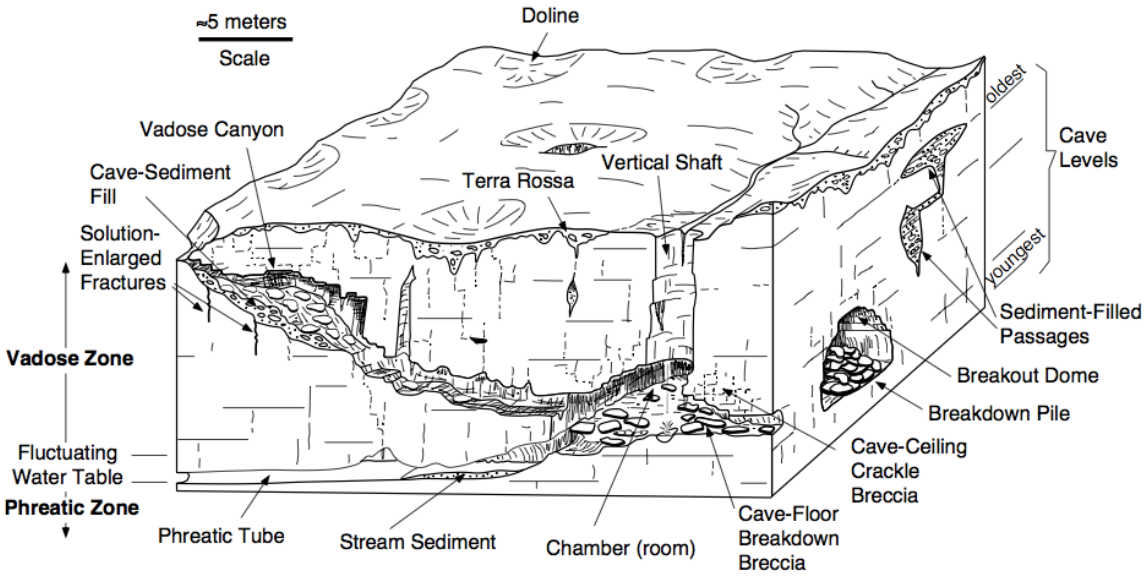

Figure 2.2.1-2: A typical karstic terrain. Figure derived from Loucks (1999).

Karstic terrains have characteristic features and are often easily recognized. Figure 2.2.1-2 illustrates a typical karst landscape exhibiting caves and extensive underground water systems formed in soluble carbonate rocks (Ford and Williams, 2013). There will also often be development of surface features, like dolines, grikes, karren and sinking streams, usually called exokarst. The process of karst formation is led by removal of rock volume by chemical and mechanical erosion, which will lead to an increase in porosity and permeability in the rock. This process can also lead to the formation of secondary porosity, and with this improvement of the reservoir quality (Nordeide, 2008).

Caves are a typical diagnostic feature for a karstic sub terrain, and they can create substantial cave networks in the subsurface (Ford and Williams, 2013). Caves will be further discussed in chapter 2.2.4. In connection with the caves there can be found several other distinctive features like breccia pipes, collapse dolines and speleothems.

2.2.2 Paleokarst

Paleokarst is defined by Walkden et al. (1974) as ancient karst, which is commonly buried by younger sediments or sedimentary rocks and thus includes both relict paleokarst and buried paleokarst. A more accurate definition is supplied by Loucks (1999), who defines paleokarst as karst systems that no longer is active. Paleokarst can however be reactivated, and there is often clear signs of two or more karstification events in a paleokarst system. It can be difficult to get hard data for paleocave systems, because well-exposed outcrops, particularly in 3D are relatively rare.

Paleokarst is often related to unconformities at all scales ranging from brief episodes of subaerial exposure, to regional events lasting several million years. There are examples of paleokarst throughout earth's history reaching back to Achaean age paleokarst surfaces documented on the Canadian Shield (Ford and Williams, 2013).

2.2.3 Paleokarst as a reservoir

Worldwide there are several proven petroleum reservoirs in paleokarst systems (e.g. (Kerans, 1988, Choquette and James, 1988); some of these contain record breaking wells in terms of production.

The Cerro Azul #4 in Mexico (1916) is known to be the most productive well in history, and is still producing today from a paleokarst zone (Blickwede and Rosenfeld, 2010). The Yates field in West Texas of Permian age is also a well-known example of this, with 1556 documented caves. The field was discovered in 1926 and is reported to have 5 billion bbl. oil in place (Tinker, 1995).

The Kirkuk Field in Iraq has been producing for over seven decades, and is one of the most important oil fields in Iraq (Trice, 2005). The Middle East is known for its massive carbonate reservoirs, and many of them have been producing for decades.

The Kashagan oil field located in Kazakhstan is one of the largest oil fields in the Caspian Sea region, and has an estimated 7-9 billion bbl. recoverable reserves (Kaiser and Pulsipher, 2007).

In China, the Ordos and Tarim basins are well known for its vast reserves of oil and gas in paleokarst reservoirs. The Jingbian Field in Ordos Basin is the largest paleokarst gas reservoir in China, with an estimated 11 trillion cubic meters of gas reserves in place (Li et al., 2008).

This is only a few of many known paleokarst reservoirs around the world, and proves the importance of a deeper knowledge when dealing with these reservoirs.

The porosity and permeability in paleokarst systems is linked to several factors; but chiefly to geometry of the initial karst system, depositional processes (including collapse and infill) and diagenetic history. Karst and paleokarst reservoirs typically exhibit a high degree of heterogeneity associated with porosity and permeability values (Trice, 2005). Karst is developed along pre-existing fracture networks and will prograde gradually through the system. For prediction of porosity it is important to have knowledge about when and why the process of karstification started, and what factors controlled its evolution over time (Esteban, 1993). Figure 2.2.3-1 shows a conceptual diagram illustrating the changes in porosity and pore diameter during the different stages of cave development.

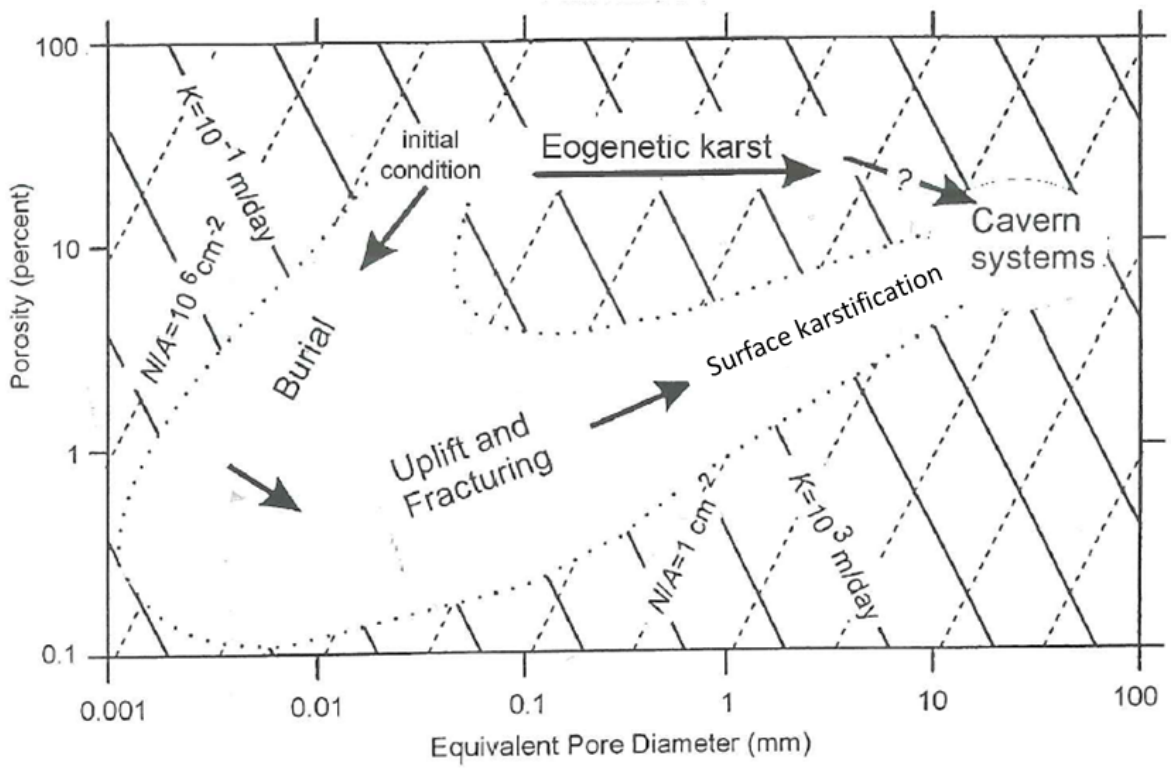

Figure 2.2.3-1: The changes in porosity and pore diameter, from the initial stage to formation of caves. The lines in the background are contours of hydraulic conductivity. Figure modified from Vacher and Mylroie (2002).

According to Palmer (1991) the porosity of the matrix in the host rock associated with cave systems will generally be low in areas where the karst is continental. Cave systems usually form in carbonates with limited matrix porosity where fluid flow is focussed along fault and fracture networks (Loucks, 1999). Where parts of the cave previously have experienced collapse, interbreccia will often be present. If and when cave passages and the large interbreccia pores collapse, the fine-interbreccia porosity will increase and then decrease, and the pore types resulting from fractures will be more abundant. As long as the brecciated paleocave is not filled with cements or eliminated by compaction, paleocaves may form localized high-quality reservoirs (Shen et al., 2007). Esteban (1993) also found that the probability for preserving karst porosity increases when the system has been subjected to rapid transgressions.

According to this conceptual evolutionary model of paleokarst porosity development, shallow cave systems like the Yates field in west Texas, will exhibit cavernous, interbrecciated and fractured porosity (Loucks, 1999). In deeply buried paleokarst reservoirs, the porosity network will mainly consist of crackle breccia and fracture porosity. Thrailkill (1968) and others found a high degree of lateral heterogeneity associated with the porosity in modern karst systems. Extensive cave rooms commonly exhibit host-rock pillars that could act as baffles to fluid-migration, assuming that the permeability of the host rock is low (Kerans, 1988).

According to Kerans (1988) the part of caves that are filled up or almost filled up with cave sediments, will normally not form reservoirs. Loucks and Anderson (1985) found that the major fluid storage area will be formed by the interbreccia and matrix porosity, and that the major permeability pathways will be controlled by the tectonic fractures.

Loucks (1999) states that most paleocave reservoirs are a product of coalesced collapsed paleocave systems, and not products of isolated collapsed passages. These coalesced paleocave systems can be up to several thousand meters across, and are believed to form much bigger reservoir exploration targets than individual passage targets. Loucks believes that some systems are too large and continuous to be a result of collapse of a single isolated cave passage or system, and must be a result of several

stages of development. Stein-Erik Lauritzen (pers. Comm. 2016) has later challenged the general validity of this hypothesis as rocks more than 1 diameter away from the cave passage appear unaffected by the weakness introduced by this cavity (Lauritzen, 2015). Provided the mechanical strength of the rock is sufficient, the collapse will not propagate laterally outside a strain envelope extending one diameter away from the cave passage (see figure 2.2.3-2). Thus, unless cave passages are either densely spaced or surrounded by a weak host rock, collapsing cave passages will most likely not coalesce in the manner envisaged by Loucks (1999).

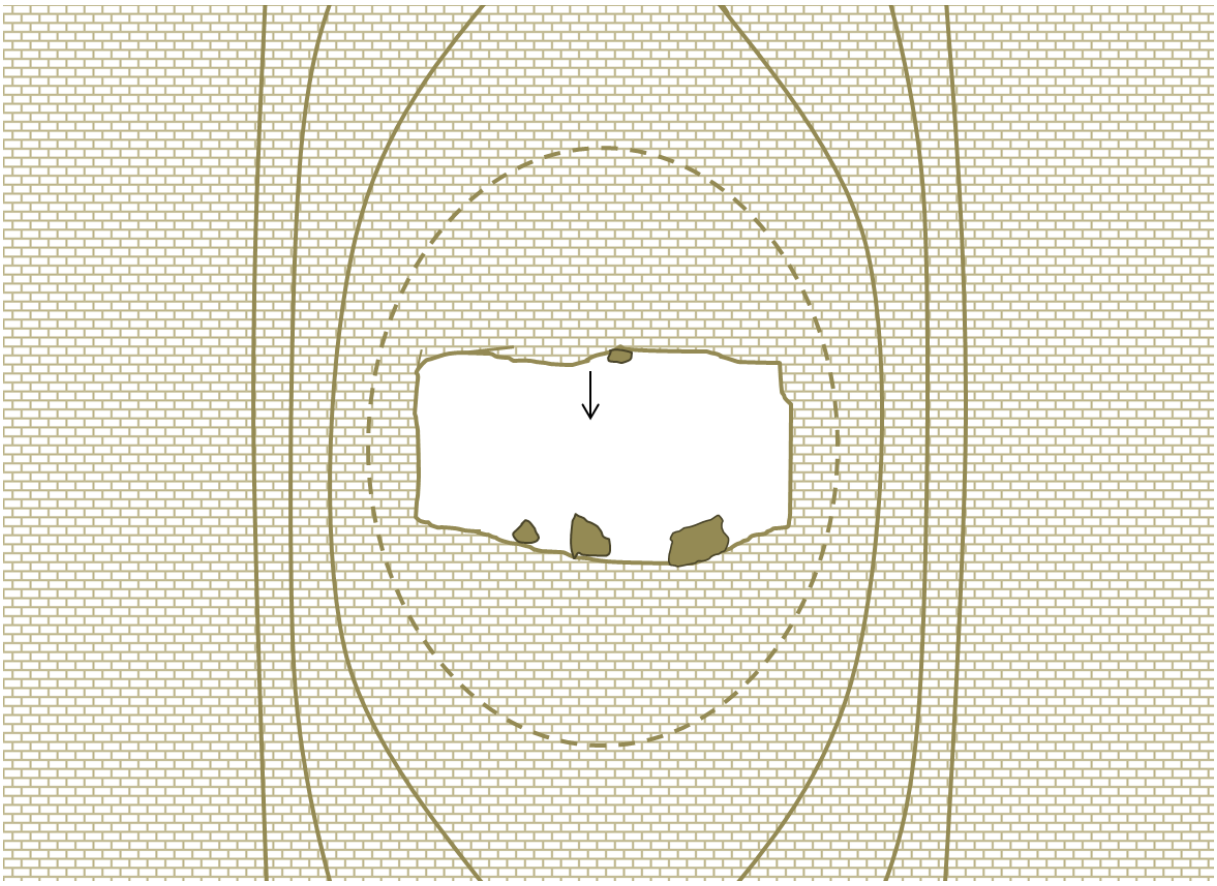

Figure 2.2.3-2: Tension field around a cave passage. Only 1 diameter from the passage, the surrounding rocks will be unaffected by the cave. Figure redrawn from Lauritzen (2015)

Due to their ubiquity and importance, modelling and production of paleokarst reservoir is not something new. There are several ways of incorporating paleokarst reservoir features into reservoir models, and established techniques for handling production. First, it is necessary to try to prove that there actually is a paleokarst reservoir in the subsurface. Mazzullo and Chillingarian (1996) found that identifying unconformities in carbonate sequences usually is the most effective method of doing this, as these are focal

points for karstification and consequently the likely location of paleokarst reservoirs. Paleokarst related to unconformities can be found by using data from wireline logs, cores, bit drops and seismic surveys. Typical, sometimes subseismic-scale, karstic features like fractures, faults and heterogeneous matrix can be identified using image logging tools (Shen et al., 2007). Structural elements associated with paleokarst reservoirs can be identified on seismic data as sag features above missing reflectors (Loucks, 1999), cylindrical karst features (Lucia, 1995) and cylindrical faults. The information collected from these investigations should be included into a possible plan of development.

Once the presence of a paleokarst reservoir can be proven, the incorporation of paleocave systems into modelling and production curves can be done. The high permeability zones associated with the collapsed cave system that is typically present in these reservoirs need to be accounted for (Botton-Dumay et al., 2002). The best paleokarst reservoirs are usually found in affiliation with overlying sags, thus the modelling and production from the reservoir should be focused around these features (Lucia, 1996).

2.2.4 Caves and formation of caves

A cave can be defined as a "natural underground opening in rock that is large enough for human entry". This is the definition that is used by the International Union of Speleology, and is widely accepted in the research community.

The development of caves is typically a near-surface process, and is initiated by dissolutional excavation in the vadose or phreatic zone (Loucks, 1999). Mixing of fresh and meteoric water will lead to mixing corrosion in the phreatic zone (Esteban, 1993). Unsaturated freshwater will also lead to dissolution of the surrounding rocks, and excavation in cavities and fractures. The excavation is initiated around fractures and bedding planes, and when the conduit reaches a diameter of 5-10 mm it is considered a true cave conduit. At this diameter the velocity of fluids increases and the turbulent flow of the water will be competent enough to transport sediments (Ford, 1988).

As long as the passage stays in the phreatic zone at or under the water table, sub-circular, phreatic tubes will develop, see figure 2.2.4-1, (Ford and Williams, 2013). The orientation and further development of a phreatic system will be controlled by fracture density and orientation, as well as the attitude of the strata (Smart and Whitaker, 1991). With unrestricted access to unsaturated water, the evolution of the phreatic cave passage may develop phreatic loops and passage systems extending for long distances (Ford and Williams, 2013).

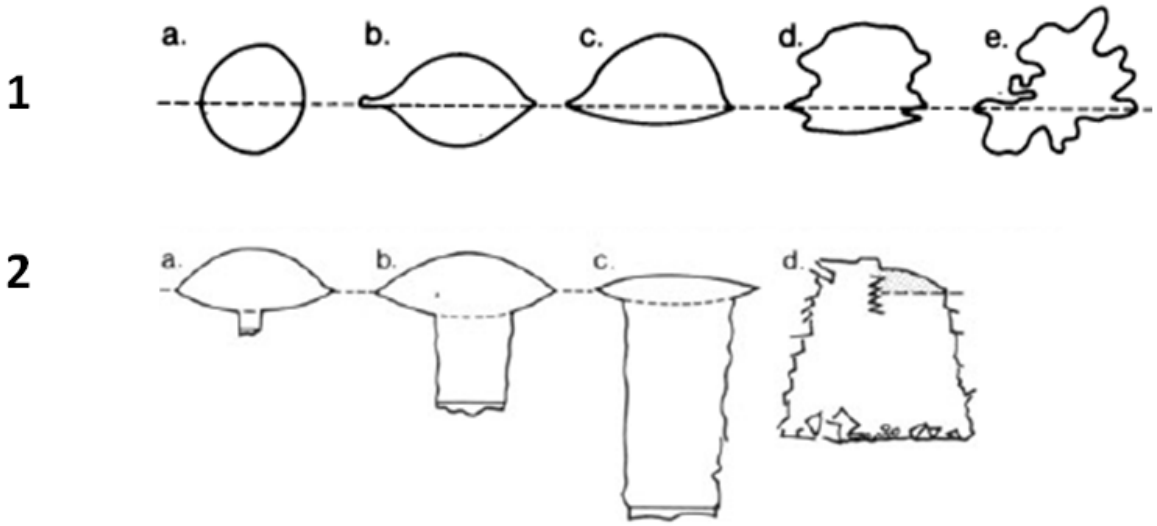

Figure 2.2.4-1: The difference between phreatic and vadose passages. 1 a-e is the typical evolution of a phreatic tube, and 2 a-d is the typical evolution of a vadose passage. Modified from Choquette and James (1988).

With a sinking water table a phreatic system will gradually transform to a vadose system. Continuous flow of water through the previous phreatic passages will lead to formation of vadose canyons and vertical shaft passages. Loucks (1999) observed in several of the modern cave systems he studied that abandoned phreatic tubes on different levels were connected by erosive vadose canyons and vertical shafts. The Setergrotta cave which will be modelled in this thesis consist of both vadose canyons and phreatic elements (Lauritzen, 1996).

The morphology of caves is dependent on several different factors; the location of the cave is controlled by the distribution of soluble carbonate rocks and the presence of discharge and recharge points, the pattern of the cave passage is controlled by the

ground-water recharge, and the different individual cave passages is controlled by the geomorphic history, phreatic and vadose flow and geological structures (Palmer, 1991). This give rise to a wide range of cave geometries which can be classified and to some extent can be linked back to the factors controlling their formation.

2.2.5 Cave collapse and breccia pipes

All caves will eventually collapse with increasing stress. The strength and size of the ceiling is controlled by the thickness of the strata in the ceiling. This was presented by White (1988) who states that cave passages typically start to collapse when the width of the passage is close to 30 meters. White and White (1969) presented a formula for the critical thickness of the strata supporting the ceiling, where it is clear that the collapse of the ceiling is controlled by the density of the bedrock (ρ), the width of the passage (L) and the flexural strength for the supporting strata (S):

$$T_{crit} = \frac{\rho L^2}{2S}$$

A breakout dome will form in the ceiling above the passage, normally in the vadose zone (Ford and Williams, 2013). The dome will gradually expand with increasing stress, which is ultimately relieved by collapse of the rocks within the stress zone. If mechanical processes do not remove the collapsed material, it will pile up beneath the collapse dome as breccia; the collapse terminating as the breccia build-up reaches the roof and stabilizes it forming a breccia filled pipe. Breccia pipes are sub-circular to cylindrical features with a diameter of some tens of meters and filled with collapse-breccia originating from overlying strata of the surrounding host rock (Ford and Williams, 2013). However, if the breccia accumulating below the collapse is removed, the collapse will not stabilize, but continue its upward propagation until it reaches the surface forming sinkholes called dolines. Breccia pipes can reach 500 m in height and may propagate through any overlying lithology (Choquette and James, 1988). There have been observed breccia pipes with a height of up to 1000 meters in the Redwall limestone in Grand Canyon, but this is unusual (Weinrich and Sutphin, 1994).

White and White (1969) state that water supports 40 % of the ceiling weight in the phreatic zone. Should the water be removed, i.e. the cave regime changing to vadose, the ceiling will be weakened and possibly collapse. Collapse of a cave passage will usually take place in the vadose zone or in an abandoned passage. As caves and surrounding strata are buried in the subsurface, cave sedimentation and near-surface dissolutional excavation will terminate (Loucks, 1999). Large clasts will break down into smaller clasts until the interbreccia pores and voids are filled up with cement during burial of an uncemented cave.

When burial of the system continues, collapse of the remaining passages will create collapse structures and breccia pipes. Collapse of the passages will not always be the result; open cavities in modern caves are found at depths as great as 3000 m below the surface (Ford and Williams, 2013). There have been several reports on open cavities in petroleum reservoirs like the Yates field in West Texas, and in the Madison reservoirs in the Garland field, Wyoming (Loucks, 1999). These examples are proof that some parts of a passage may remain open due to local conditions, even at great depths. It is important to be aware of open cavities and fractures, as they may result in water breakthrough problems (Shen et al., 2007) and constitute a hazard for drilling operation.

2.2.6 Classification of cave fills

Classification of breccias and clastic deposits has been done in several different ways. Loucks (1999) presented a triangular diagram based on the composition of the cave infill, see figure 2.2.6-1. Three end-members are presented; crackle breccia, chaotic breccia and cave sediment.

- Crackle breccia is a result of fracturation and are mostly found in the ceiling of the cave. The different clast segments are separated by small-scale fractures.
- The chaotic breccias are a result of collapse of the cave, and consist of clasts from the walls and ceiling of the cave.
- The cave sediment is the third end-member, and is a product of cave forming mechanisms that were deposited before the cave collapsed.

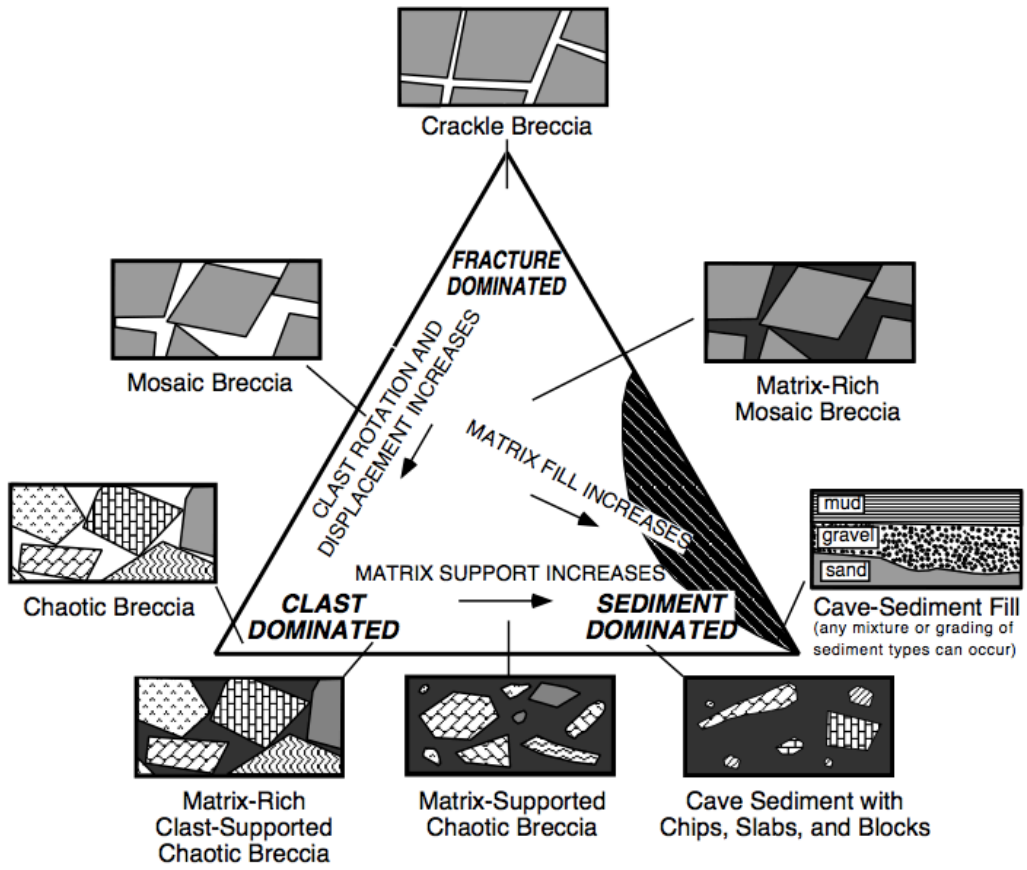

Figure 2.2.6-1: The three end-members for the classification of breccias and clastic deposits, derived from Loucks (1999). Crackle breccia is the dominating end-member in the paleokarstic reservoirs, and chaotic breccia can be found inside the collapsed cave.

2.3 Modelling of paleokarst reservoirs

2.3.1 Challenges and previous work

Modelling of paleokarst, and especially paleocave reservoirs for the ultimate purpose of forecasting subsurface fluid flow has proven to be a challenge. Part of the problem lies in the fact that characterization of these reservoirs straddle the interface between speleology and traditional reservoir geology. The two disciplines represent two different schools with respect to aims of their research and methods employed. Cave mapping has centuries' long traditions, but the aim of these maps was commonly to chart their current impact of groundwater flow, rather than consider their future as paleokarst reservoirs. On the other hand, few petroleum geologists care much about what recent karst systems can tell them. Thus previous studies involving modelling of paleokarst split into two branches: modelling of karst cave conduits, and characterization of subsurface paleokarst reservoirs.

The geometric complexity and internal heterogeneity of the features exhibited by these systems make them difficult to integrate into the existing modelling frameworks employed by the industry. Cave structures and paleokarst systems have traditionally been rendered in reservoir models, using variogram-based methods, but this method fails to provide a precise representation of the actual geology of the reservoir (Erzeybek Balan, 2012). Modern cave network mapping on the other hand employs point data sets, which emphasize passage shapes and dimensions. This data is sometimes difficult to adapt to rigidly gridded templates without losing details.

Fournillon et al. (2010) presented a "genetic" approach for characterizing karstic networks using 3D geological modelling. Their method relies on the classification of different elements in the karstic system according to their orientation. The aim of this approach is to provide several different possible models based on hard data from other karstic systems to find a realistic flow pattern for the system.

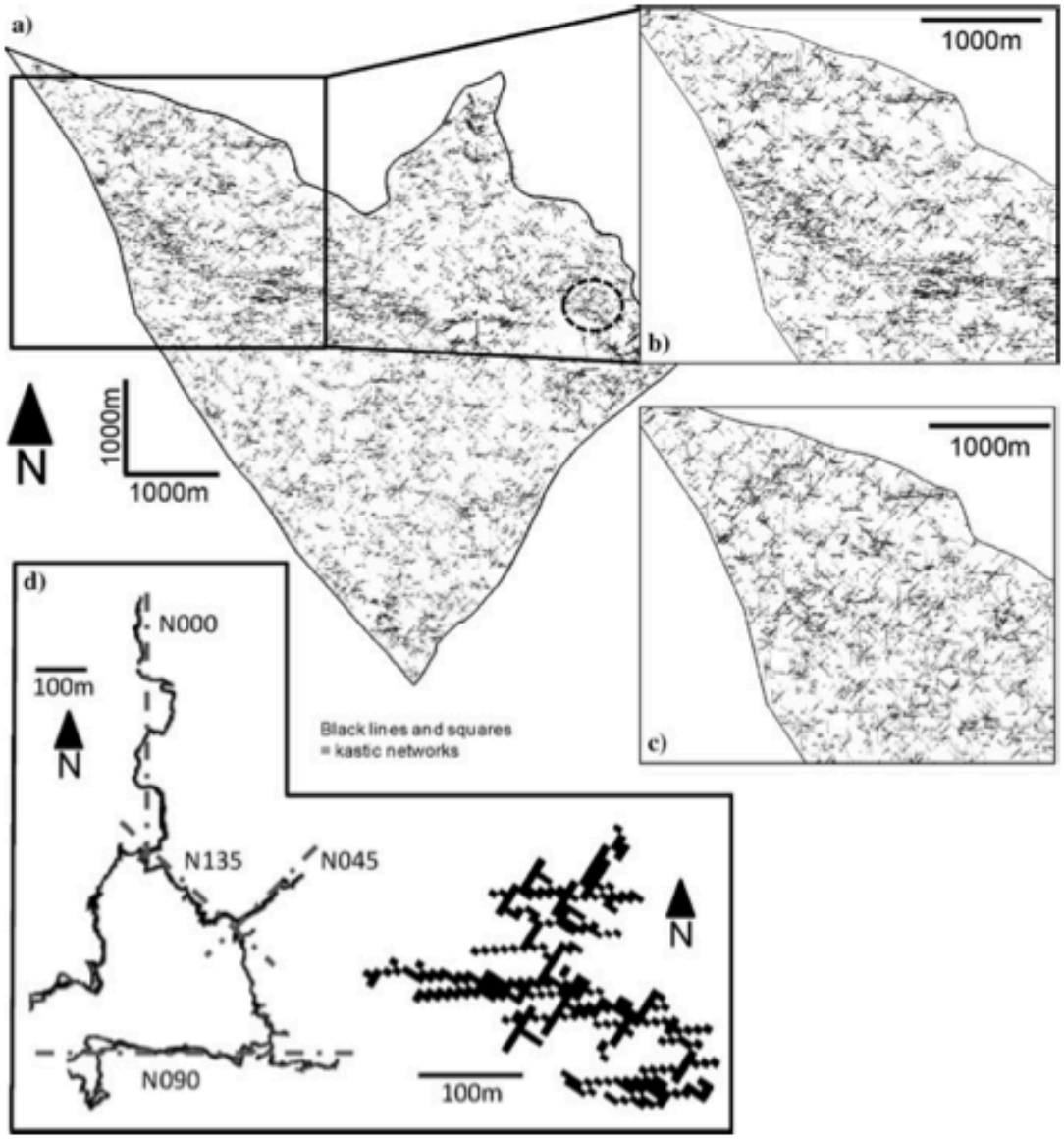

Figure 2.3.1-1: Resulting karstic network, where a, b and c shows the result of the simulation and d shows a comparison to a real cave, and the simulated network. Figure from Fournillon et al. (2010).

Borghi et al. (2012) presented a pseudo-genetic stochastic method for modelling karstic conduits in a manner that honours speleogenetic processes and field measurements. Their method has 4 main steps; 1) building a 3D model of the region, 2) conduct stochastic simulation of heterogeneity features like bedding planes, 3) identify potential in- and outlets of the system, as well as identifying base level and different phases of karstification, 4) generate a karst network using a fast marching algorithm, see figure 2.3.1-2. This method allows the integration of a broad range of data into the model, and potentially provides a more accurate forecasting of karstic conduit networks.

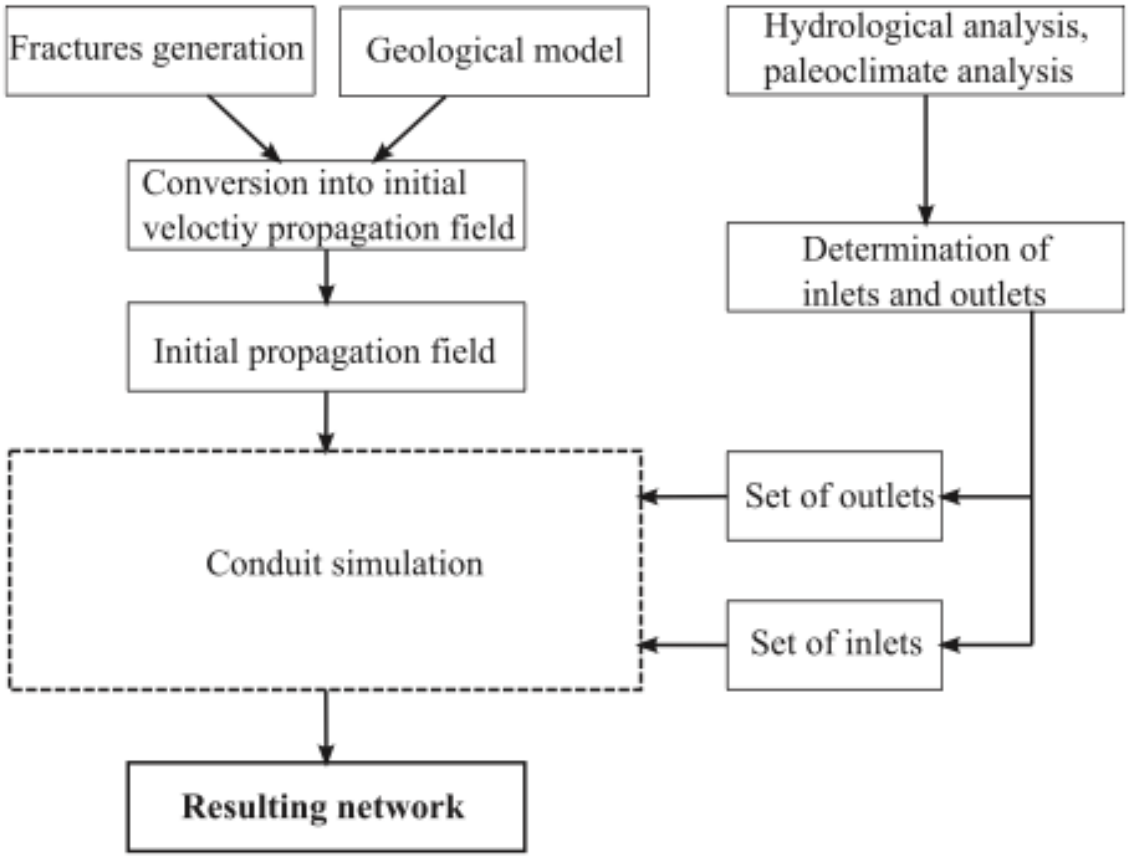

Figure 2.3.1-2: Workflow for the algorithm generated to simulate the karst network. Figure from Borghi et al. (2012).

Erzeybek (2012) presented a method of modelling and simulating the distribution of cave structures in a paleokarst system which involved the use of non-gridded MPS analysis (fig. 2.3.1-3). Statistics are gathered and calculated from modern cave networks, and the cave is modelled by applying a pattern simulation algorithm based on the statistics. An algorithm is created to simulate the cave facies and cave zone thickness.

To test the validity of the method, the algorithms were applied to Wind cave in South Dakota and to the Yates Field in West Texas. Fluid simulations were performed on the model created for the Yates Field to further investigate the validity of the cave facies simulations. This method allows construction of paleocave system models where the geometric complexity of the reservoir is rendered in a better way than a gridded MPS technique would be able to.

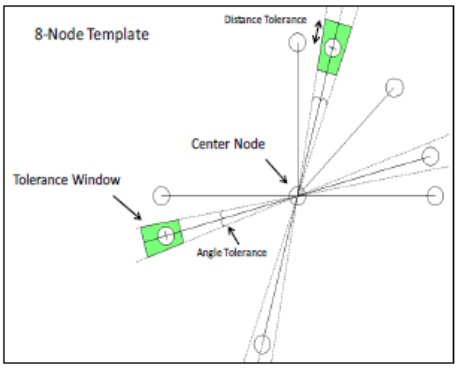

a. Define a template with angle and distance tolerances

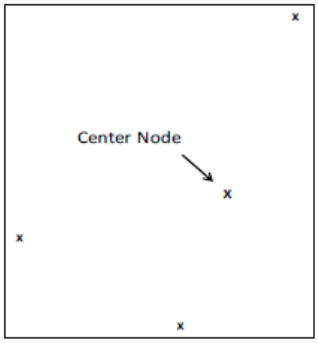

b. Select a node location from the data set.

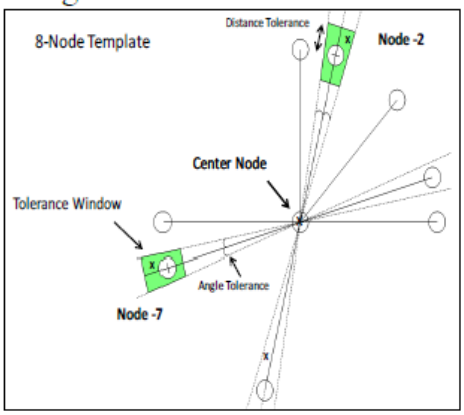

c. Center the template around the selected node and scan current pattern of surrounding data.

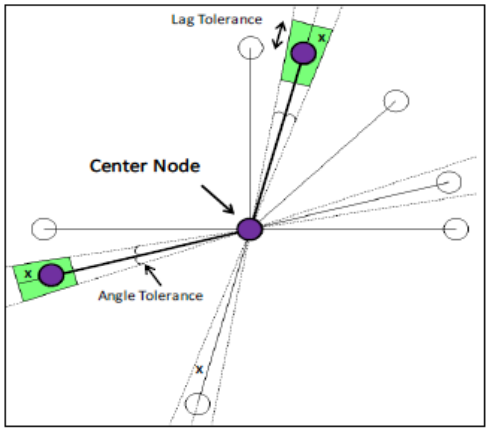

d. Pattern of data observed at the current location of the template.

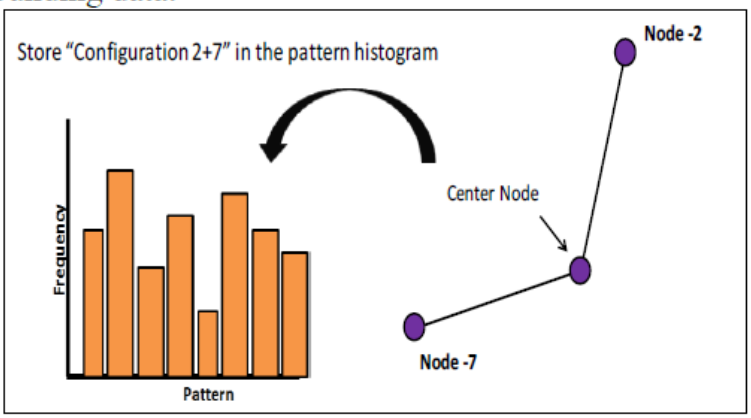

e. Update the pattern frequency by translating the template over the entire data set and compute the resultant pattern histogram.

Figure 2.3.1-3: Method developed by Erzeybek, modelling of paleokarst reservoirs with the use of a non-gridded MPS analysis. Figure from Erzeybek (2012).

Furnée (2015) presented a workflow for modelling paleokarst reservoirs employing forward modelling of cavity collapse (fig. 2.3.1-4). A pre-defined cave system was used to supply geometric constraints. The geo-model was built using the industrial reservoir modelling software suite RMS*TM*, and subsequently exported to Eclipse for fluid-flow simulation purposes. The workflow provided by Furnée (2015) allows forecasting of likely paleokarst reservoir geometries and properties deriving from a given cave geometry, and provides a tool for investigating the impact of different model parameters on flow performance.

In his workflow, skeleton lines combined with calculated geometric distance from the skeleton lines were used to recreate the geometry of the cave passage. A limitation introduced by the use of geometric distance from a mapped cave centreline is that the passages and modelled collapse halos are rendered as circular in cross-section. Although Furnée (2015) provides a robust method for modelling caves by capturing 3D cave traces and subsequent infills, it does not address explicit rendering of 3D geometry of the cave passages.

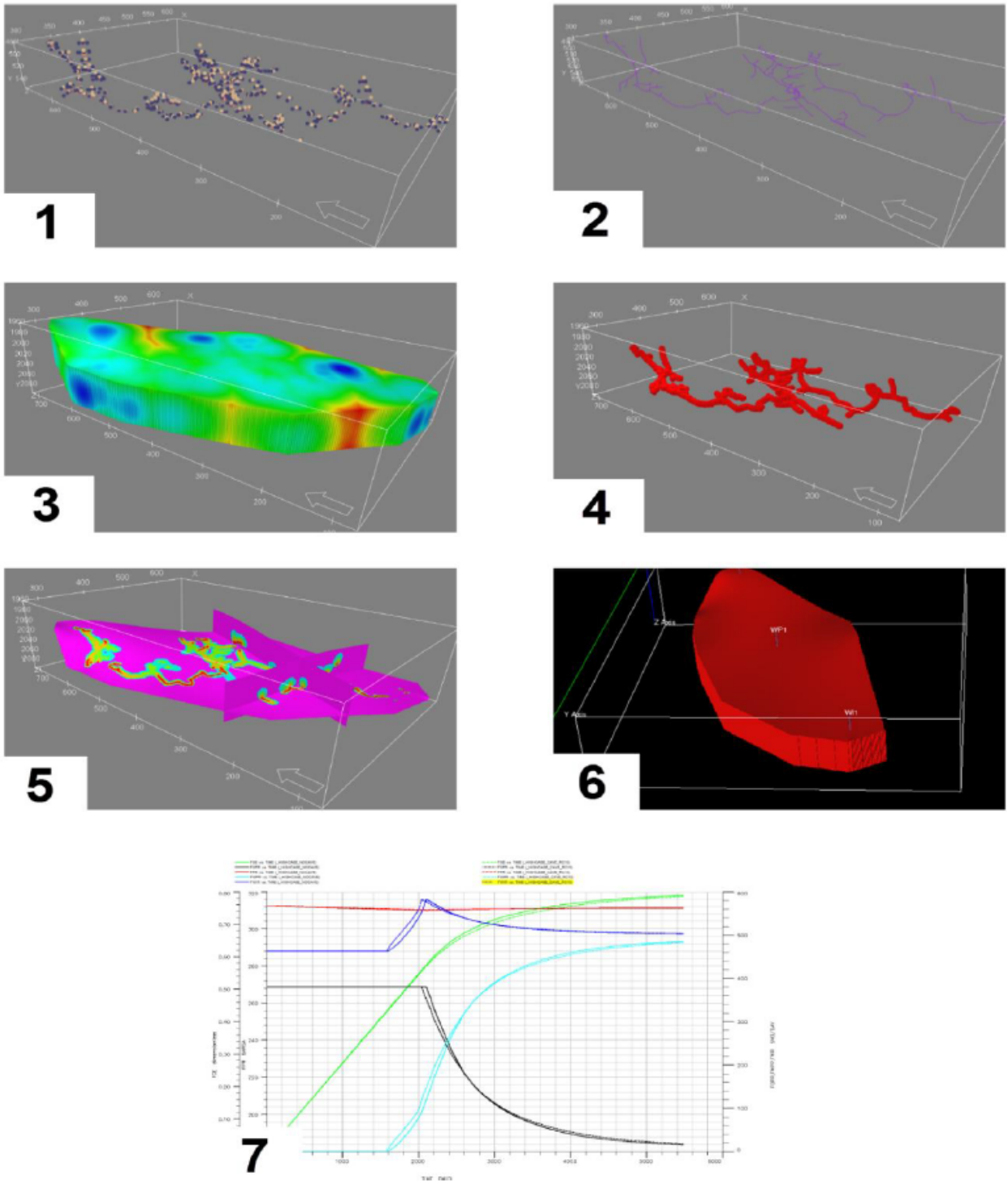

Figure 2.3.1-2: Step-by-step method for the stochastic modelling of caves done by Furnée, from the import of the skeleton lines, to export to Eclipse. Figure from Furnée (2015).

2.3.2 The Setergrotta cave

The Setergrotta cave is located in Mo i Rana (See fig.2.3.2-1), in the northern parts of Norway, and is according to Lauritzen et al. (2005) one of the largest known limestone caves in Norway.

Figure 2.3.2-1: Location of the Setergrotta cave

The cave is located in the upper limb of a recumbent fold as a result of the NW-SE compressional regime present during Silurian times and the Caledonian orogeny. The cave is approximately 3430 meters long, has a depth of 81 meters (Lauritzen et al.,

2005) and has an estimated minimum age of 15000 years (Øvrevik, 2002). The cave morphology is dominated by large vadose canyons but also some phreatic elements, and extensive breakdown (Lauritzen, 1996). It has a typical cave geometry with varying width and height of the cave passages, and are present in several layers of the reservoir, which proved to be a challenge for the RMS modelling tool. Mapping data used as input for this thesis was produced in 2005 by Stein-Erik Lauritzen and R.Ø. Skoglund (2005).

3 METHODS AND SOFTWARE TOOLS

This chapter will only briefly present the tools and concept that have been used, and the basis of some of the work done in the thesis. The full method will be presented in chapter 4.

The aim of the project has been to provide new methods for reservoir modelling of paleocave reservoirs, particularly how to incorporate geometric variation of the cave passages and resulting collapse halos. Paleokarst reservoirs exhibit a variety of geometries mirroring their origin from different cave geometries ranging from seemingly random patterns in flank-margin caves to highly structural single and multiple storied networks. Capturing the complexity of these reservoirs is a substantial challenge considering some of the limitations posed by today's reservoir modelling tools. The greatest challenges encountered while working on this thesis have been the modelling of the cave geometries in different levels, and to correctly model the collapse of the passages.

Previous work by Furnée (2015) was used as a basis for the present thesis. It employs the same database, but the aim in this study was to focus on a method for capturing and controlling the geometry of the cave passages in a more precise manner. As no extant studies specifically addressing this problem in a reservoir modelling context could be found, the workflow presented in this thesis was largely developed using a heuristic approach. This involved "trial-and-error" of concepts and set-ups in order to produce a functioning solution. Shortcomings of current reservoir modelling tools force the use of untraditional methods for the modelling of paleokarst reservoirs.

3.1 Modelling software

The software used in this thesis is RMS*TM* 2013.1.2, which is a geo-modelling tool developed by Roxar Software Solutions. The software is a standard industrial tool for 3D reservoir modelling and simulation. Methods for modelling paleocave features are not present in RMS, and for this reason alternative methods and "out-of-the-box" thinking is necessary to be able to do this. As input for the modelling tool, real cave data was used. The reason for this is partly to ensure a realistic cave geometry, but also to see how speleogenetic data collected using standard methods can be transferred to a reservoir modelling framework. The Setergrotta was surveyed by R.Ø. Skoglund (2005) with the use of a laser and a PDA. The survey is not yet published.

The skeleton of the cave is based on this survey (see figure 3.1-1) and has been imported into RMS as GPS data. In addition to the skeleton of the cave, other point data was imported. When surveying a cave, skeleton points are recorded as well as points and coordinates from the roof, walls and floor. This way a complete geometry of the cave in that location is recorded and can be imported into RMS as XYZ coordinates.

Figure 3.1-1: The skeleton of the cave, used to define the general trend of the cave

3.2 Flow simulation

The initial idea was to export the RMS models to the flow simulation tool ECLIPSE in order to compare model performance to the extensive flow simulation results by Furnée (2015). Due to time-constraints imposed by the difficulty of producing a robust geo-model, this task was not performed. A comparison between the two modelling methods in terms of impact on flow performance should be conducted at a later point, and at a higher level of detail than time allowed for here.

Instead of conducting a full ECLIPSE simulation study, a streamline simulator was used to provide at least an initial impression of the flow behaviour of the reservoir model. Streamline simulation is a tool in RMS that provides an estimate of the fluid flow through the reservoir in the form of streamlines, and are mainly used as a visualization tool. Figure 3.2-1 shows one of the simulations executed on the reservoir model.

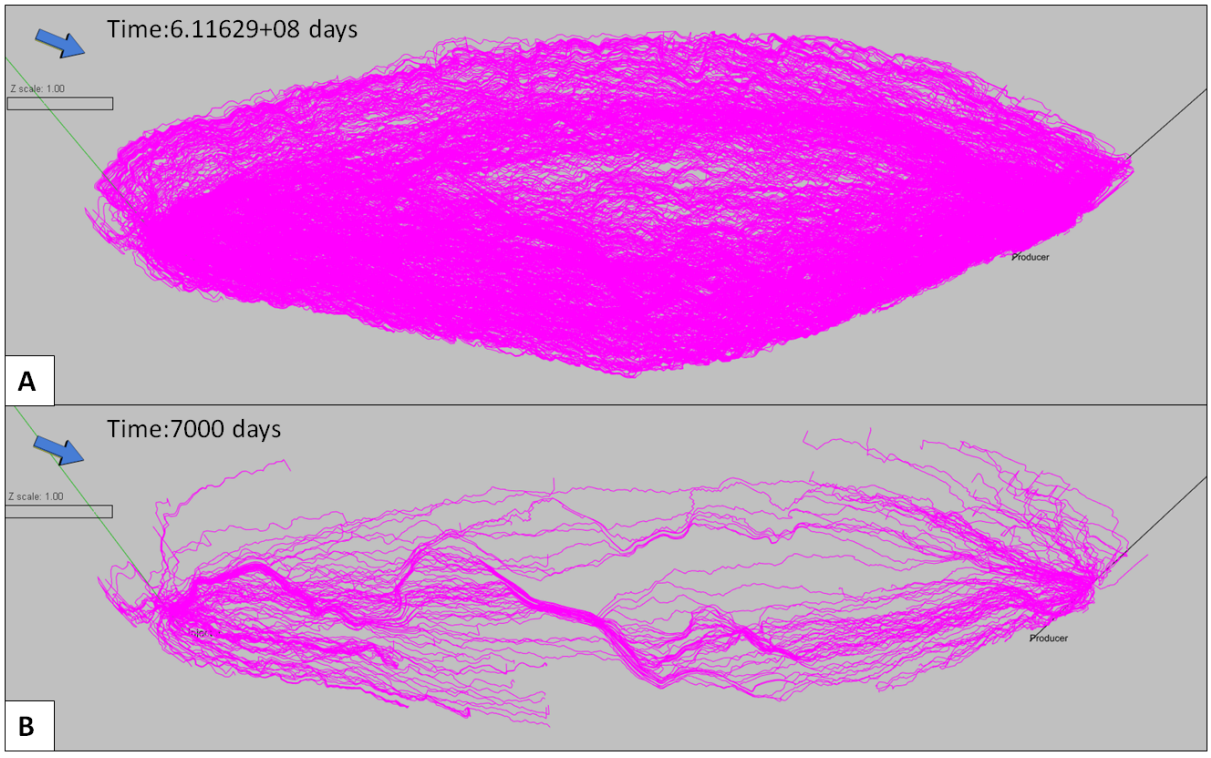

Figure 3.2-1: Streamline simulations made for the reservoir model. A is not filtered on time, and B is filtered on time.

The streamline simulator produces streamlines between wells, in this case one producer, and one injector. The effect the different degree of upscaling had on the grids were investigated, and also some experimenting with the petrophysical values used for the simulations were rendered. The streamlines can be filtered on time to investigate the development of the fluid flow through time. The petrophysical values chosen for the simulations are approximately the same as those Furnée (2015) used in his study with the low case for the background.

4 WORKFLOW DESCRIPTION

Chapter 4 describes the final workflow in detail. The modelling procedure can easily be employed for other caves using similar input data. The method provides an accurate rendering of natural cave geometries when using reservoir modelling tools, but there are some unresolved software issues which need to be addressed at a later stage (see chapter 5). The RMS project can be found on the USB memory stick attached to all hard-copies of this thesis. Figure 4-1 is a conceptual model of the workflow created in this thesis.

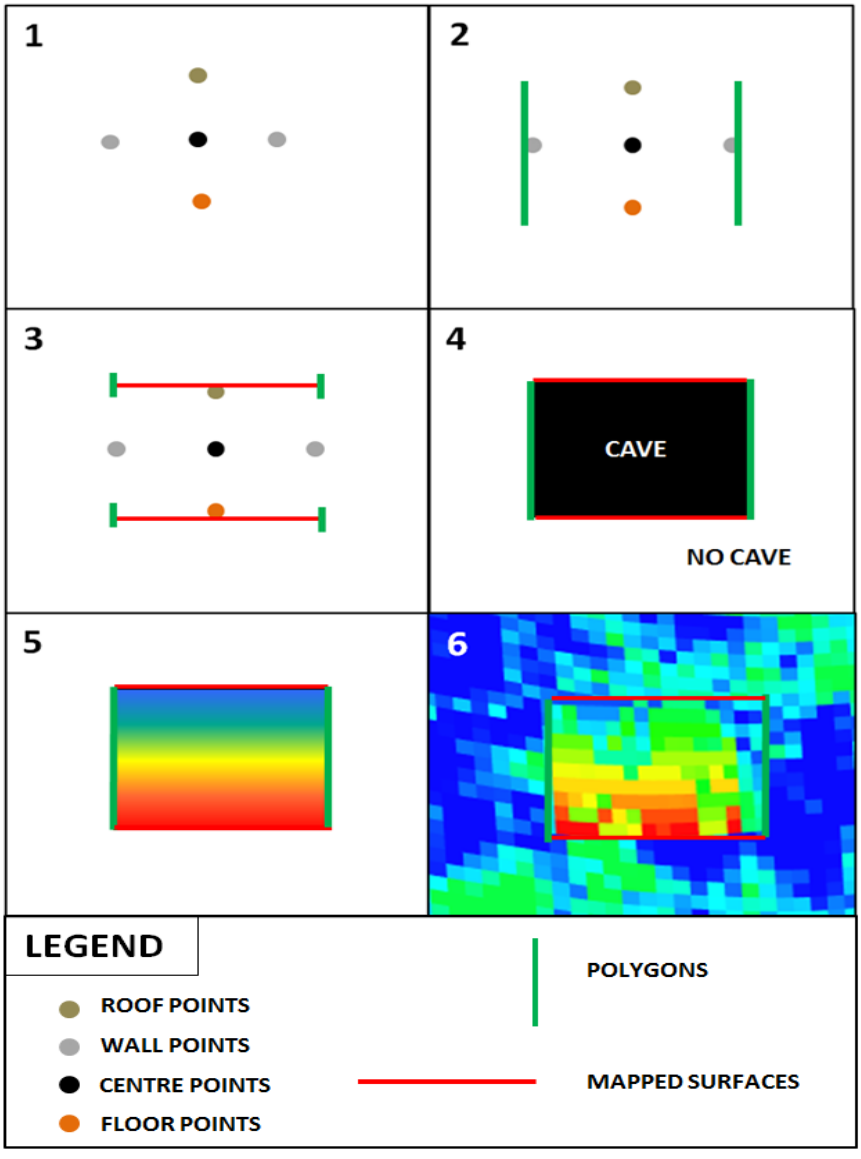

Figure 4-1: Simplified workflow generated in this thesis. A more detailed workflow can be found in appendix 8.2.

4.1 Input data and preparation

A real cave, the Setergrotta cave, is used as input for the reservoir model. Cave maps were provided as global 3D coordinates showing the geometry of the cave. The original data was retrieved from an in-house cave-modelling software called “Grottolf” by Lauritzen (2003) and needed to be reformatted and edited prior to being imported into RMS. In Excel, all points were multiplied with -1 to remove any negative coordinate values. The points were imported into RMS as general 2D data and are named *XYZwallsImport*, *XYZfloorImport*, *XYZroofImport* and *XYZoctaImport* and placed on the clipboard. See figure 4.1-1 for the points visualized. *XYZoctaImport* are points shot to make a cross section through the cave passage at each stop where points for the roof, walls and floor are taken. All objects with given names in RMS will from now on be written in *italics*! A complete list of all labels employed in the RMS project, and specifics of the objects they pertain to can be found in Appendix 8.1. With the use of scalar operations, 1518 meters was added to all depth values in order to transpose the model to a more realistic depth.

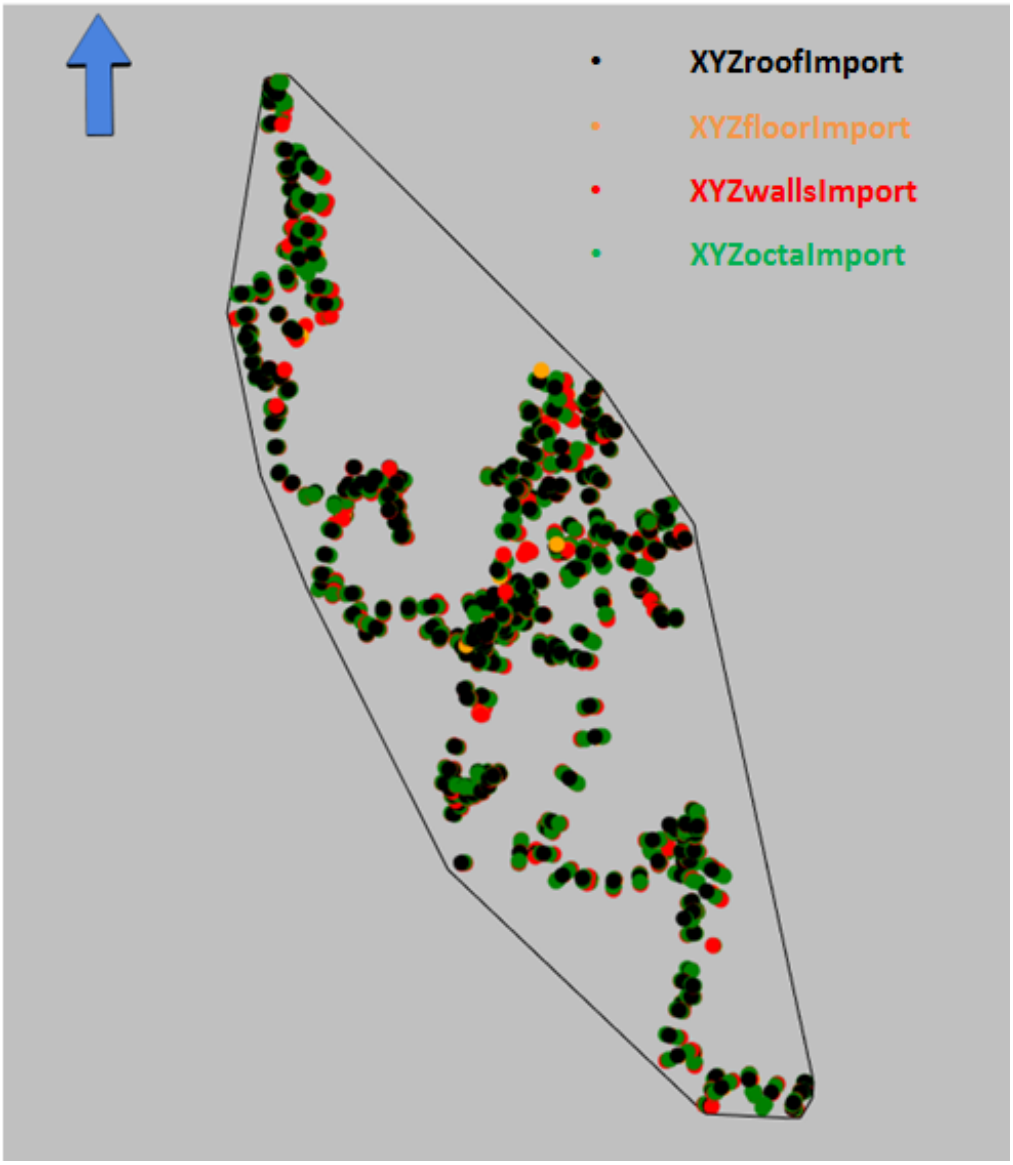

Figure 4.1-1: All imported XYZ points, with the project boundary

SkeletonLines are the centre points of the cave passages. The outer limit of the skeleton lines are used for defining the project boundary. The boundary is created using the "create boundary" function in *skeletonLines.* A manual editing check is carried out in order to eliminate any intersections between the imported datasets and the boundary, thus avoiding potential loss of information. Two copies of the project boundary are made, and with the use of scalar operations one of the boundaries are moved up 43 meters and named *boundary43up*, and the other is moved 27 meters down and named *boundary27down*. They are both located on the clipboard and will be used for modelling the top and bottom of the reservoir model later (see chapter 4.2.2).

4.2 Modelling of the original cave

The paleokarst reservoir modelling is performed in two steps; modelling of the original cave, and modelling of the collapsed cave. The procedure is largely similar, but the preparation of the data is different. Capturing accurate geometry is probably the most challenging part of modelling caves in RMS. There is presently no practical method that allows exact rendering of cave geometries in reservoir models, and implementation must rely on finding functioning work-arounds.

Caves are mapped using a laser range finder from a series of selected positions along the cave passage. A centreline in the middle of the cave, as well as the roof, floor and both walls of the cave is measured by the laser and automatically loaded into a handheld PDA. The centreline is a good approximation of the overall geometry, dip and direction, of the cave system and is used as an input to RMS.

4.2.1 Defining the original cave passages

The greatest challenge regarding the geometry of the cave passages is to find a method of defining the width and height of the individual passages, and to be able to integrate this geometry in the gridding of the model. The wall coordinates, *XYZwallImport*, can be used for this purpose, bur they represent point measurements rather than continuous polygons, and resolution may vary. The wall points and skeleton lines are used together to provide a map-view of the cave passages. A polygon is created by tracing the wall points, were the passage can be defined. The polygons have to be closed, and due to the geometrical complexity of the cave, passages need to be split into several segments. All together 24 polygons (labelled *polygon_1*, *polygon_2* etc.) are generated for the model, see fig. 4.2.1-1. The individual polygons are merged into a single polygon named *AllPolygons* by using the “append” operation.

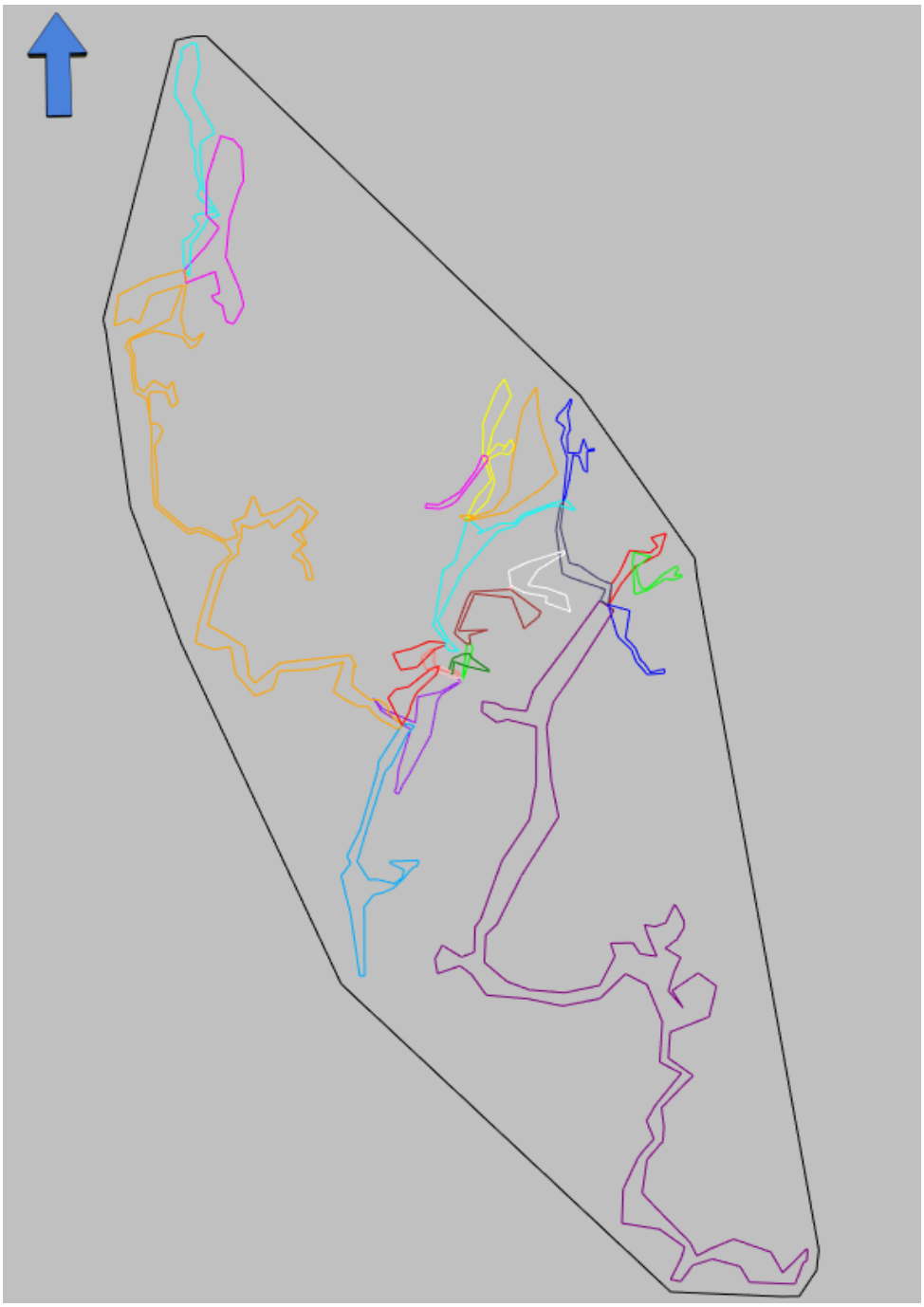

Figure 4.2.1-1: All polygons created with project boundary shown in black.

All the individual polygons are mapped using the "horizon mapping" functionality. The wall coordinates in the form of polygons serve as input. The surfaces have a grid increment of 0.5*0.5 meters to be able to define the narrowest cave passages. The surfaces are rotated 15 degrees to have the best fit along the most prominent structural trend of the passages. The resulting 24 passages are placed on the clipboard under the folder *MappedSurfaces*, and are mapped using local B-spline algorithm.

Surfaces cannot have multiple points with identical XY values. However, caves are often multi-storied, which means that surfaces representing overlapping cave passages must be split into several elements. For this reason the surfaces and polygons were divided into three different groups, representing different cave levels.

The 24 individual surfaces are each assigned to a cave level, and merged using the "Logical" operation. The operation presents several different choices for combining different surfaces. The first surface of the level is duplicated to be used as a basis for the new level, and for each new surface that is added as surface B, the operation "A or B" is chosen and the job is run i.e. *MappedSurface1* serves as surface A and *MappedSurface2* serves as surface B.
This process is repeated until all surfaces are merged into the right level. The new mapped surface is named according to the surfaces that have been gathered. The process is executed for all three main levels, and results in the surfaces *MappedSurfaces_Cave1*, *MappedSurfaces_Cave2* and *MappedSurfaces_Cave3*. These three levels of surfaces will be used for the further mapping of the cave in the project (figure 4.2.1-2).

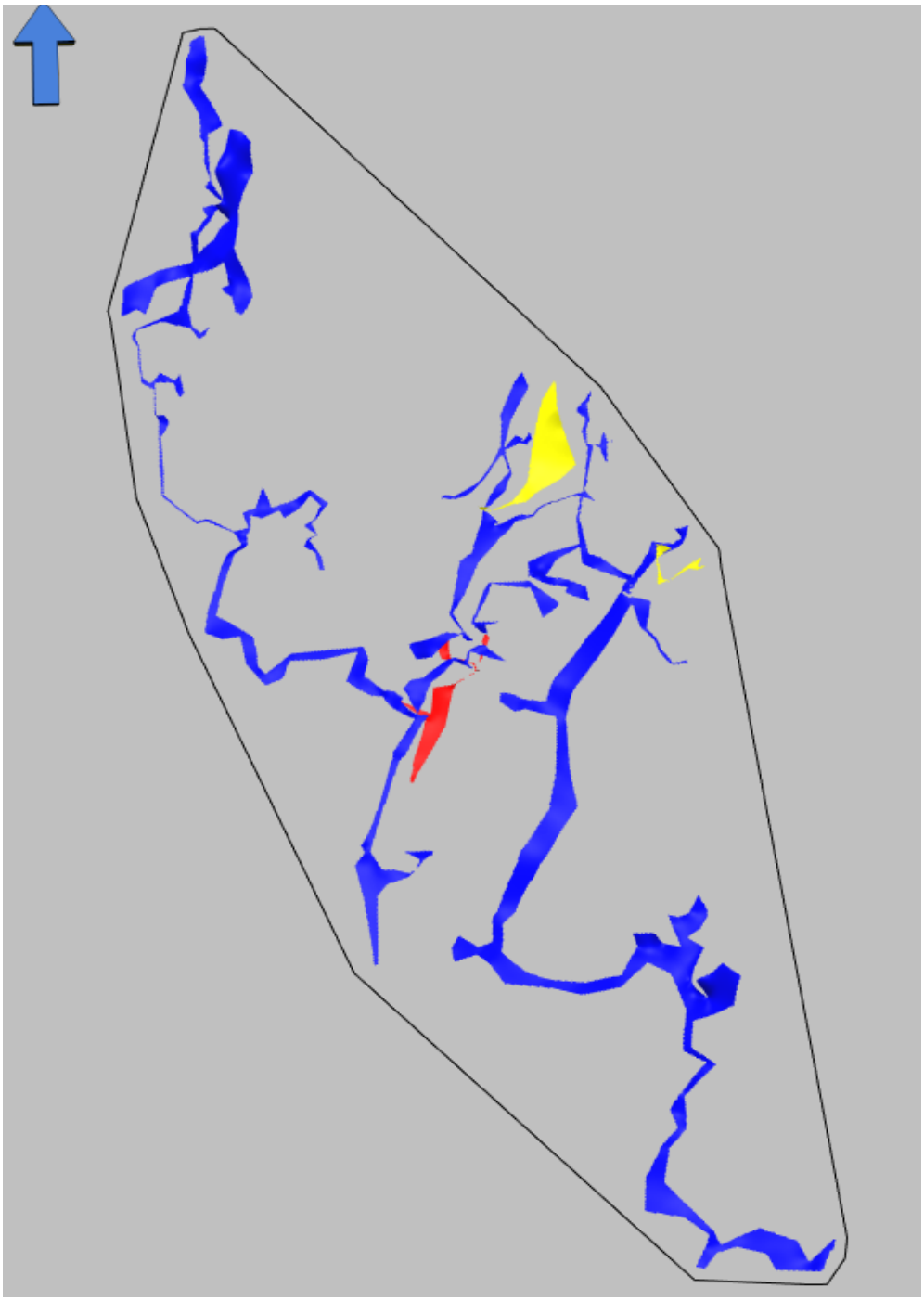

Figure 4.2.1-2: 3 levels of mapped surfaces. The blue cave is cave 1, the red is cave 2 and the yellow is cave 3.

The levels are:

- *Cave1*
- *Cave2*
- *Cave3*

And contain the mapped surfaces and polygons:

LEVEL	SURFACE/POLYGON
Cave 1	1-8, 11, 13-15,17-22 and 24
Cave 2	9,10,12
Cave 3	16 and 24

Table 4.2.1-3: Different levels of the cave, and the surfaces and polygons they contain.

The imported roof and floor coordinates are used to define the cave floor and cave roof. These coordinates need to follow the same division into levels as the mapped surfaces and polygons (see table 4.2.1-3). Three folders called *Points_Cave1, Points_Cave2* and *Points_Cave3* are created on the clipboard. Each folder contains two sets of points representing the coordinates for the roof and the floor in each of the three levels.

The original points for the cave roof and floor, *XYZroofImport* and *XYZfloorImport*, contains all points, so to be able to separate the points into the correct levels the "Filter" operation is used. This operation presents the option for filtering out points in different ways. The option "inside limit" is chosen in the filter operation, and the mapped surfaces for each level is used as input. For the filtering of the roof and floor points within cave 1 for example, the *MappedSurfaces_Cave1* is used as input. The operation has to be done twice for each level, once for the floor coordinates for cave 1, and once for the roof coordinates for cave 1.

A maximum and minimum value for the filter can be chosen. The maximum and minimum values represent the upper and lower distance from the surface. The filtering job will keep all points located within the maximum and minimum values. For the filtering job for the roof points a maximum value of 4 meter, and a minimum of 1 meter is chosen. This way only the points above the surface will be filtered. For the floor a

maximum of 1 meter, and minimum of 4 is chosen for the same reason. The output of this process is a set of points that fit the criteria. With the filter method it is likely that at least a couple of the points get neglected.

A manual method of visualising all points, either the *XYZroofImport* or the *XYZfloorImport*, and their point table has to be done. The filtered points for the different levels of the cave are also visualized, and their point table. The points that have been neglected during the filtering job are identified, i.e. for the roof of cave 1, and the coordinates for the point can easily be copied from the point table of the *XYZroofImport* in to the point table for the filtered *PointsXYZ_Cave1_Roof*. This process is executed for all three main levels. These points will be used for the mapping of the 3 main levels of the cave, and has to be mapped individually.

4.2.2 Mapping the original cave passages

For gridding of the cave passages, a stratigraphic framework has to be created. This is done in the "Horizons" tab. A total of 8 horizons are created which are:

Horizon	Type	Based on:
Cave_top	Interpreted horizon	*Boundary43up*
Cave3_roof	Calculated horizon	*PointsXYZ_Cave3_roof*
Cave3_floor	Calculated horizon	*PointsXYZ_Cave3_floor*
Cave1_roof	Calculated horizon	*PointsXYZ_Cave1_roof*
Cave1_floor	Calculated horizon	*PointsXYZ_Cave1_floor*
Cave2_roof	Calculated horizon	*PointsXYZ_Cave2_roof*
Cave2_floor	Calculated horizon	*PointsXYZ_Cave2_floor*
Cave_bottom	Interpreted horizon	*Boundary27down*

Table 4.2.2-1: The horizons created for the mapping of the original cave, the type they are, and what they are based on.

Cave_top and *Cave_bottom* are defined as Interpreted horizons, while the other horizons are Calculated horizons. In the tab Data types, *GeneralPoints* and *GeneralSurface* are chosen for the calculated horizons and *GeneralPoints*, *GeneralSurface* and *SkeletonLines*

are chosen for the interpreted horizons. Cave 3 is set at the top of the structural framework because this is the highest part of the cave, and will be the upper zone, cave 1 will be the middle zone and cave 2 will be the lower zone. See chapter 4.2.3 for the final zonation of the cave.

For *Cave_top* and *Cave_bottom* the boundaries *Boundary43up* and *Boundary27down* located on the clipboard are dropped on top of the *GeneralPoints* and are used for the mapping of the horizons. This process is executed in the horizons tab under horizon mapping. The *GeneralPoints* are used as input and the project boundary are used as a polygon to limit the extent of the mapping. The result of the horizon mapping is the *GeneralSurface*.

For the horizons defining the main levels of the cave passages, cave 1-3, the *GeneralPoints* are used as input for the modeling of both roof and floor of the cave. The points filtered on the clipboard are dropped on top of the *GeneralPoints* (see chapter 4.2.1). For the horizon modelling the *GeneralPoints* are used as input. The polygon corresponding to the level is used for the clipping of the horizon. The increment is set to 0.5*0.5 meters to prevent the loss of the narrowest passages, and the grid is rotated 15 degrees to fit the general orientation of the passages. This process is done for all the three levels, both for the roof and the floor.

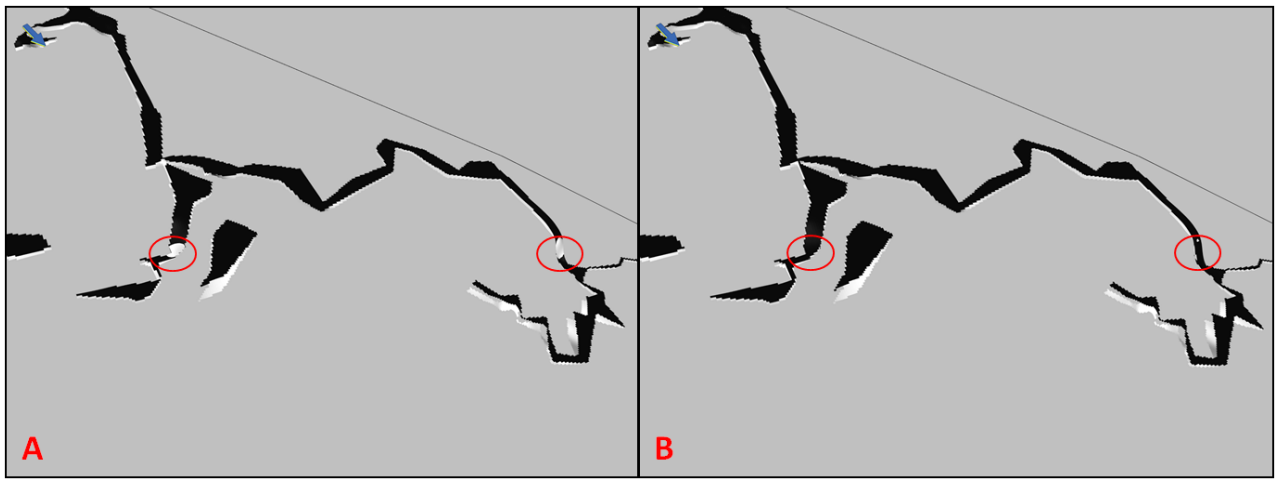

Figure 4.2.2-2: The unedited (A) and edited (B) roof surfaces. The black surface is the roof, and the white is the floor. This is the surface for cave 1.

Parts of the cave 1 level required some manual adjustments. In some parts of the cave, the roof coordinates are located lower than the floor coordinates, and the roof is dipping down underneath the floor, see figure 4.2.2-2. This is probably caused by errors made during the mapping of the cave. This is obviously not realistic in the natural world and needs to be adjusted. The surfaces are visualized and the roof points that are located underneath the floor are moved 1 meter up. This process is done for the *Cave1_roof.* The old, unedited points and roof surfaces can be found on the clipboard under the folder *PointsAndHorizonsOriginal.* For the mapping of the cave, the edited points are used, and are located on the clipboard in the filtered points folders, *Points_Cave1*. Under the horizons, both the horizons cut by the polygons and the uncut horizons can be found, but it is the *GeneralSurface* that is used to create the grids and for the structural model.

4.2.3 Creating a structural model

The structural model set-up defines the horizons and zones that will be used in the grid. A new structural model, *CaveOriginal*, is created in depth domain. The model box, defining the outer limits of the model domain is based on the range from the project boundary, by using this as input. The XYZ coordinates were slightly adjusted to avoid losing any information. See table 4.2.3-1 for the adjusted XYZ coordinates. The model box has no rotation.

	CENTRE	LENGTH
X	475.90	500.00
Y	394.46	750.00
Z	2036.75	250.00

Table 4.2.3-1: Model box set-up

There are no faults in the model domain, so any aspects relating to faults can be ignored in this case. The Horizon model on the other hand is needed for generating a grid. Under the tab Stratigraphy, the vertical resolution is set to 20 meters. All available horizons are selected and *GeneralSurface* is chosen as data input. To avoid erosion by underlying cave zones it is necessary to specify the transitions between the cave levels as "depositional" (i.e. conformable), see figure 4.2.3-2.

Capturing the transition from cave 1 to cave 3 in the horizon modelling proved difficult. In most cases the horizon modelling produced geometric distortions or unrealistic surface relations. The cause for this is most likely linked to the way points and polygons are assigned to the three levels. This challenge is more thoroughly discussed in chapter 5.1. The encountered problems highlight the importance of assigning input data in a careful manner when employing this method on a multi-storied cave system.

A number of different settings were tested to overcome or at least improve this issue. The best result was obtained when the *Cave3_roof* horizon is set as an "unconformity", and the isochore from cave 3 is used as additional input. For the horizon *Cave3_floor* the data conditioning is set to "hard", to avoid some of the zonation issues. Under the tab "Modelling" the Grid X-Y increment is set to 2 for all horizons. The output for this job are the zones and horizons located under the new structural model. A total of 8 horizons and 9 zones have been created from this job (fig.4.2.3-2).

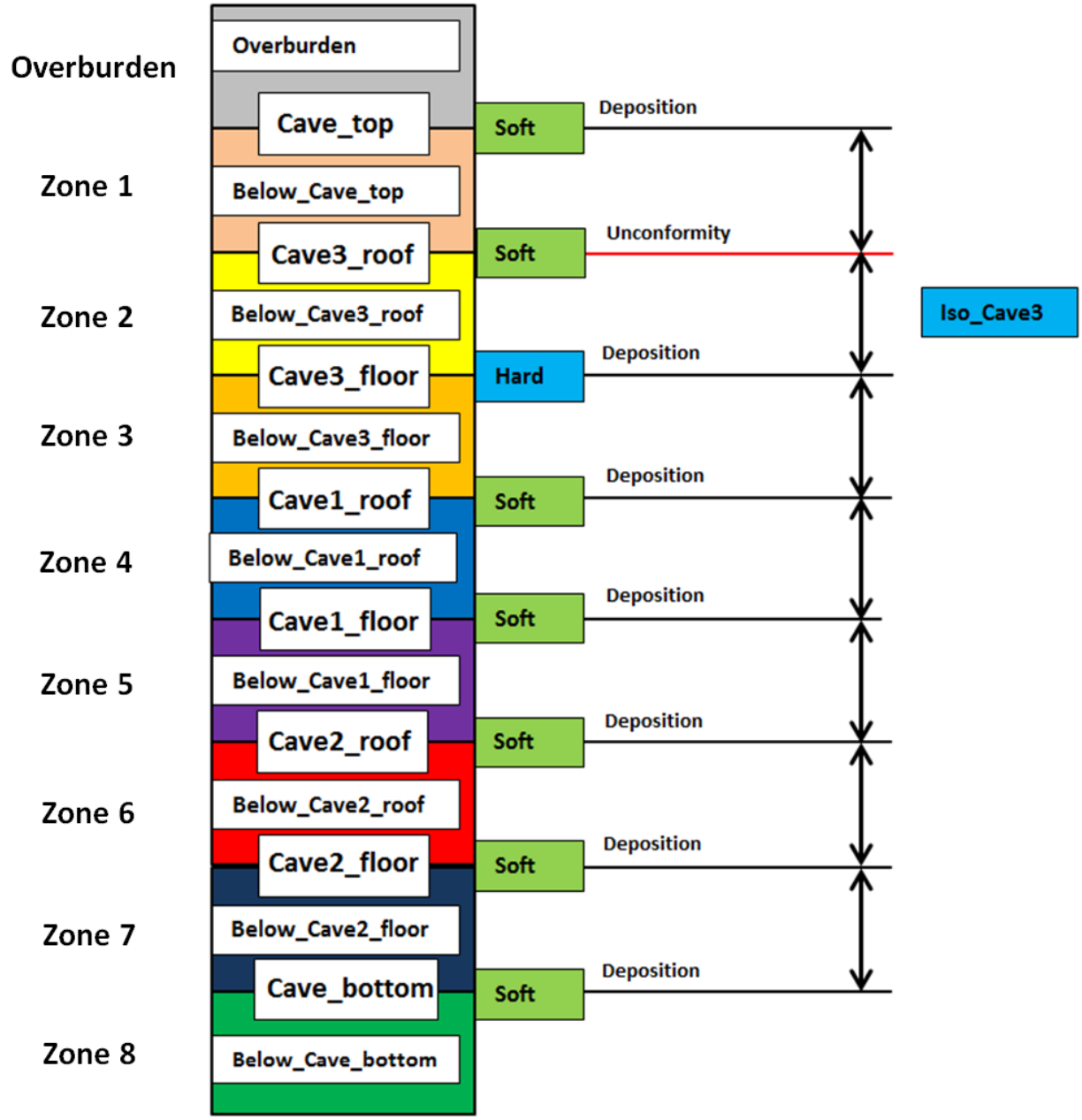

Figure 4.2.3-2: Structural model set-up for the original cave. The horizons are the same that were defined in chapter 4.2.2, while the zones are the ones in the coloured boxes, named Below_Cave_top, Below_Cave3_roof and so on.

In the grids, the lower zone *Below_cave_bottom* and the *overburden* will not be accounted for, as this is not a real part of the reservoir, but is created by RMS.

The zones are numbered consecutively from the top:

- Zone 2, *below_Cave3_roof* contains cave 3
- Zone 4, *below_cave1_roof* contains cave 1
- Zone 6, *below_Cave2_roof* contains cave 2

This partitioning will be used for the rest of the modelling. See figure 4.2.3-3. There are some issues regarding the zonation, this will be discussed in chapter 5.1.

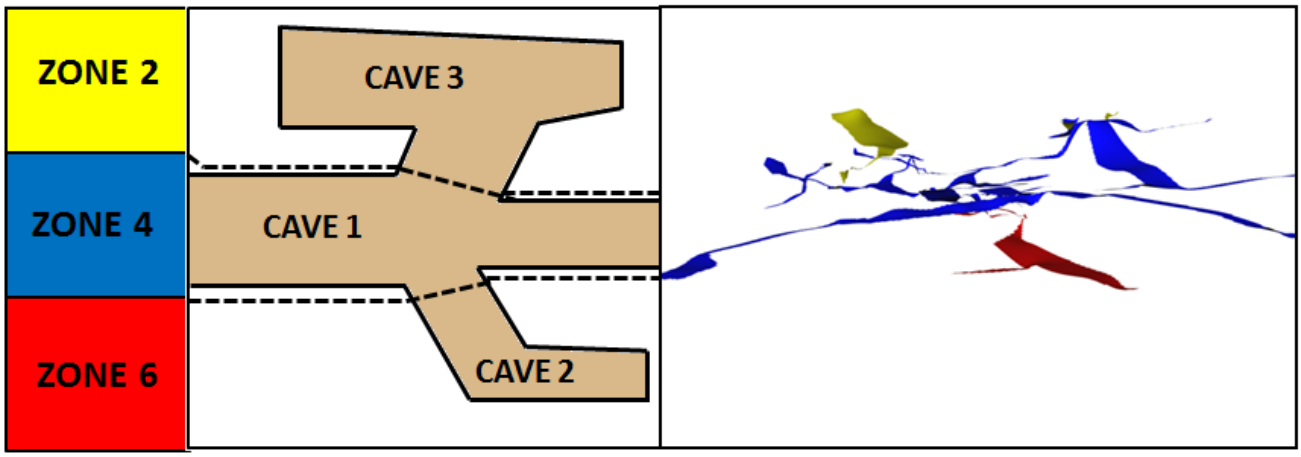

Figure 4.2.3-3: The zonation of the cave. Zone 2 contains cave 3, zone 4 contains cave 1 and zone 6 contains cave 2.

4.2.4 Gridding of the original cave passages

Four grids were generated; one for each of the 3 different levels of the cave, and one where all three levels have been merged into a single grid. The grids are labelled:

- *Grid_cave1_Original*
- *Grid_cave3_Original*
- *Grid_cave2_Original*
- *Grid_AllCaves_Original*

All of the grids have the same settings and layout (Table 4.2.4-1). Creating a new grid model, and then choosing "Create grid" will open the dialogue box for defining the grid. Under the tab "General" the *CaveOriginal* structural model is chosen as input. Under the tab "2D layout", the project boundary is used for constraining the lateral extent of the grid. The "Auto-calculate best fit" option is chosen, and the increment is set to 1*1 (Table 4.2.4-1). The grid is rotated 15 degrees to provide the best fit for the mapped surfaces.

	CENTRE	LENGTH	GRID DIMENSIONS Increment
X	473.03	490.19	1
Y	390.87	584.01	1
Rotation, clockwise:		15	**degrees**

Table 4.2.4-1: 2D layout of the grids for the original caves.

The choice of XY grid resolution (here 1*1m) is a compromise between the actual diameter of the cave passages and cell size, while keeping in mind that an increase in cell numbers add CPU cost when running property models and flow simulations. Where the passages are narrow, too coarse grid resolutions could pose a problem as some cells may end up only being connected along cell-edges. This will influence connectivity and create artificial barriers to fluid flow in the model. For the present model this was not a problem as the chosen grid resolution of 1m*1m retains the observed physical continuity of the cave passages in the model. Problems regarding the connectivity were encountered during upscaling of the model, this is further discussed in chapter 5.3.1.

Under the tab "Zone layout" the vertical grid-layout is specified for each of the 7 zones. The number of cells is tested to have the best fit for the representation of each zone. This is done be creating the grids and checking the representation of the cave within the zones with different vertical cell resolution. It was found that the Number of cells for the zones *Below_Cave_top* and *Below_Cave2_floor* is set to 30 and 20, and for the rest of the zones, the Number of cells is set to 10 (Table 4.2.4-2). It is important to find the right number of cells in the vertical direction. Some of the cave passages have a very limited height, for this reason a too high vertical resolution will lead to loss of passages. If the vertical grid-resolution was set too low, the representation of the cave in a vertical direction was compromised during the geometrical modelling. The geometrical model

used in this thesis is discrete, and only assigns the values 1 for “cave”, and 0 for “no cave”. If the vertical resolution was much higher that the cave height, the cave facies were ignored and wrongly given the value 0, “no cave”. The top and lower zones sometimes has a significant height, and the vertical resolution is set to 30 and 20.

Zones	Type	Dimension
Below_Cave_top	No of cells	30
Below_Cave3_roof	No of cells	10
Below_Cave3_floor	No of cells	10
Below_Cave1_roof	No of cells	10
Below_Cave1_floor	No of cells	10
Below_Cave2_roof	No of cells	10
Below_Cave2_floor	No of cells	20

Table 4.2.4-2: The vertical resolution of the zones in the grid.

For the three grids *Grid_Cave1_Original*, *Grid_Cave3_Original* and *Grid_Cave2_Original*, the “geometric modelling” option in RMS was used to create a parameter discretising the cave passage. Here the “Assign Values Between Surfaces” functionality is used. This functionality assigns grid cell parameter values between two input surfaces and can be laterally constrained using polygons (ROXAR, 2016b). The cave roof and floor surfaces created earlier (see section 4.2.2) are used for input together with their corresponding polygons. The cells between the surfaces (i.e. the modelled cavity) were given the value 1, and the other cells (host rock surrounding the cavity) were assigned the value 0. This procedure was performed for all three grids. The resulting parameters can be found under each grid and is named *GeometricAVBS_Cave1_Original*, *GeometricAVBS_Cave2_Original* and *GeometricAVBS_Cave3_Original*.

Somewhat surprisingly this process-step turned out to be extremely time-consuming to run. The cause for this is likely to be found in the manner the software handles interplay between “cut” surfaces, such as the roof and floor, and the full 3D grid based on “un-cut” surfaces. The issue of making this process more CPU efficient should be referred to the programming team at Roxar.

For further work the three grids representing the three levels of the cave were merged into one grid labelled *Grid_AllCaves_Original.* The "Resample parameters" operation is used for this purpose. The "Nearest node" option is chosen for the resampling and the undefined value is set to 0. The nearest node option allows a search radius to be specified by number of cells, and will be the best option for resampling discrete values (ROXAR, 2016f). The job has to be run three times to be able to gather all three parameters into the new grid, *Grid_AllCaves_Original*. The procedure resamples the three discrete parameters *GeometricAVBS_Cave1_Original*, *GeometricAVBS_Cave2_Original* and *GeometricAVBS_Cave3_Original* into the same grid adding the prefix "res".

The three resampled parameters then have to be merged into one parameter using the "Merge parameters" operation. The operation has to be performed stepwise; first the parameters *res_GeometricAVBS_Cave1_Original* and *res_GeometricAVBS_Cave3_Original* are merged, and named *merged_Cave1andCave3*, second, this parameter is merged with the *res_GeometricAVBS_Cave2_Original*. The result is the *mergedAllOriginal* parameter which shows the entire 3D architecture of the Setergrotta cave, see figure 4.2.4-3 and 4.2.4-4 for the result.

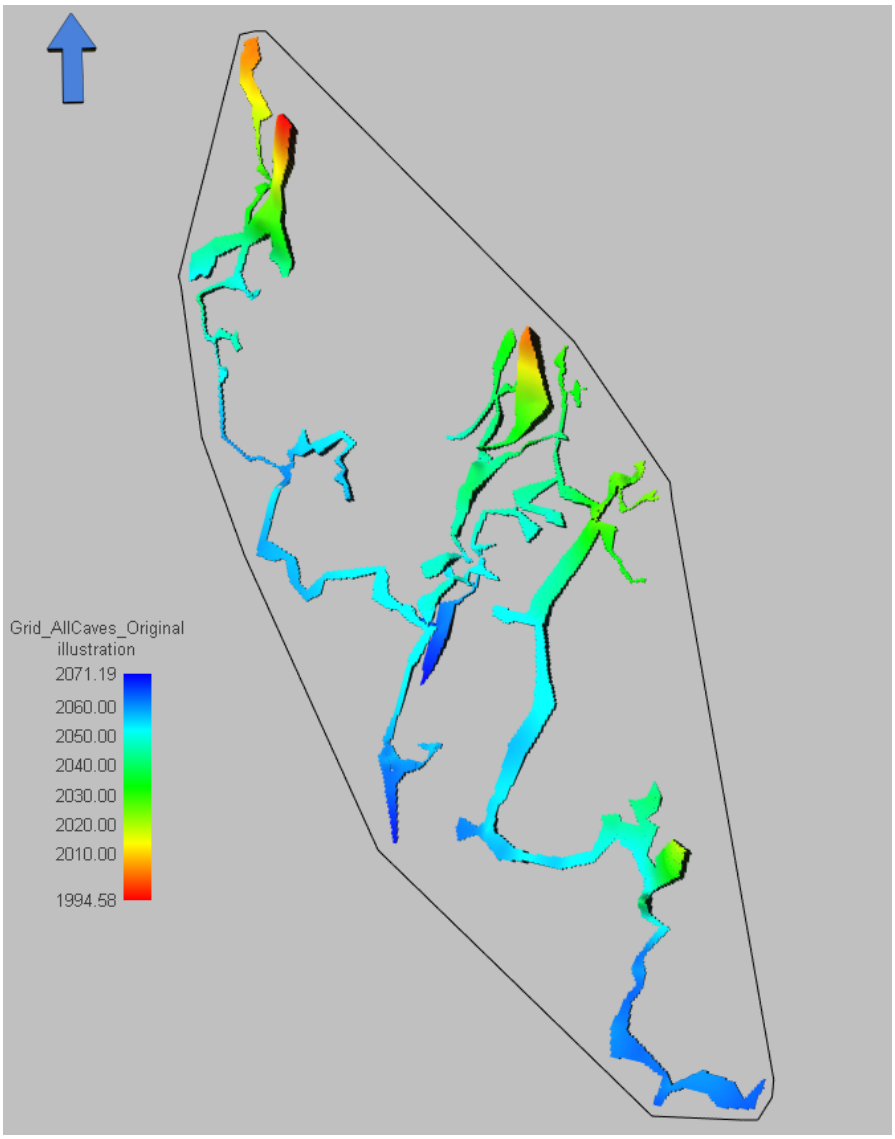

Figure 4.2.4-3: The whole cave, shown as the parameter illustration, created from mergedAllOriginal. The colouring illustrates the depth of the cave, where the blue is the lower parts of the cave, and the red is the higher parts.

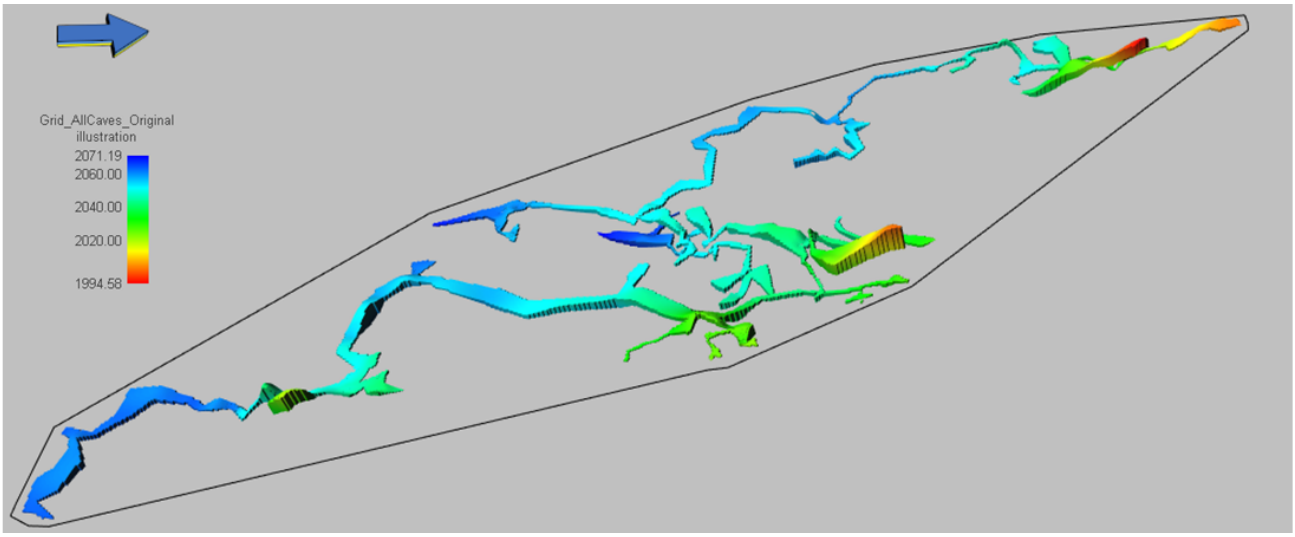

Figure 4.2.4-4: The original cave seen from another angle, the same colouring is used.

4.3 Modelling of the collapsed cave

Having established the geometry of the initial cave system, the next step is to provide a model rendering its likely post-collapse configuration. The main difference between the geometry of the initial cave and the collapsed cave is the height of the cave roof and the width of the cave passages. For the collapsed cave we also need to take into account that the passages are filled with material originating from the collapse process. In modelling terms this entails creating a new structural model, which takes into account the changed height and width of the initial cave passage. As these changes are related to the physical process of collapse, it is possible to estimate how the geometry of the cave passage will change as it collapses and is filled by breccia.

4.3.1 Defining and mapping the collapsed cave passages

Collapse of the cave passages causes upwards and lateral expansion. The collapse process will terminate when the pile of collapsed material reaches the roof and stabilizes it. This can be termed the maximum height of the cave passage (H_t). Mathematically this can be expressed as:

$$H_t = H_g \left(\frac{p_1}{p_1 - p_2}\right) \quad (1)$$

H_g is the original height of the cave, p_1 is the density of the background rock, in this case a typical density of limestone is chosen, 2,6 g/cm^3, and p_2 is the density of the collapsed, brecciated cave fill. Collapsed material typically has a 20-40 % greater volume than the original background rock, and will have a density of about 2,0 g/cm^3 (Lauritzen, 2015). The formula is based on a cave with a cylindrical cave passage with a flat floor and roof, which is the case in this project, but is not the most natural form of a cave passage. Note also that the formula is only valid if the collapsed material remains in place – if it is transported away the collapse will continue to propagate upwards until the debris pile catches up with it. Figure 4.3.1-1 illustrates the gradual collapse of a cave.

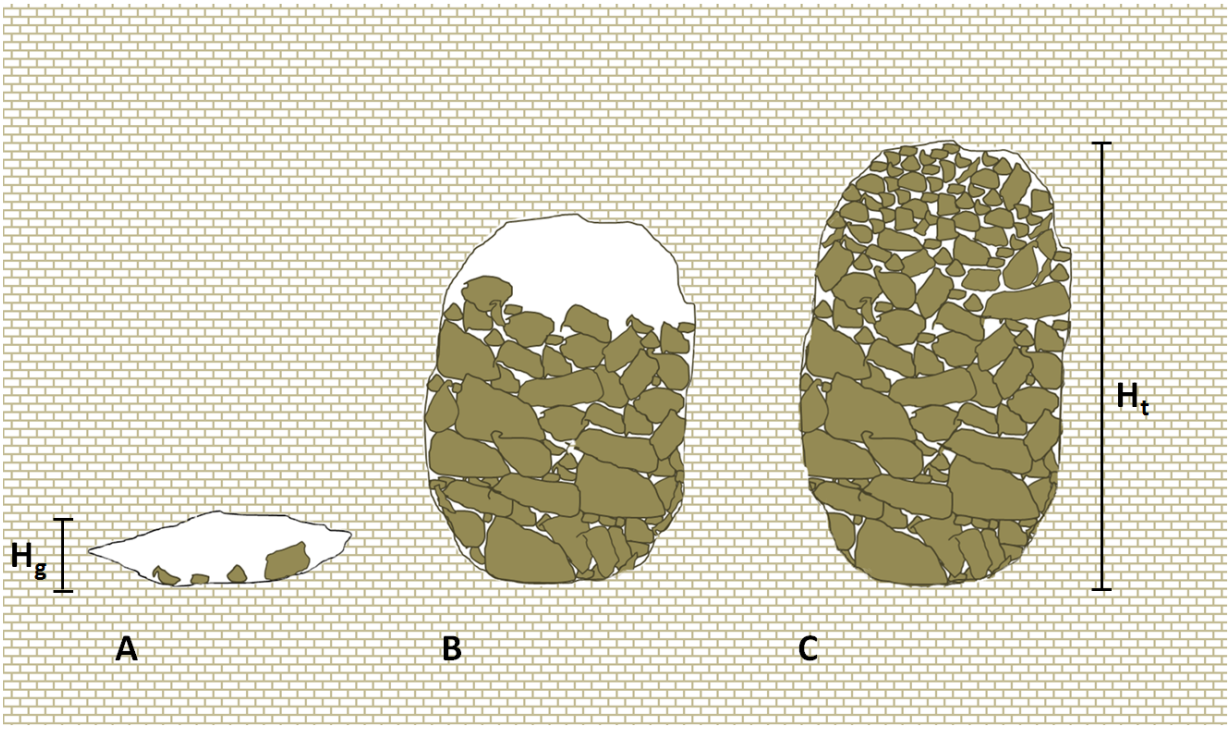

Figure 4.3.1-1: The collapse of caves. Cave A is the original cave, with height (H_g), Cave B is an actively collapsing cave, and Cave C is the fully collapsed cave, with height (H_t).

For the collapse-related lateral expansion of the cave, the mapped floor surfaces for the three different cave levels, cave 1 to 3, are copied and placed in the folder *FolderIsochores* on the clipboard. These surfaces will be used to create new lateral expanded surfaces for the modelling of the post-collapse cave. After discussions with SE Lauritzen (pers. Comm., august 2016) the lateral expansion of the collapsed cave was set to be 2 meters.

The operation "Interpolate" is used for defining the lateral expansion. This operation provides the possibility to expand surfaces for a specific distance. Within the "Interpolate" operation, the "Expand the area" is chosen and the floor surface is used as input. The surface is interpolated 2 nodes each, corresponding to 1 meter in each direction. One node represent one grid cell. This results in a total lateral post-collapse expansion of 2 meters. This is executed for all of three levels. When the procedure has been done for all levels, the operation Create new boundary is used to create a new polygon around the interpolated surface, representing the new lateral expansion of the collapse for all levels. The boundaries created can be found in the same folder on the clipboard, and will be used for the later mapping of the collapsed cave.

Isochores between the original roof and floor of the caves are generated with the use of isochore mapping under the structural models tab. The original roof and floor surfaces from the horizon modelling are used as input for the job, and the increment is set to 0.5*0.5 meters. The isochores represent the height of the original cave, and will be used to calculate the height of the cave post-collapse. A total of three isochores, corresponding to each of the three levels are created using this process.

The calculated isochores represent Hg (original cave height) and are used to calculate the total height of the collapsed cave, using Equation 1. The calculation is carried out using Excel. A direct import from RMS to Excel is not possible because the complete data set with XYZ coordinates is too big for Excel to handle. In order to decrease the number of data points, the isochores are copied into the folder *FolderIsochores* located on the clipboard, and cut by using the "Logical" operation "A or B" and the polygon created from the interpolated surfaces (corresponding to the post collapse positions of the cave walls).
When this process has been executed, the isochores can be exported from RMS as surfaces in the Gocad Tsurf test format, which exports the surface in an XYZ format. In Excel, Equation 1 is used to calculate the total height of the cave after collapse in every point along the passage.
The surface is then imported into RMS as points and put in the folder *FolderIsochores* with the interpolated surfaces and the polygons created from the interpolated surfaces.

In the horizon tab, new isochores are created between each level of the cave, making a total of three isochores, corresponding to isochores for zone 2, 4 and 6. Under data type, *DepthPoints* and *ThicknessSurface* are added for the isochores. The imported points from Excel (representing the post-collapse roof) are dropped into *DepthPoints*. Isochore mapping under the tab "Horizons" is used to map the *ThicknessSurfaces* using the *DepthPoints* as input. The isochore surface grid increment is set to 0.5*0.5, and the project boundary is used as boundary. This process is executed for all three levels.

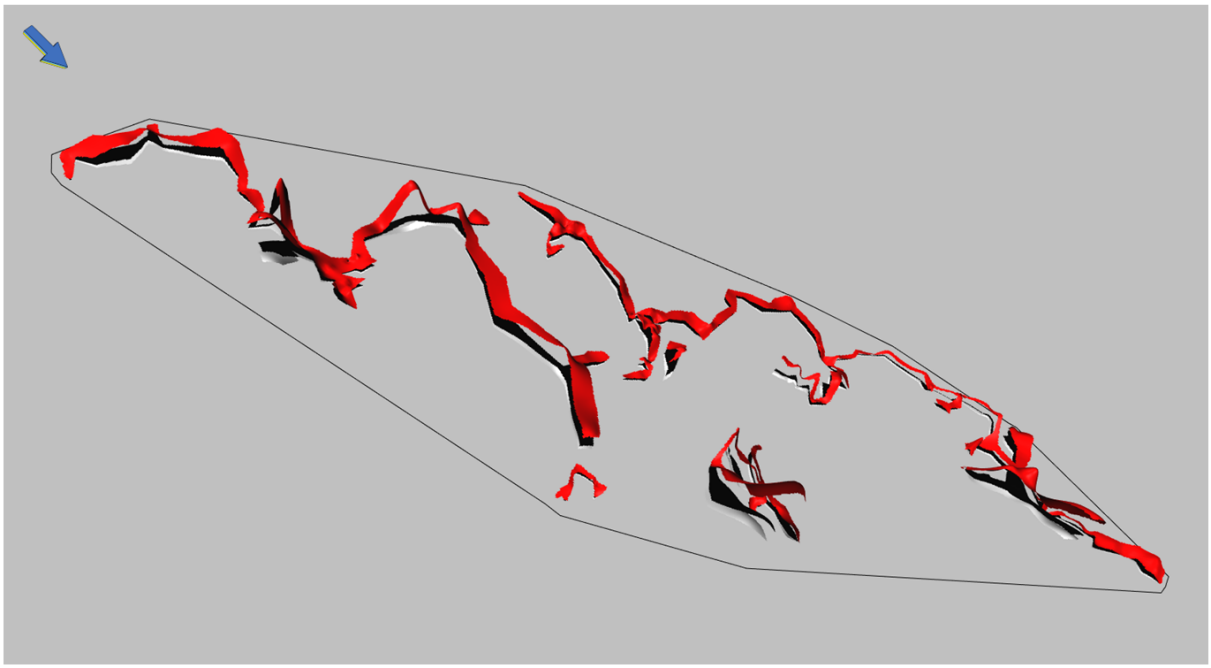

Figure 4.3.1-2: The difference between collapsed and original roof for the cave 1 level. The red surface is the collapsed roof, the black surface is the original roof and the white surface is the original floor. Notice the varying increased height of the roof in some areas.

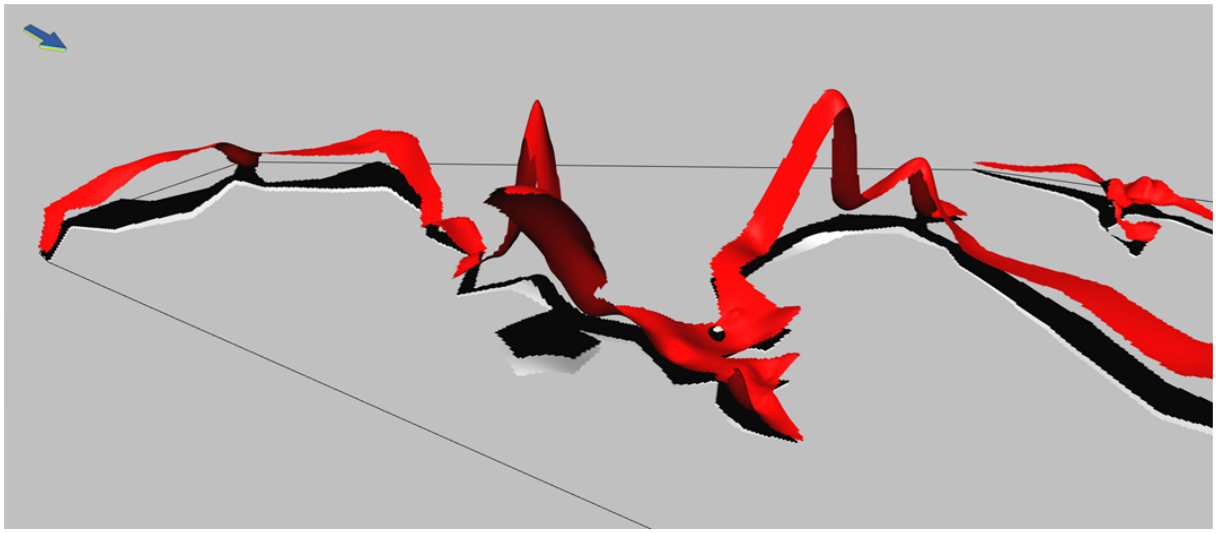

Figure 4.3.1-3: A zoomed in perspective on the difference between original cave roof (black) and floor (white), and the collapsed roof (red).

In order to generate a grid for the collapsed cave, new surfaces have to be used. Under "data type", the new surface *CollapsedSurface* is added. For the floor surfaces, the same points that were used to map the original cave are used, but the surfaces are now laterally constrained by the new interpolated polygons representing the post-collapse lateral expansion of the cave. For mapping the roof, the floor surface is dropped in the *CollapsedSurface*, and the operation "Surface-surface" is used to take the floor surface minus the isochore *ThicknessSurface*. Now two surfaces can be found under each

horizon, and the collapsed cave can be gridded. Under the horizons, both the horizons cut by the polygons and the uncut horizons can be found, but it is the *CollapsedSurface* that is used for the structural model and the subsequent gridding. Figure 4.3.1-2 and 4.3.1-3 illustrates the initial floor and roof of cave 1 as well as the calculated collapsed roof.

4.3.2 Creating a new structural model

The geometry of the collapsed cave passages differs from the initial cave configuration, which necessitates the definition of a new structural model. The model box is set to the same dimensions as the first (pre-collapse) structural model *CaveOriginal*, see chapter 4.2.3. For the new structural model, the *CollapsedSurface* is used as input for the surface and zone modelling. As the collapse expands above the top surface of the initial model, a new boundary, *boundary73up* is created and used as input for calculating a new *Cave_top* surface. All horizons are set as "hard" data except the *Cave_top* and the *Cave_bottom*. All stratigraphic boundaries are defined as "depositional" (conformable). The isochores from the collapsed levels are used as additional input, to minimize the zonation issues previously mentioned in chapter 4.2.3. The vertical resolution is set to 20. The new structural model is named *CaveCollapsed*. The output of the modelling job are the horizons and zones shown in figure 4.3.2-1.

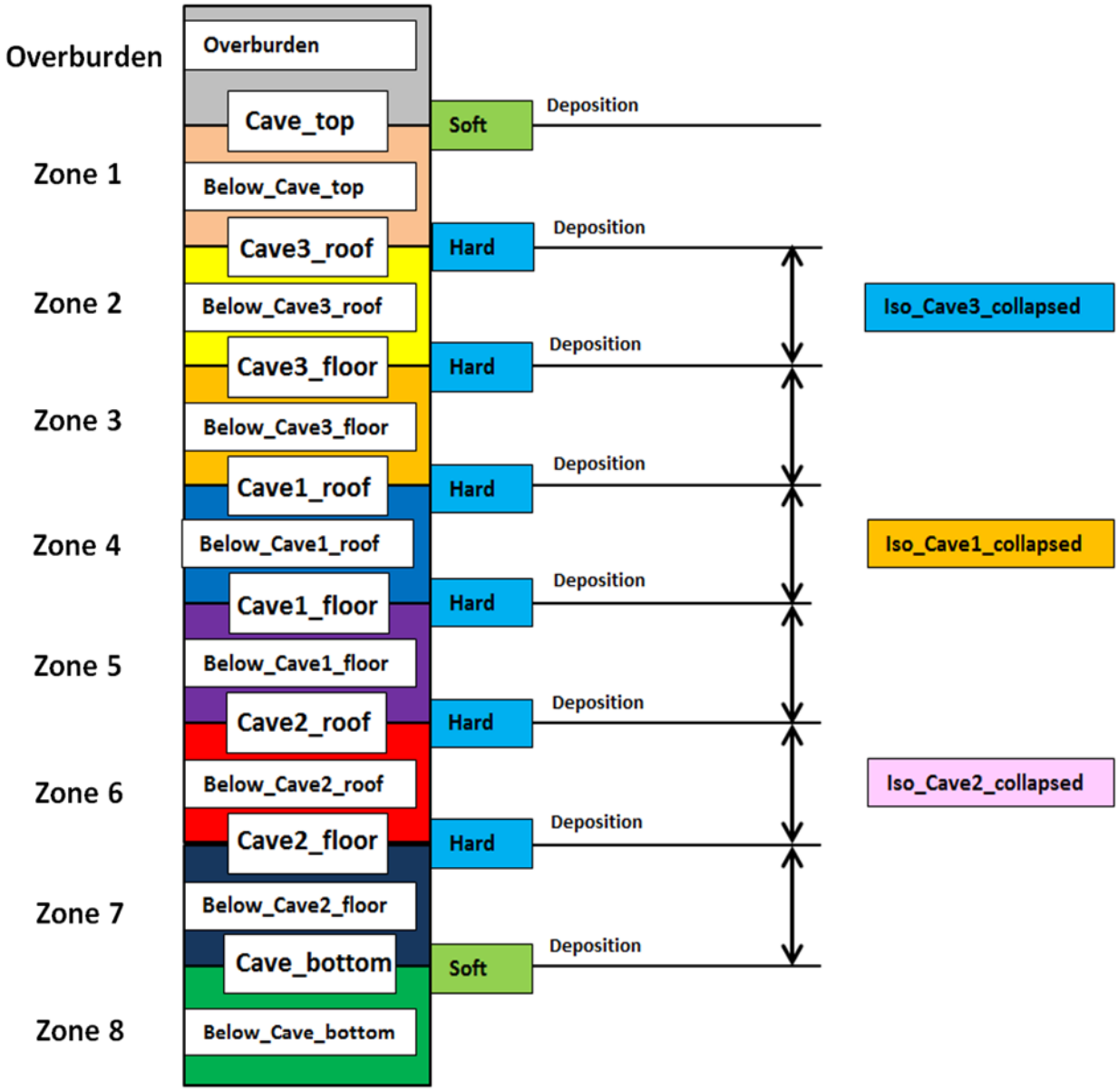

Figure 4.3.2-1: Structural model set-up for the collapsed cave.

Similar as with the zonation of the pre-collapse model, there are some technical issues concerning the zonation of the different levels of the cave in the grid, especially with respect to the interaction between cave 1 and cave 3. As can be seen in figure 4.3.2-2 and 4.3.2-3 there are spatial overlaps between the zones. Several workarounds were explored, but no good solution was found. A new subdivision cannot be done since cave 1 and cave 3 are overlapping, but a new definition of the polygons created in the beginning of the project, defining the walls of the cave, could improve the result. For the present case excluding the cave 3 level from the model might offer a solution, but the aim of the modelling exercise should also involve identifying and addressing

problematic features which may turn up during the modelling process. This problem will be discussed further in chapter 5.1. While this problem make the result a bit "messy" it does not create any significant problems for the further work on the model. The petrophysical modelling and streamline simulations run the model as one, and not divided into zones.

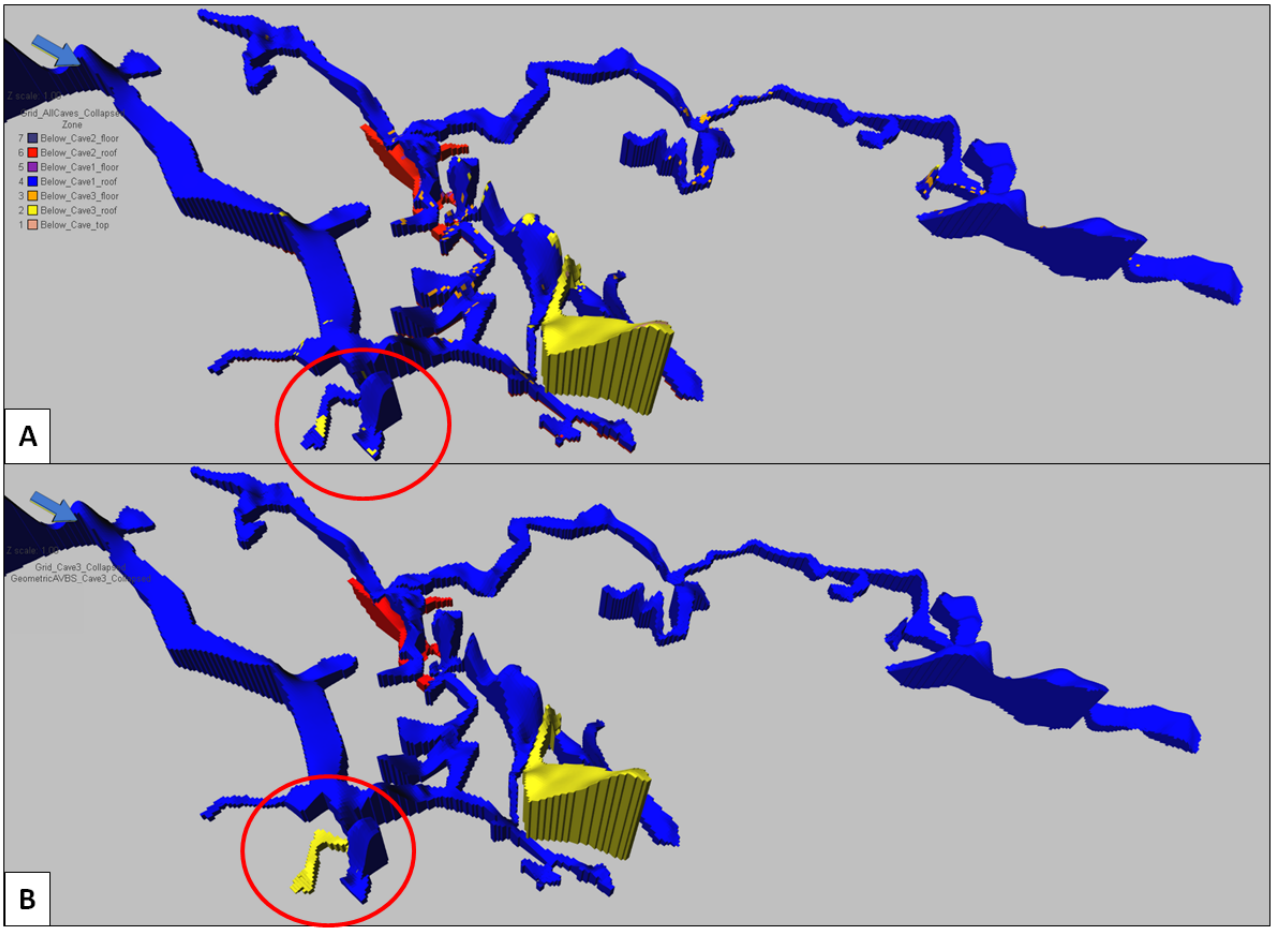

Figure 4.3.2-2: The issues regarding the zonation. Figure A is the whole merged cave filtered on the zones. It is clear to see that a part of cave 3 is located in the same zone as cave 1 (red circle). Figure B is illustrating how it should be. The blue part of the cave is cave 1, the red is cave 2, and the yellow is cave 3.

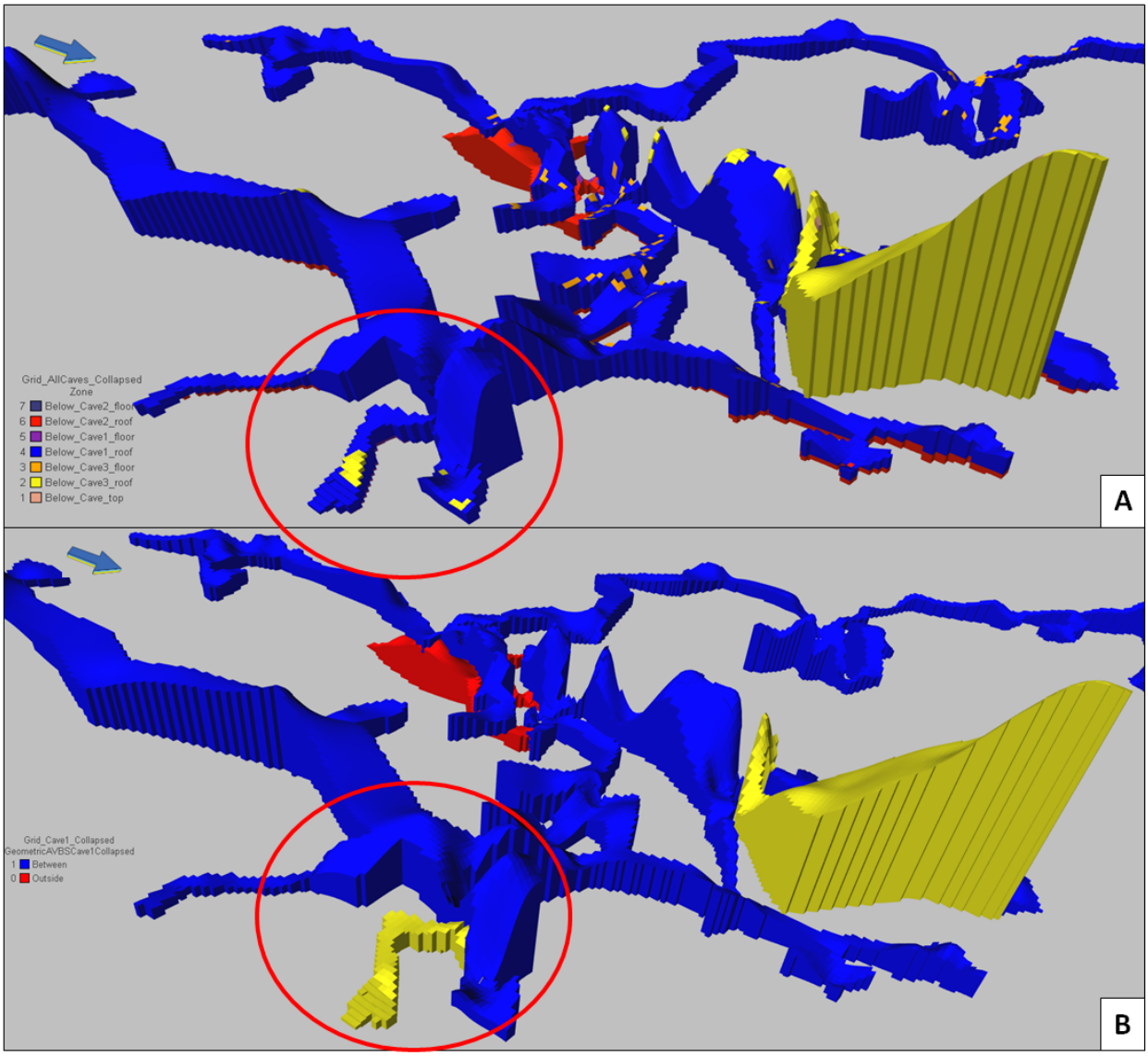

Figure 4.3.2-3: A more zoomed in perspective of the most problematic area. Once again Figure A illustrates how the zonation is, and figure B illustrates how the zonation should be.

4.3.3 Gridding of the collapsed cave passages

Gridding of the post-collapse cave model uses the new structural model *CaveCollapsed* as input, but is otherwise identical to the pre-collapse grid model set-up (see above). Four identical new grid models are created:

- *Grid_Cave1_Collapsed*
- *Grid_Cave2_Collapsed*
- *Grid_Cave3_Collapsed*
- *Grid_AllCaves_Collapsed*

The 2D layout is slightly adjusted compared to the original cave, and the vertical layout is the same as for the original cave (Table 4.3.3-2).

	CENTRE	LENGTH	GRID DIMENSIONS Increment
X	475	450	1
Y	390.87	584.01	1
Rotation, clockwise:		15	**degrees**

Table 4.3.3-1: 2D layout of the grids for the collapsed cave.

Zones	Type	Dimension
Below_Cave_top	No of cells	30
Below_Cave3_roof	No of cells	10
Below_Cave3_floor	No of cells	10
Below_Cave1_roof	No of cells	10
Below_Cave1_floor	No of cells	10
Below_Cave2_roof	No of cells	10
Below_Cave2_floor	No of cells	20

Table 4.3.3-2: Vertical layout for the grids containing the collapsed cave.

All three cave levels are gridded and the geometric modelling feature "Assign values between surfaces" is used to create a discreet parameter defining the position of the cave passages in the grid. The new polygons created from the interpolated surfaces, representing the XY positions of the post-collapse walls, are used as boundaries for this operation. The resulting discreet binary parameters (1 = cave, 0 = No cave) are resampled into the grid *Grid_AllCaves_Collapsed* and the parameters are subsequently merged into a single parameter, *MergedAllCollapsed,* see the result in figure 4.3.3-3. This

parameter is used for defining the position of the breccia-filled collapsed cave and is employed for subsequent trend modelling and for the petrophysical modelling.

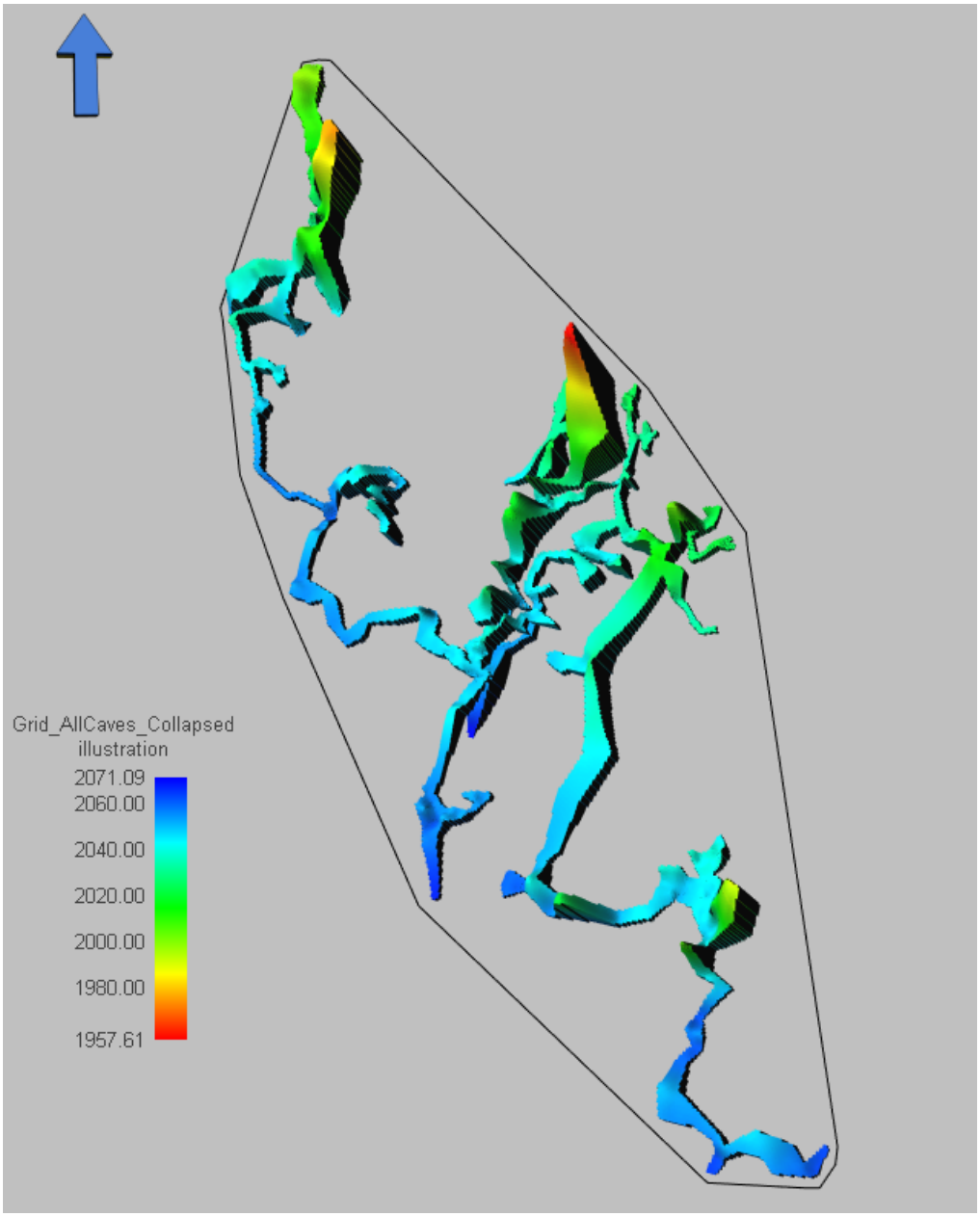

Figure 4.3.3-3: The collapsed cave, shown as the parameter MergedAllCollapsed, and filtered to remove the background facies. The colouring illustrates the depth of the cave, with the higher parts shown in red, and the lower parts shown in blue.

The *MergedAllCollapsed* parameter will serve as input for the rest of the modelling jobs, and for the later flow simulations. The difference between the original cave and the collapsed cave is quite significant, especially with respect to the height of the passages. See figures 4.3.3-4 and 4.3.3-5 for a comparison.

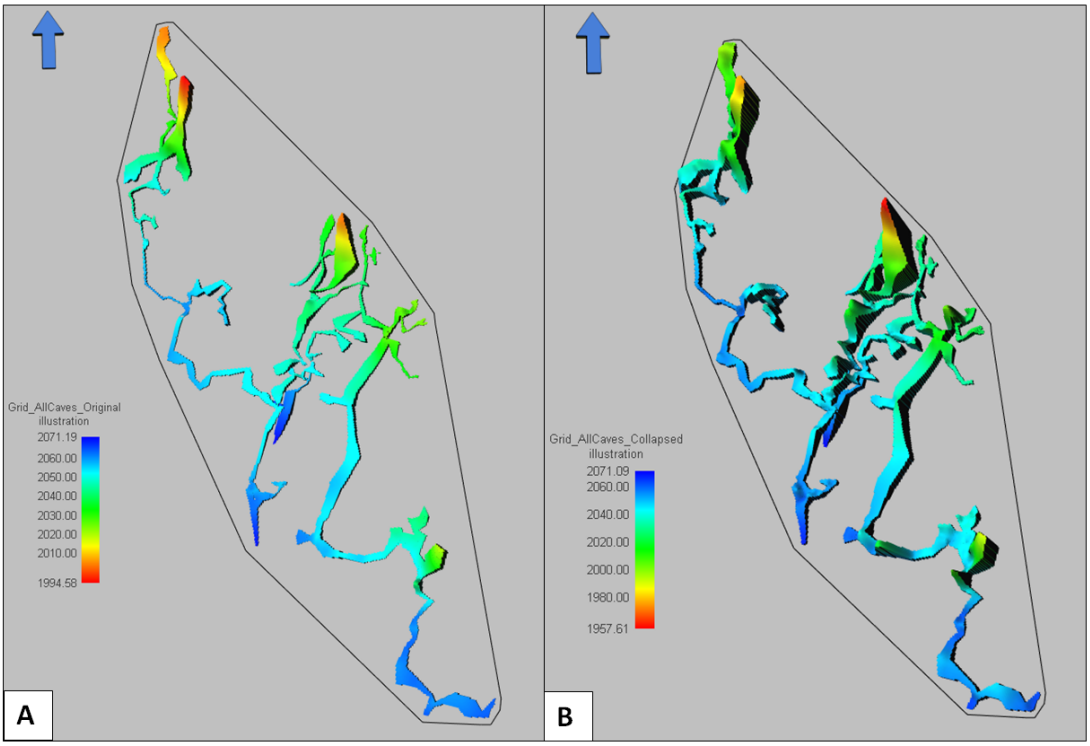

Figure 4.3.3-4: The two gridded caves. A is the original cave, and B is the collapsed cave. Notice the difference on the thickness of the passages.

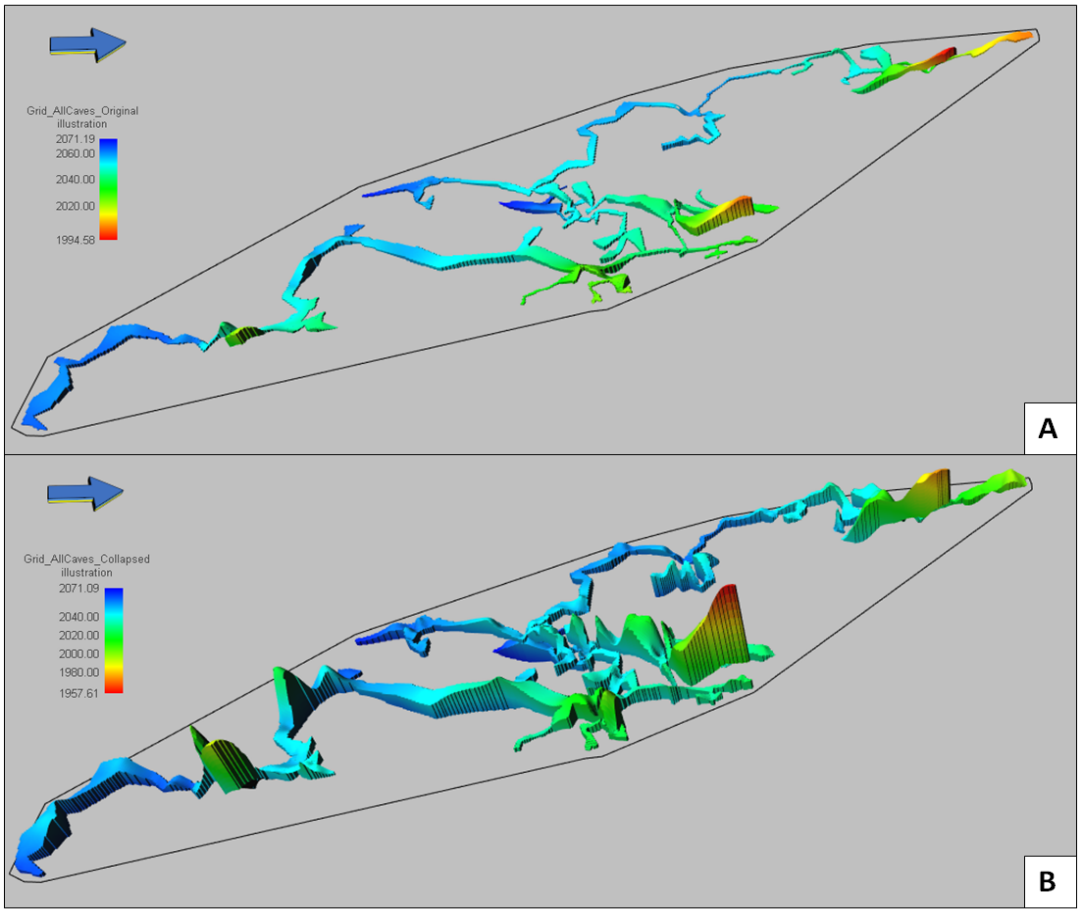

Figure 4.3.3-5: This figure illustrates the difference of the height of the passages. A is the original cave, and B is the collapsed cave. Notice the local collapse of the passages in the collapsed cave and the corresponding height of the ceiling in the original cave.

4.4 Trend modelling

For further work on the model, a trend parameter is needed. The trend parameter is used to create a trend for the petrophysical modelling within the cave, to avoid a completely random distribution of the petrophysical values. Within the cave the porosity and permeability will be at its highest near the floor of the cave, and gradually decrease upwards. The trend created in this chapter focus on this, and are used as input for the petrophysical modelling. By using the "Grid index parameter" tool, and filtering the cave on each zone, the trend parameters are created. This way a trend is created for each zone of the cave and can be used as input for the petrophysical modelling.

4.4.1 Creating a trend for the cave

For the trend modelling, it is important to note that the vertical structuring of the grid is proportional for each zone. This implies that each zone has a constant number of cell layers, which will vary in thickness as a proportion of the total thickness variation of the zone. The zonation created from the structural model is used to create a trend which is distributed evenly within the cave. In the reservoir model there are three main zones that contains cave geometries; Zone 4 mostly contains cave 1, Zone 2 contains cave 3 and Zone 6 contains cave 2. In each zone there are 10 layers, and these layers will be used to create the trend.

The trends were created like this:

- In the grid *Grid_AllCaves_Collapsed* a discrete parameter Zone is created with the use of the function "Grid Index Parameters" which creates a parameter where each zone is represented by a value.
- The filter function is used to filter out one of the zones containing cave geometries, i.e. zone 4 for cave 1. With the filter enabled, a new Grid Index Parameter is created, this time the Simbox Layer parameter.
- The Simbox Layer parameter is created and each layer within the chosen zone is given a value according to the number of layer it is, the parameter is called *SimboxLayer_Zone4* for zone 4 and so on.

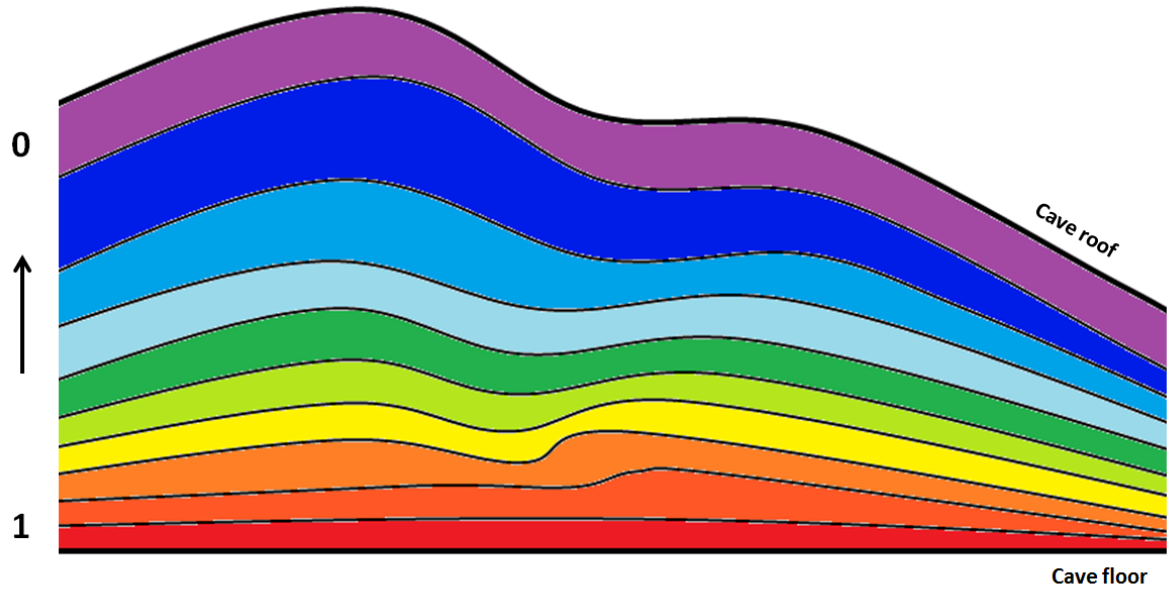

Figure 4.4.1-1: How the trend of the cave passages is distributed in the grid layers. Values are ranging from 1 on the cave floor to 0 on the cave roof.

The parameter has 10 layers with corresponding values reflecting the layer in the grid, i.e. for zone 4 the values are ranging from 60 to 51. For the trend parameter we want values ranging from 1 to 0. The process of fixing the values from 1 to 0 was done using the scalar operation:

- The scalar operation is used to get values ranging from 1 to 10 by subtracting the values with 50.
- A new continuous parameter is created and named *Cave1Trend* for the trend parameter for cave 1. The values from the corresponding Simbox Layer parameter for cave 1 are dropped in to the new trend parameter.
- To have values ranging from 1 to 0 the scalar operation is used again, the values are divided by 10. The result is a trend varying from 1 in the base, to 0 in the top for passages with all thicknesses.

Figure 4.4.1-1 illustrate how the trend values are distributed. A total of 3 trend parameters are created this way, *Cave1Trend*, *Cave2Trend* and *Cave3Trend*.

4.5 Petrophysical modelling

Forecasting petrophysical properties for paleokarst reservoirs is highly challenging due to their highly complex nature. Any chosen modelling solution will commonly be left open to criticism for either including too little or too much detail, or for omitting factors considered crucial to some workers. For the present thesis the accuracy and details of the petrophysical model are not a crucial factor as the aim of the thesis is to provide a workflow for modelling paleokarst reservoirs rather than conducting a study for a specific case. For the present purpose the standard stochastic tool for petrophysical modelling in RMS was used. Parameters were generated for porosity and permeability (X, Y and Z) for the cave fill and surrounding host rock.

4.5.1 Assigning petrophysical values

The setup for the petrophysical modelling in RMS, which can be found under the "Property modelling" tab in the grid, is summarized in Table 4.5.1-1 and 4.5.1-2.

In order to allow comparison with Furnée (2015) similar porosity and permeability values were utilized for constraining the petrophysical model set-up. It should, however be noted that Furnée (2015) employed a deterministic rather than stochastic approach for populating his model with petrophysical values.
The generated petrophysical parameters are subsequently combined with the fracture model (see chapter 4.5.2) to create the final petrophysical model.

In chapter 2.2.5 we assumed that for the fully collapsed cave, the passage will be completely filled with breccia and collapse material from the host rock. The cave infill commonly exhibit a fining upwards trend towards the top of the collapsed dome (e.g. Kerans (1988) and Nordeide (2008)) and a corresponding decrease in porosity and permeability can be expected. A trend function (see chapter 4.4) is used to capture this feature. If cements or other allochtonous sediments subsequently fill the cave, different petrophysical may be expected. This only illustrates the challenges of estimating petrophysical values.

Note that the petrophysical properties of the host rock are deliberately kept low in order to highlight flow through the cave passages during later simulation.

The petrophysical modelling tool (ROXAR, 2016d) performs a stochastic simulation which generates realizations based on a specified set of constraints. The "Advanced" set-up option is employed. In the "General" tab for the petrophysical modelling tool, the output parameters *PORO*, *PERMX* and *PERMZ* are defined. The facies parameter *MergedAllCollapsed* (showing the distribution of Cave and No-Cave facies) is used as input. Here all zones are modelled simultaneously. Model constraints for the frequency distribution of petrophysical values for each facies are specified in the "Distribution" tab (summarized in Table 4.5.1-1 and 4.5.1-2).

CAVE	Mean	Truncate Data
PORO	0,2	Keep data between 0-0,45
PERMX	200	Keep data between 0-350
PERMZ	200	Keep data between 0-350

Table 4.5.1-1: Petrophysical values chosen for the Cave facies

NO CAVE	Mean	Truncate Data
PORO	0,08	Keep data between 0-0,2
PERMX	0	Keep data between 0-0
PERMZ	8	Keep data between 0-20

Table 4.5.1-2: Petrophysical values chosen for the No Cave facies

A general 3D trend (see chapter 4.4.1) is employed to capture the gradual decrease of porosity and permeability values upwards inside the filled cave. The trend parameter is only used in zones where caves are present.

For the Cave facies, the mean and truncate values are set according to Table 4.5.1-1. In addition to these transformations, two more transformations are utilized to obtain the wanted effect of the trend within the cave and distribution of petrophysical values:

- A general 3D trend is added for each zone containing the cave facies (i.e. for zone 4 the trend *Cave1Trend* for cave 1 is used as input).
- In order to obtain the desired effect from the trend parameter, the scaling coefficient is set to 1. This produces porosity values starting at 1, but values can be re-scaled afterwards. The scaling coefficient controls the degree of influence the trend parameter will have on the distribution of porosity and permeability values.
- A general non-linear scale transformation of 1 is also added to disperse the values modelled in the whole range specified by the previous input for the porosity. For the permeability values the scale of this transformation is set to 50 within the cave.

The No cave facies only requires specification of mean, maximum and minimum values (distribution truncation) as well as the General non-linear scaling factor.

- The values for mean and truncations are listed in Table 4.5.1-2.
- The general non-linear scale is set to 5 for *PERMX*, and to 0,1 for the porosity to get the desired dispersion of the values. The desired values are the ones defined by the truncations.

For streamline simulation purposes, *PERMX* (and with this also *PERMY*) for the No Cave facies are set to 0. Higher petrophysical values for the background, No Cave facies, were tested, but this resulted in a high degree of disrespect of the Cave facies during fluid flow simulations. The permeability of the No Cave facies is populated using the fracture modelling tool (see chapter 4.5.2), however the fracture modelling tool in RMS does not generate fracture-related permeability in the Z direction. Consequently values for *PERMZ* are assigned using the petrophysical modelling tool. The values chosen for *PERMZ* corresponds with the values chosen by Furnée (2015) for the low cases he ran on his model and the resulting fracture-related permeability for *PERMX* and *PERMY*.

In the “Variograms” tab, the range is set to 10 in all directions for all zones, facies and properties. The variogram is set to 10 to be sure that it covers the whole cave system.

The resulting continuous parameters *PORO*, *PERMX* and *PERMZ* are all given the prefix “Job1”. Values for *PERMY* are duplicated from *PERMX*.

A realization from the petrophysical modelling is shown in figure 4.5.1-3. The porosity values have been post-processed by re-scaling as described above. In the cave a clear trend of increasing porosity and permeability values downward can be observed, and for the rest of the model, the properties are distributed randomly within the limits set during the petrophysical modelling job.

Screenshots from the set-up in the “Distribution” tab for the zone containing cave 1 can be found in appendix 8.3.

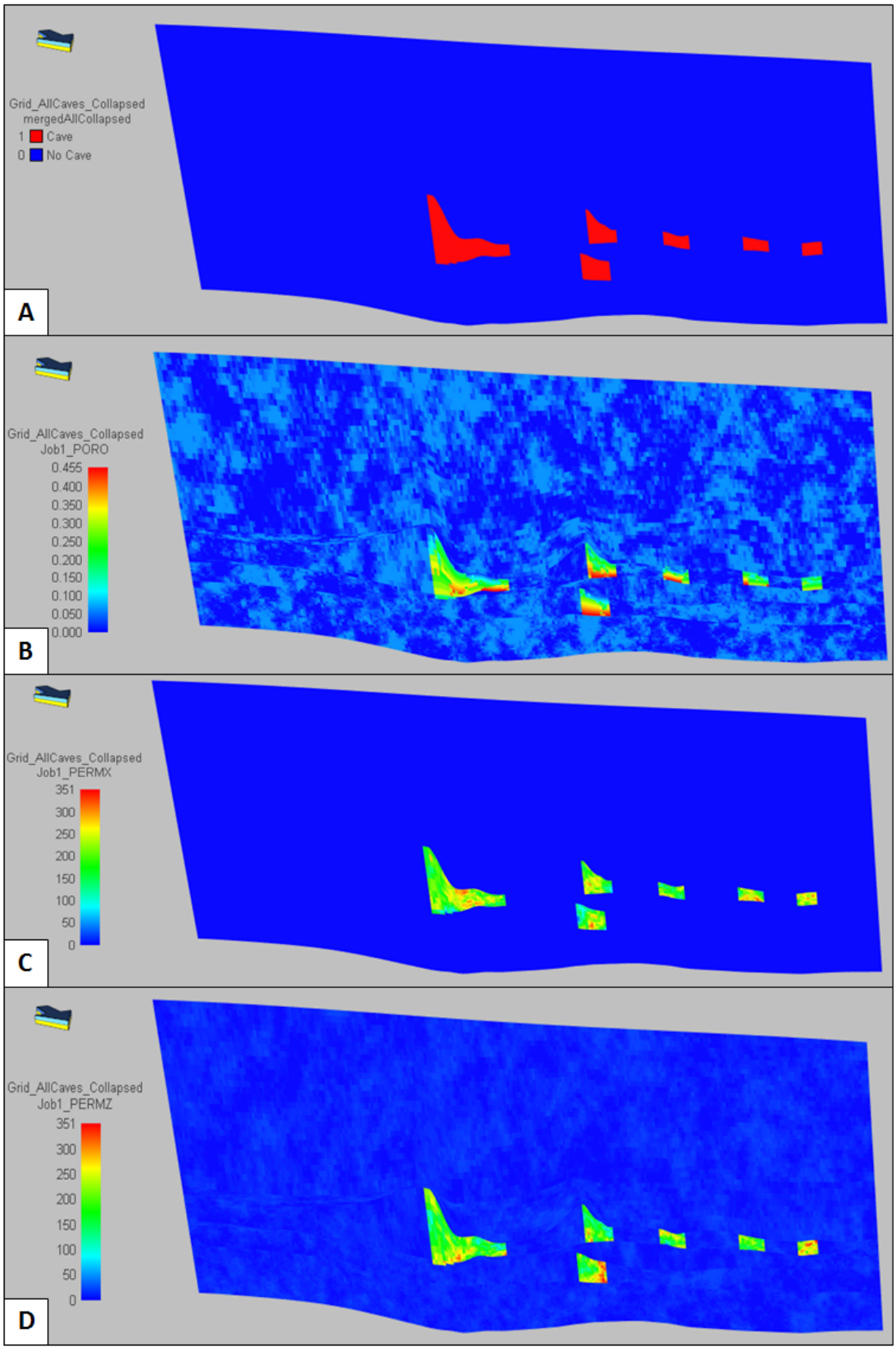

Figure 4.5.1-3: Result of the petrophysical modelling. A is before any modelling has been done, B is the PORO parameter, C is the PERMX and D is PERMZ.

4.5.2 Fracture model

Karst commonly develops in fractured rocks, and fractures are likely to form a key element of host rock permeability in paleokarst reservoirs. The main cave passages tend to develop and expand along pre-existing fractures (Shen et al., 2007).

The present model employs the RMS Fracture modelling tool to handle fracture-related permeability and porosity (ROXAR, 2016c). No dataset for fracture measurements was available for the Setergrotta site, but Furnée (2015) estimated the main fracture sets by plotting the orientations of cave passages in a rose diagram (figure 4.5.2-1). Three main azimuths were identified: 15, 90 and 170 degrees.

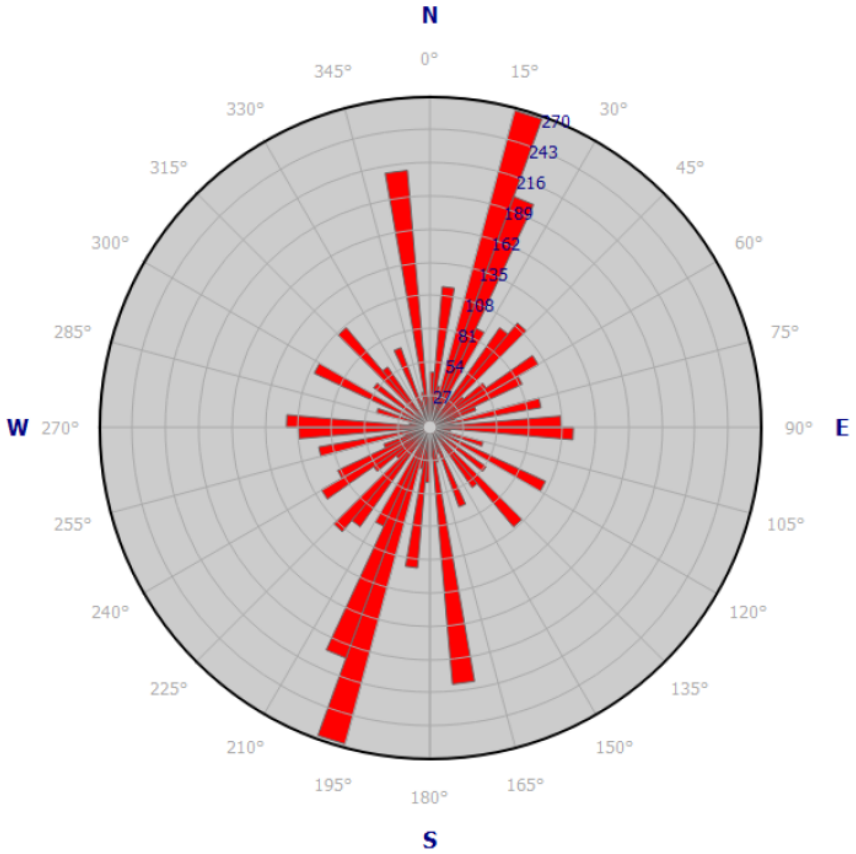

Figure 4.5.2-1: Rose diagram illustrating the main fracture orientations of the cave passages, 15,90 and 170 degrees. Figure from Furnée (2015).

Four new continuous parameters are created, *Density_1*, *FRAC_15*, *FRAC_90*, *FRAC_170*. Using the calculator *Density_1* is assigned a value of 1, *FRAC_15* a value of 15, *FRAC_90* a

value of 90 and *FRAC_170* a value of 170. The parameters are in this way assigned values and used as input for the "Create fracture model" set-up.

In the "Fracture modelling" tool, the following input is used:

Fracture name	Frac15	Frac90	Frac170
Density (Fracture/m)	1	1	1
Orientation	15	90	170
Orientation variability	5	5	5
Length (m)	50	50	10
Length Variability	5	5	1
Fracture Thickness (m)	1	1	1

Table 4.5.2-2: Input for the fracture modelling.

The rest of the settings are set to RMS default values. The default values are kept to be able to compare the results with Furnée (2015). This creates the parameter "Fracture model" which is used for the further Dual- and single-porosity modelling.

The "Dual-porosity modelling" tool is used to create the fracture-related porosity for the model, and can be found under the "Fracture modelling" tab. The fracture model created is used as input, and the parameter *FracturePorosity* is chosen as output for the job. This parameter is combined with the porosity parameter *PORO* created from the petrophysical modelling job with the use of the calculator. This is easily done by creating a new parameter, and take the *FracturePorosity* parameter plus the *PORO* parameter. The final parameter is named *PORO_FRAC*, and will be used for streamline simulations.

The “Single-porosity modelling” tool is used to create permeability parameters with the effect of fractures accounted for in the X and Y direction. The tool cannot generate fracture-related permeability in the Z direction, which is a severe shortcoming in the software. The permeability parameter *PERMX* created from the petrophysical modelling is used as input for both Perm I and Perm J, and the fracture model is used as input. The output is the parameters *PermI* and *PermJ*. These parameters will be used for the streamline simulations. *PermI* and *PermJ* now have a mean permeability of about 8 mD created by the fracture permeability.

4.6 Streamline simulation in RMS

Streamline simulations can be used to screen fluid flow through the reservoir in the form of streamlines between wells. Some basic reservoir properties are defined and the result provide a preliminary illustration of the fluid flow in the model. The model grid has a resolution of 1*1 meters yielding 26 280 000 grid cells. Attempts to run the Streamline simulations at this resolution failed, as pressure solutions failed to converge. In order to allow streamline simulations to be run, the model was upscaled.

4.6.1 Model upscaling

Upscaling involves minimizing the number of grid cells by merging them - preferably without the loss of critical details that may have an impact on the behaviour of the fluid flow. The process assigns effective properties to the new, coarser cells without the loss of important information (ROXAR, 2016a). Upscaling can cut CPU cost of flow simulation significantly.

For the streamline simulations that will be executed on this model, the grid is upscaled to a grid with a 2*2 meter X-Y resolution. The new grid is called *Grid_Upscaled2*. Apart from the resolution it is identical to the initial grid in XY direction.

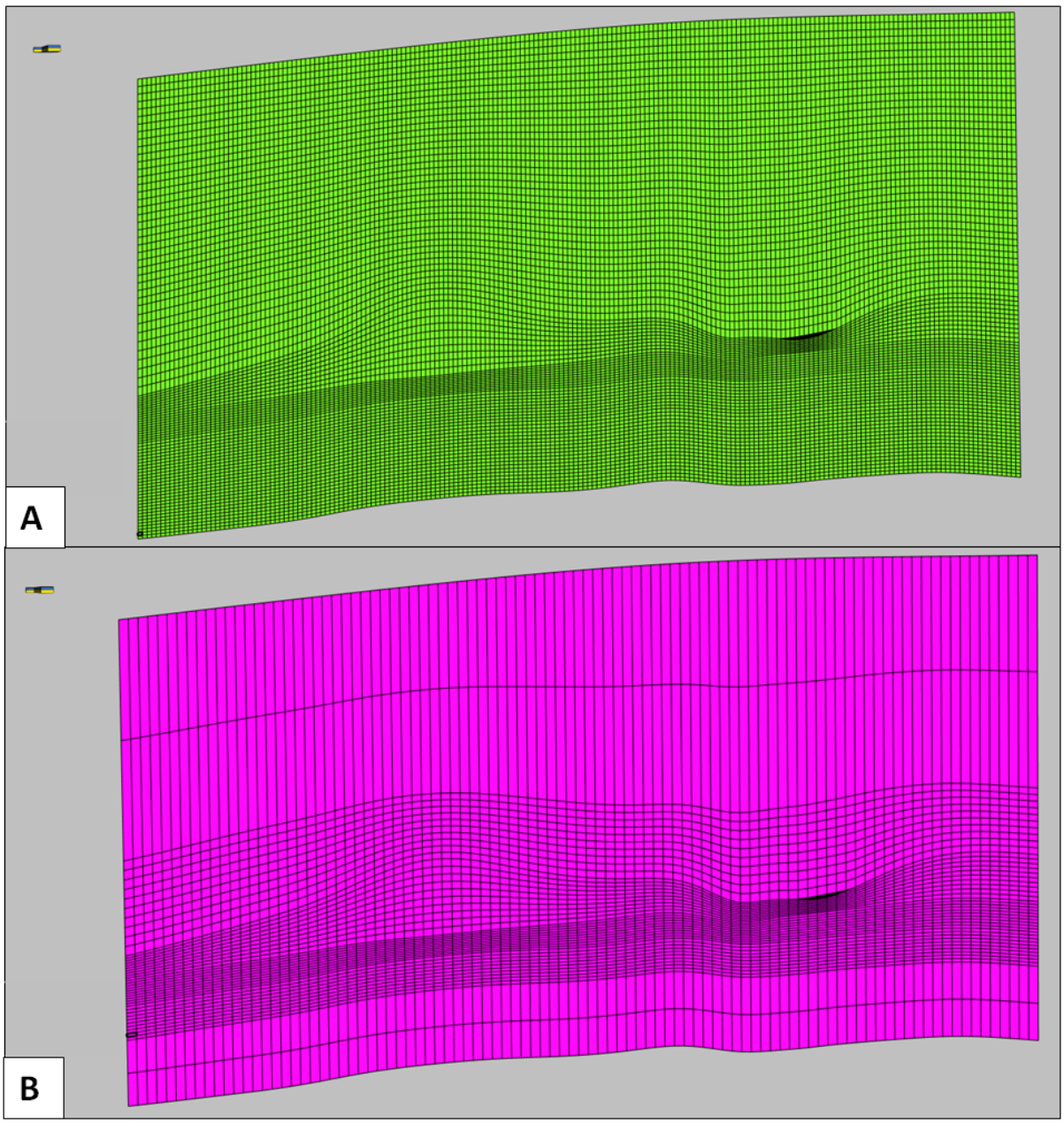

Figure 4.6.1-1: The difference in vertical upscaling between the initial Grid_AllCaves_Collapsed grid (A) and the upscaled Grid_Upscaled2 grid (B).

The vertical resolution is set to 2 for the upper and lower zones of the grid, as these zones do not contain the cave, and 10 for the rest (Fig. 4.6.1-1). The upscaled model contains 3 061 800 grid cells, which is small enough to allow streamline simulation. Figure 4.6.1-2 illustrates the difference between the initial *Grid_AllCaves_Collapsed* grid and the upscaled *Grid_Upscaled2* grid shown with petrophysical values that was used for the streamline simulation.

Grids with XY resolutions of 4*4 and 6*6 were also created, for the sake of investigating the effect upscaling has on the streamline simulations. These will be more closely studied in chapter 5.3.1.

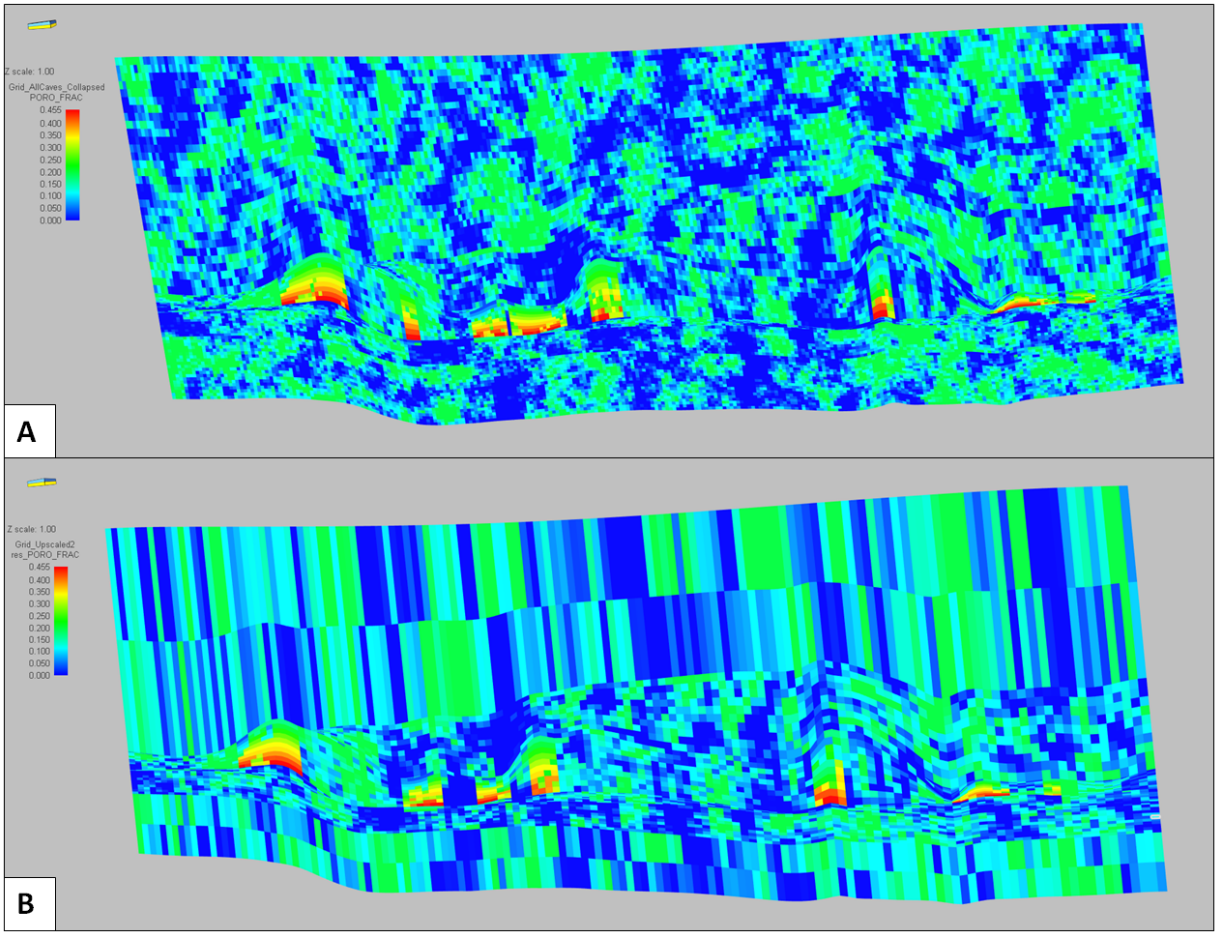

Figure 4.6.1-2: The difference between the original grid (A) and the upscaled grid (B).

4.6.2 Streamline simulation

The streamline simulation tool can be found under the tab “Flow modelling” in the grid. It is used as a visualization tool to create an image of the fluid flow through the reservoir. It produces a series of streamlines through the reservoir representing the fluid flow during production and injection.

Here, two vertical wells, one producer and one injector, are created and placed at opposing ends of the cave system. Position and depth intervals for the wells are listed in Table 4.6.2-1.

WELL	X (m)	Y (m)	Z (m)
Producer	344	674	1800-2100
Injector	605	111	1800-2100

Table 4.6.2-1: Well coordinates for the two wells in the system.

In order to carry out the simulation in the grid *Grid_Upscaled2*, the two wells must be blocked. Blocking of wells up-scales the well data to the same resolution as the 3D grid (ROXAR, 2016e). The parameters needed to execute the streamline simulations are *PermI*, *PermJ*, *PORO_FRAC* and *PERMZ*, and which are rescaled from the initial grid, *Grid_AllCaves_Collapsed* into the upscaled grid, *Grid_Upscaled2*.
In order to reduce the number of cells even further, the upper and lower parts of the grid, zone 1 and 7, which only include host rock are filtered out prior to running the streamline simulations. The aim is to focus on the fluid flow through the part of the reservoir containing cave facies. Some information, particularly relating to fluid movement out of the paleokarst system and into the overburden may be lost here, but this does not affect the overall aim of the present thesis.

In the tab "Grid data" under "Streamline simulation", the different resampled petrophysical parameters are used as input. Everything else in this tab is set as default. In the "Properties" tab, initial reference depth and pressure are set to 2000 meters and 200 bar respectively, as most of the reservoir is located at approximately 2000 m depth. The simulation is run as an oil-water scenario. Since the simulations are for test and internal comparison purposes only, RMS default settings are kept for all parameters. In the "Wells" tab, the blocked wells are used as input and the wells *Producer* and *Injector* are chosen. Production and injection rates are kept identical at 1000 m^3/d. The bottom-hole pressure (bhp) is set to 160 bar for the producer, and 260 bar for the injector.

The generated streamline realizations may look chaotic at first but with the use of the visual settings, the streamlines can be filtered for the total travel time, and patterns highlighting the fluid flow pathways through the reservoir emerge. Figure 4.6.2-2 shows an example.

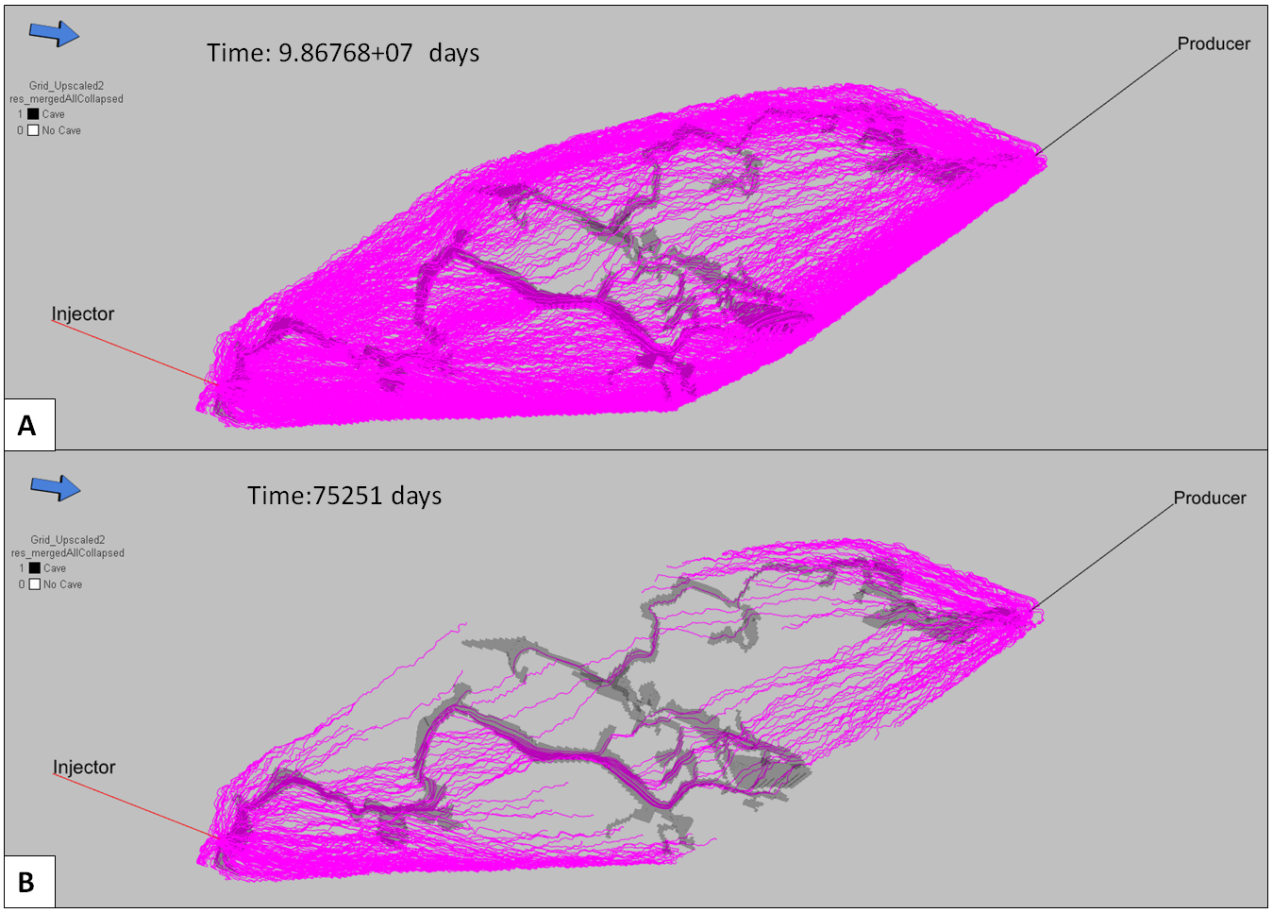

Figure 4.6.2-2: Streamline simulations executed on the grid Grid_Upscaled2. Figure A is unfiltered, and figure B is filtered on time, the fluid flow after 75251 days is shown. The cave can be seen in darker grey.

Report files from the simulations can be found in Appendix 8.4. The outputs from streamline simulations are not only streamlines; several other parameters describing the behaviour of the reservoir during production are generated and can be analysed. The outputs are:

- TFI (Time From Injector)
- TTP (Time From Producer)
- INJREG (Injection Regions)
- PRDREG (Production Regions)
- PRESSURE
- INITPR (Initial Pressure)
- PORVOL (Pore Volume)

The detailed results from the streamline simulation are presented and discussed in chapter 5.3 below.

4.6.3 Drainage functions

In order to gain a qualitative understanding of reservoir behaviour during production, drainage functions for the different upscaled grids are created. This facilitates a quantitative analysis of the results from the streamline simulations, for each well in terms of time and volume. Drainage functions were generated for all grids where streamline simulations were performed. The input parameters (listed in Table 4.6.3-1) are derived from the streamline simulation job.

Producer volume	PORVOL
Producer time	TTP
Producer region	PRDREG
Injector volume	PORVOL
Injector time	TFI
Injector region	INJREG

Table 4.6.3-1: Input for drainage functions

The drainage functions produced can be plotted as a graph showing injection and production volume over time as shown in figure 4.6.3-2.

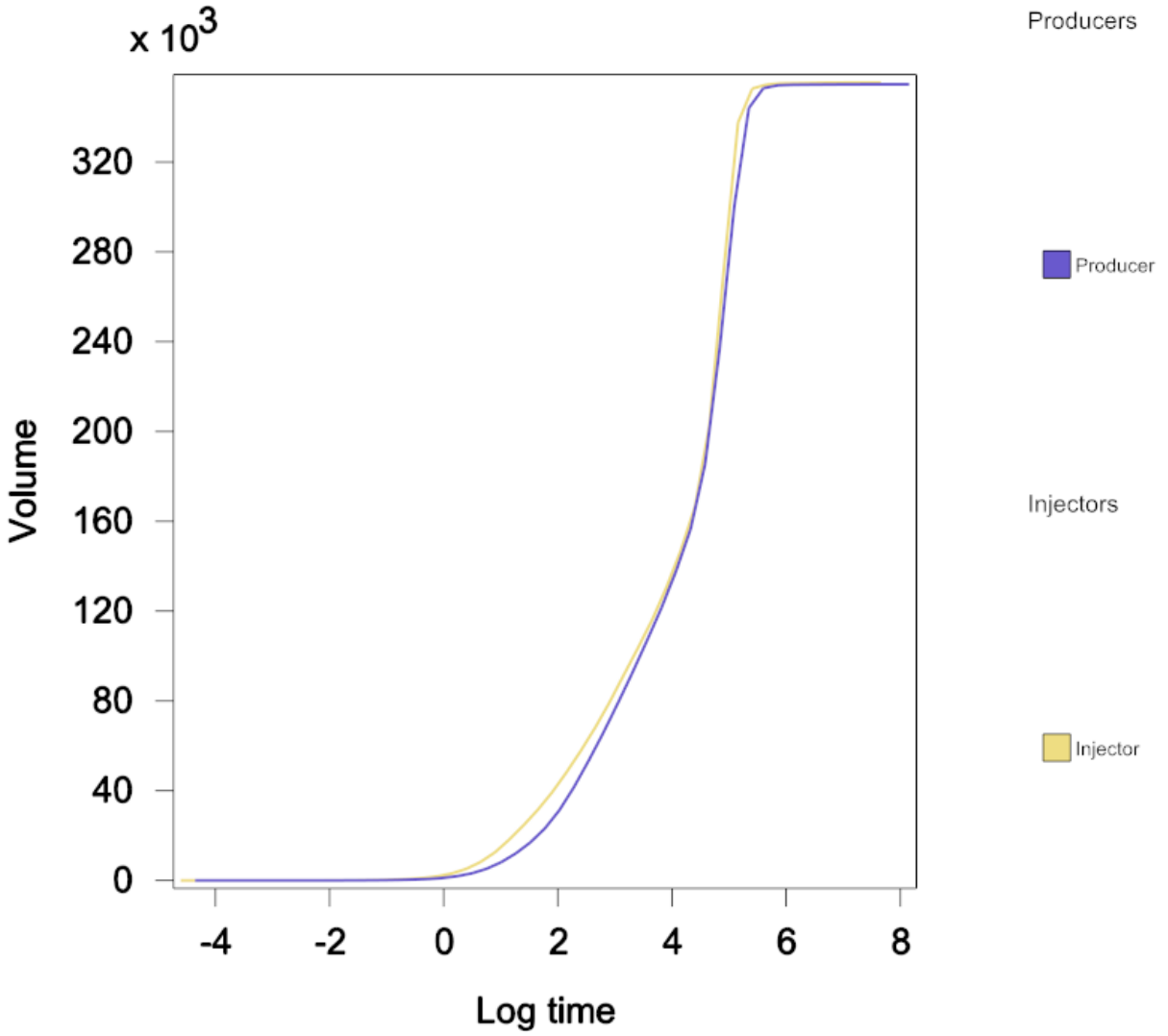

Figure 4.6.3-2: Drainage function from Grid_Upscaled2. The purple line is the producer, and the yellow is the injector. Time scale is in days (logarithmic) and volume in m³.

4.6.4 Volume calculations

Volumetric calculations were performed in RMS both to obtain in-place volumes, but also to check the impact of upscaling on the volumetric estimates. The volume calculation tool can be found under the grid in the "Volumetrics" tab.

Volume calculations were only executed for the zones containing the cave system. This can be chosen in the "General" tab. In the "Calculations" tab the "Main types" is set to Oil/condensate and the parameters "Bulk", "Net", "Pore", "HCPV" and "STOIIP" are selected as output. Negative cell volumes are set to zero.

OIL VARIABLES	
Oil/water contact	2100
Water saturation	0.1
Bo factor	1
FORMATION VARIABLES	
Net/Gross	1
Porosity	PORO_FRAC

Table 4.6.4-1: Input for the volumetrics job.

The volumetric calculation generates the parameters:

- Oil bulk, commonly seen as the structural volume
- Net bulk
- Oil pore, pore volume in the reservoir
- HCPV, Hydro Carbon Pore Volume
- STOIIP, Stock Tank Oil In Place

Table 4.6.4-2 shows the results of the volumetric calculations for *Grid_Upscaled2*.

GRID	BULK	NET	PORE	HCPV	STOIIP
UPSCALED2	3928309	3928309	362861	326575	326575

Table 4.6.4-2: Results of volumetric calculations for Grid_Upscaled2.

The results will be further discussed in chapter 5.4.

5 DISCUSSION

The workflow procedure outlined in the preceding chapter provides a robust approach for capturing some of the main characteristics of collapsed cave systems by using standard industrial reservoir modelling tools. The method is largely a product of a systematic "trial-and-error" approach, where different ways of employing a given dataset and process understanding (i.e. cave survey data plus collapse processes and products) were explored in order to produce features known and expected in paleokarst reservoirs. Although likely to represent an improvement compared to previous efforts at modelling paleokarst, it is by no means a "perfect" or "final" solution. Work has been constrained by time as well as technical challenges and shortcomings posed by the software. Furthermore, the present modelling effort is focused on meter-scale rendering of paleokarst, which underplays and simplifies known petrophysical heterogeneities and flow effects at finer scales.

Chapter 5.1 will discuss the method developed in RMS, the challenges encountered while creating the model and the shortcomings of the current software. Chapter 5.2 will compare the model to the one by Furnée (2015) who used the same dataset, but employed a different modelling method. In Chapter 5.3 the streamline simulation results from RMS and the features affecting the simulations will be discussed. Finally the results from the Volumetric calculations are discussed in Chapter 5.4.

Standard reservoir modelling suites lack specific functionalities and workflows that facilitate implementation of caves and collapsed, breccia-filled paleocaves. For this reason quite a lot of creativity and work-arounds has to be employed for creating "realistic" geo-models for this type of reservoir. Some steps in the workflow presented in this thesis are however, quite time-consuming. If this cannot be improved on, the question presenting itself is if the amount of time used to create the model is justified by the quality of the new simulation results or any improvement of our understanding of the fluid dynamics of these reservoirs.

Most of the previous work done on modelling of paleokarst reservoirs has been stochastic modelling of caves. As far as is known to the author deterministic modelling of cave passages and "forward modelling" of paleokarst architectures using reservoir modelling tools has only been attempted by Furnée (2015).

5.1 Modelling in RMS

The modelling method presented in this thesis provides complete control on cave passage geometry, and renders expected paleokarst geometries on meter scale. A schematic summary of the modelling concept employed here is shown in Figure 5.1-1.

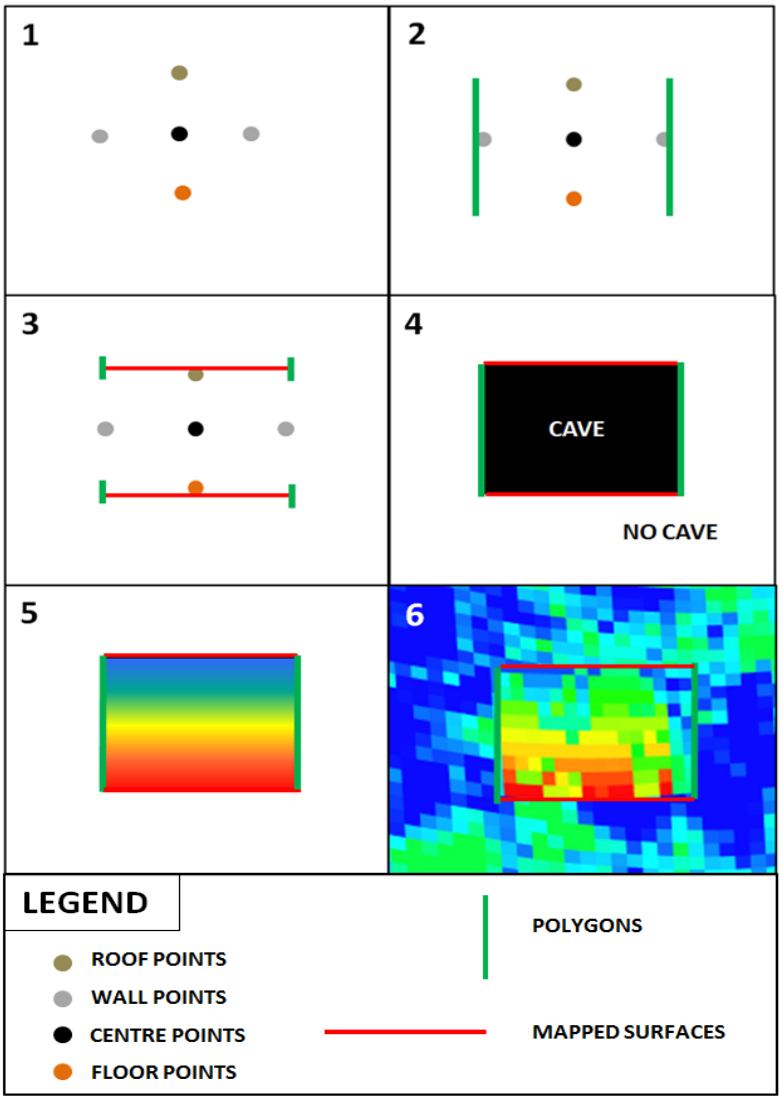

Figure 5.1-1: Summary of the modelling concept employed for this thesis. Step 1 is the import of the cave survey, step 2 is the creation of polygons representing the cave walls and step 3 is the mapping of surfaces. Step 4 is the geometric modelling, defining the cave, step 5 is the trend modelling for the cave interior and step 6 is the petrophysical modelling. Note that Steps 1 to 4 are employed to model the initial cave passages. Post collapse geometry of the cave follow the same steps, but with adjusted wall polygons in step 2 and adjusted roof polygons in step 3 before proceeding to steps 4 to 6 (see chapter 4.3).

The challenges encountered while working on the model will be examined more closely below. The detailed workflow as employed in RMS can be found in Appendix 8.2.

The most prominent issue when trying to model caves using reservoir modelling software is that they lack tools for defining cave-systems like objects. Several time-consuming methods had to be applied to create a work-around for this issue. Also the fact that surfaces cannot be traced over several superimposed cave-levels proved to be a major issue. This caused difficulties related to the definition of different zones in the grid.

5.1.1 Modelling of paleokarst

For a reservoir with suspected paleokarst features it is important to be able to identify these in seismic and well data. The different methods of identifying the features are presented in chapter 2.2.3. Paleokarst reservoirs are extremely complex, and are known for their high degree of spatial lithological heterogeneity. In practice this implies that well data such as cores and logs is not likely to provide representative statistical data for spatial mapping of reservoir properties.

Open cavities and structures associated with collapse and infill are typical features of paleokarst reservoirs, but their spatial distribution is commonly difficult to predict as individual features often are below seismic resolution and may be impossible to identify. The vertical resolution of seismic data will play a big role for the identification of paleocaves. For a reservoir at 1500-2000 m depth, vertical resolution will typically be on the order of 10-25 m depending on the depth of the reservoir and the equipment used. This implies that important features in the reservoir, such as paleokarst, might go undetected. If the cave system has a limited height, it may be below the vertical resolution of the seismic, and potentially go entirely unnoticed. Figure 5.1.1-1 illustrates what could be the result of limited vertical seismic resolution. The black surface illustrates what can be identified from the seismic. All features located on top of the surface (fig. 5.1.1-1 A) can be identified, but everything underneath the surface (fig. 5.1.1-1 B) will go unnoticed.

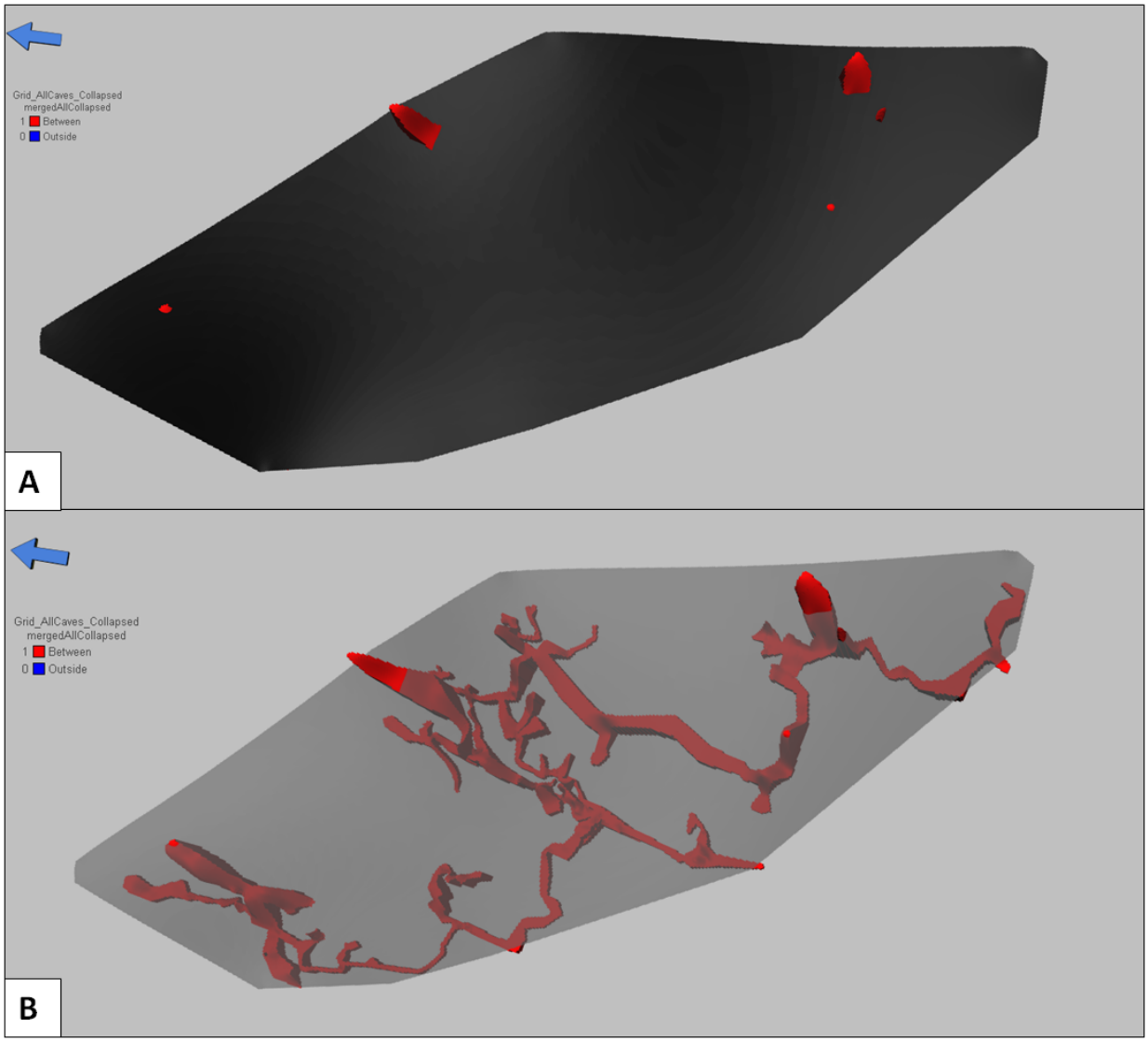

Figure 5.1.1-1: The effect of limited seismic resolution. Figure A illustrates what could be noticed on the seismic, and figure B shows what could be missed underneath due to the seismic resolution.

In a natural environment there would be found sags above the highest collapsed zones (Loucks, 1999), and cylindrical faults associated with the collapse (Lucia, 1995). The sags and cylindrical faults located above paleokarst systems are important characteristics for these types of reservoirs that can be observed on seismic data. Features like this may be interesting to take into account for further work on the modelling of these reservoirs.

To be able to map and grid the cave geometries in the reservoir using existing tools, several time-consuming methods are required. The definition of the cave passages with the use of polygons provides an accurate and realistic representation of the passage

thickness and geometry, but the process is very time-consuming. Ideally the software should be supplemented by tools allowing the user to map complex objects such as cave systems in a less complicated manner and facilitate the use of stochastic methods to accommodate uncertainties related to spatial positioning.

For a deterministic approach of modelling these features, a need to map and grid coherent features in different levels presents itself.

5.1.2 Mapping in different levels

In RMS, points and polygons can be located in different levels of the system, but surfaces cannot. Points on a surface cannot have multiple points with identical XY coordinates. This forces subdivision of the cave into 3 levels. From chapter 4.2.1 we know that this subdivision was executed for the polygons and for the mapping of roof and floor of the cave. The division of the cave survey dataset according to different levels in the cave results in a more complicated workflow and a greater chance for errors, as evident from the zonation overlap issues experienced for cave 3, see figure 5.1.2-1.

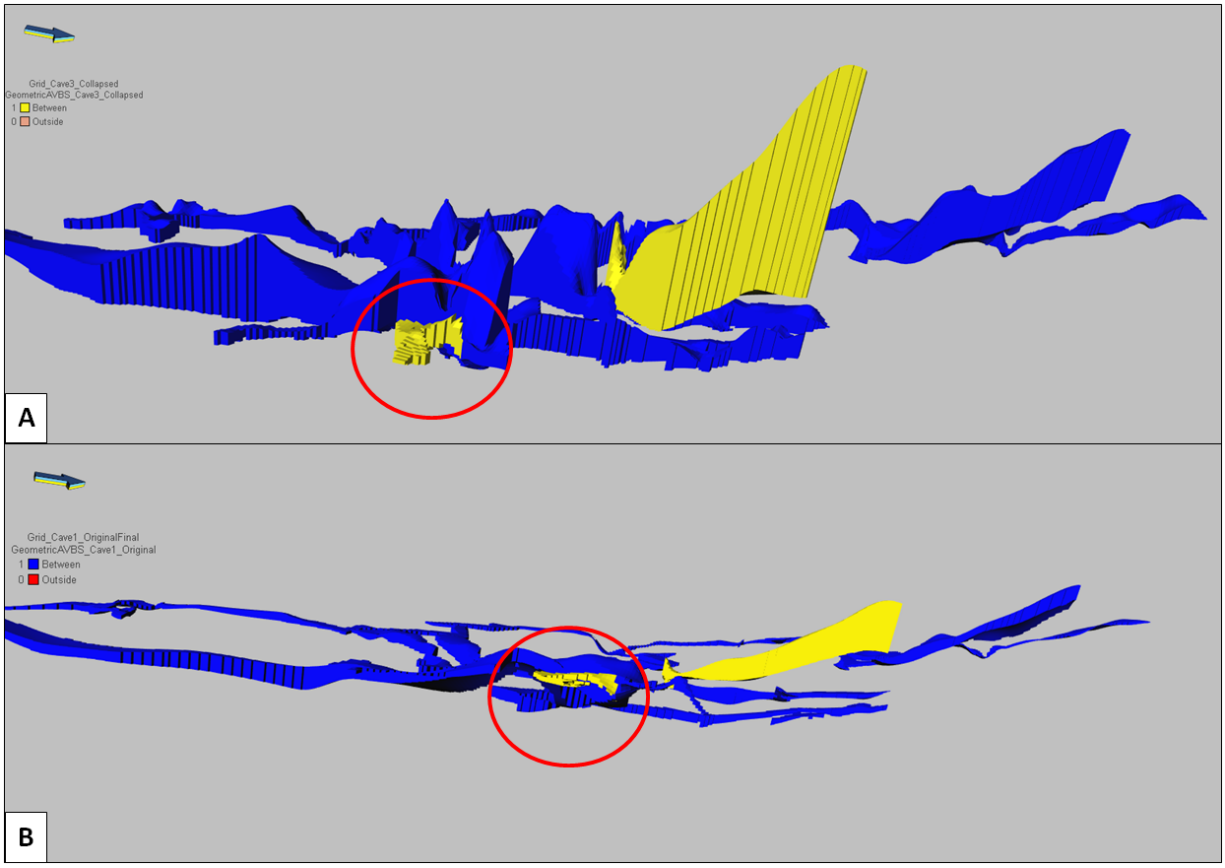

Figure 5.1.2-1: Figure illustrating the issues regarding the mapping in different levels in the model. A is the collapsed cave where cave 3 is shown in yellow, and cave 1 is shown in blue. B is the original cave with the same colour codes. There is no to little difference in height between cave 1 and cave 3 shown in the red circle, but in this area cave 3 is overlaying cave 1, so the subdivision has to be in place.

When the entire cave is finally merged into one parameter in the grid it works for further work on the model. If surfaces could be placed in different levels, this would not be a problem. This would lead to a more accurate result, with less room for errors, like the one for cave 3. The ability to map objects accurately in different levels is not only important for caves, but also for intrusions, both igneous, salt and sand (Cartwright et al., 2007). Intrusions may alter the surrounding rock in a reservoir, and needs to be accounted for in a reservoir model (Xu et al., 2015). For this reason it may be preferential to adapt the software to include the modelling of overlapping surfaces. There is a module present in RMS today for the integration of intrusions in a reservoir, but there is no way of populating the intrusions with petrophysical properties, which would be preferential.

5.1.3 Zone modelling

The model zonation is implicitly generated during the construction of the structural model. For the grids created in this thesis, the input for the structural model consists of the predefined horizons comprising of cave 1, cave 2 and cave 3, representing the different levels of the cave. These individual levels of the caves were further subdivided during the definition of the different polygons created at the start of the project (see chapter 4.2).

The need to use different cave levels creates some problems for the definition of different zones for the structural model. Especially the zones containing cave 1 and cave 3 proved difficult. Cave 3 erodes in to zone 4, which is supposed to only contain cave 1. The problematic area is located where cave 3 has a very small difference in height compared to cave 1. In the white circle shown on figure 5.1.3-1 cave 3 is located in zone 4 where the caves intersect, which forces the use of the subdivision of the cave. But the two parts of the cave are located at approximately the same height in the system (in the post-collapsed cave, cave 1 is even located higher than cave 3), and this causes the zonation issues, see figure 5.1.3-2.

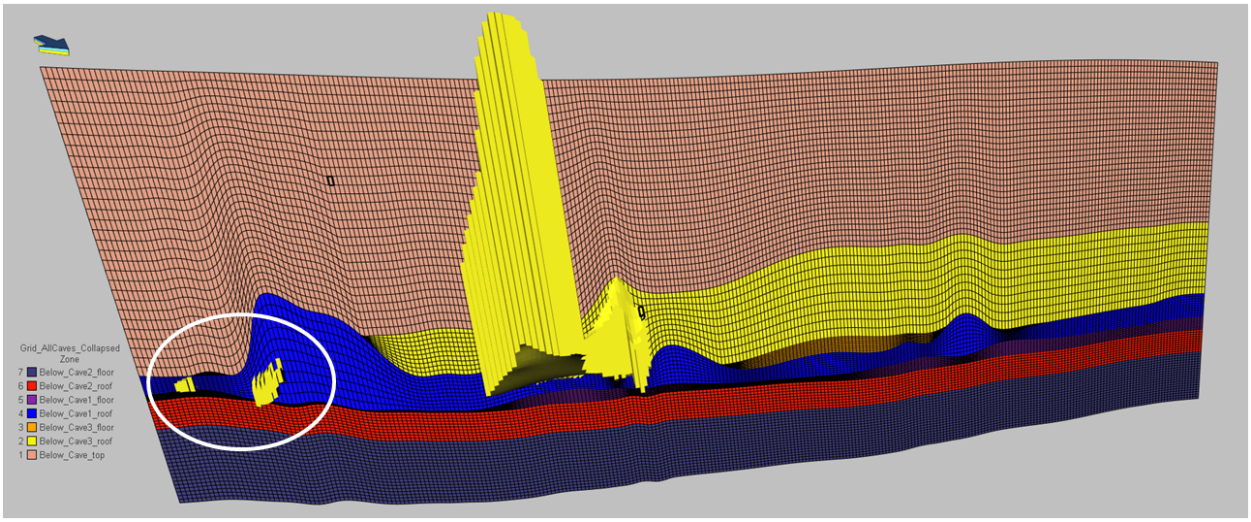

Figure 5.1.3-1: Figure illustrating the difficulties regarding the zonation of the grid. The yellow cave is cave 3, shown with the zones. The white circle indicates the problem, where cave 3 is located in zone 4, the zone that is supposed to only contain cave 1.

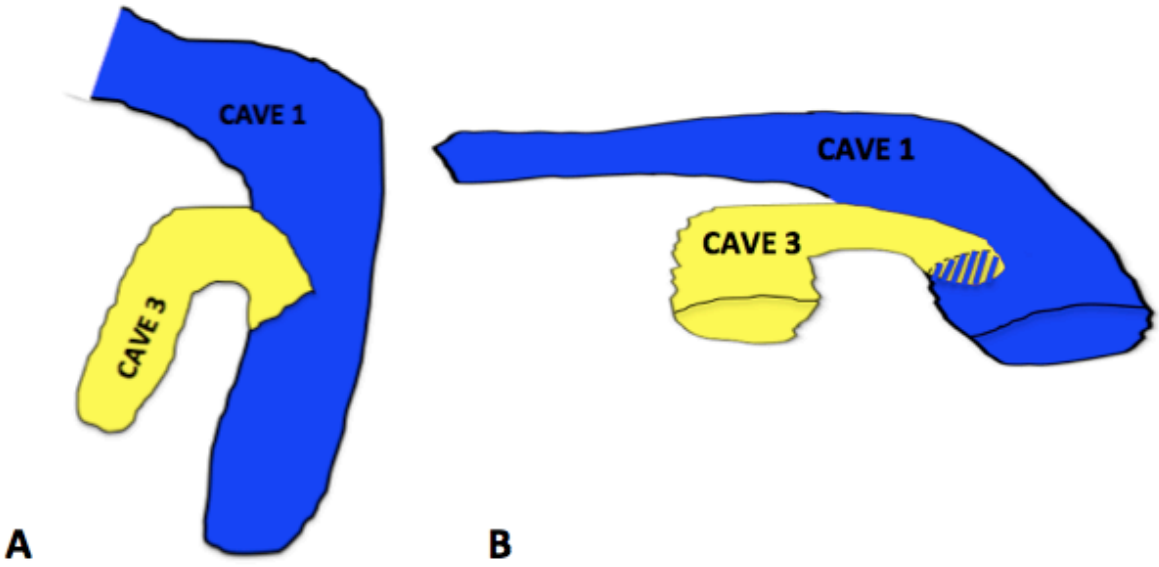

Figure 5.1.3-2: Simple sketch illustrating the most problematic area for the zone modelling. Cave 3 is located above Cave 1 where they merge. A shows the area in map view, and B shows the same area in 3D.

5.1.4 Time is money

The process of assigning each part of the cave passages its own geometry is the most time-consuming process, as there is no automated way for transferring the survey points from the cave map into the reservoir modelling software as polygons or even as a coherent body. Providing an algorithm which handles this automatically and performs a consistency check would speed up the modelling work significantly.

The narrowest cave passages present in the Setergrotta cave is only about 1 meter wide. For this reason, a fine grid is needed to ensure flow pathways inside the collapsed cave can be captured. Employing a grid with 1*1 meter resolution requires a good computer, but one is still likely to spend considerable CPU time running the geometrical models and simulations. Some of the geometric models defining the spatial position of the cave in the modelling grid took up to 32 hours to run. The main grid used for petrophysical modelling has an increment of 1*1 meters and have a total of 26 280 000 grid cells, which explains the considerable amount of time it takes to run the geometrical models.

Streamline simulations could not be run on this high resolution grid and the grid needed to be upscaled to be able to run the simulations. This will be looked at more closely in chapter 5.3.

5.2 Comparison to Furnée

The simple, yet fully functional reservoir model created by Furnée (2015) provides a time-efficient representation of the caves in the reservoir. The model illustrates the general trend and geometry of the cave system, and can easily be imported into Eclipse for fluid simulations. However, one of the key deficiencies of this model is the uniform geometry of the individual cave passages. The initial cave diameter is considered constant. Although it is possible to modulate this somewhat by splitting the cave into different segments and assigning different diameters to these, his approach fails to capture the actual geometric complexity exhibited by most caves.

The model presented in this thesis differs from the one by Furnée (2015) in two respects:

- The details and complexity of the geometry of the cave
- The method employed for modelling collapse of the cave.

5.2.1 Geometry of the cave

The geometry of a cave system is often complex and can be hard to predict. The cave passages are created in pre-existing fractures, and the further growth will be governed by hydrological factors and fracture-patterns in surrounding rock (Ford, 1988). The cave system modelled in this thesis is based on the same cave system and data sets as Furnée, but the manner in which the data has been implemented differs.

Furnée used skeleton lines from the cave survey of Setergrotta as key input, and generated the passage network geometry in the modelling grid using geometric modelling (i.e. a parameter describing the distance from the skeleton lines with a filter

set for the chosen cave diameter). The resulting cross-section geometry of the cave passages is uniform and circular for the whole cave system. This is a simplification of what is observed in nature, but the result may still be accurate enough for reservoir modelling purposes. However, the impact of omitting geometric complexity has not yet been quantified. The transition from a cave passage with one diameter to a much narrower cave passage may lead to a pressure build-up in the fluids flowing through the passage and a shift in the fluid patterns.

Figure 5.2.1-1 shows a comparison between the cave system geometry from Furnée (2015) and geometry produced using the workflow in the present thesis.

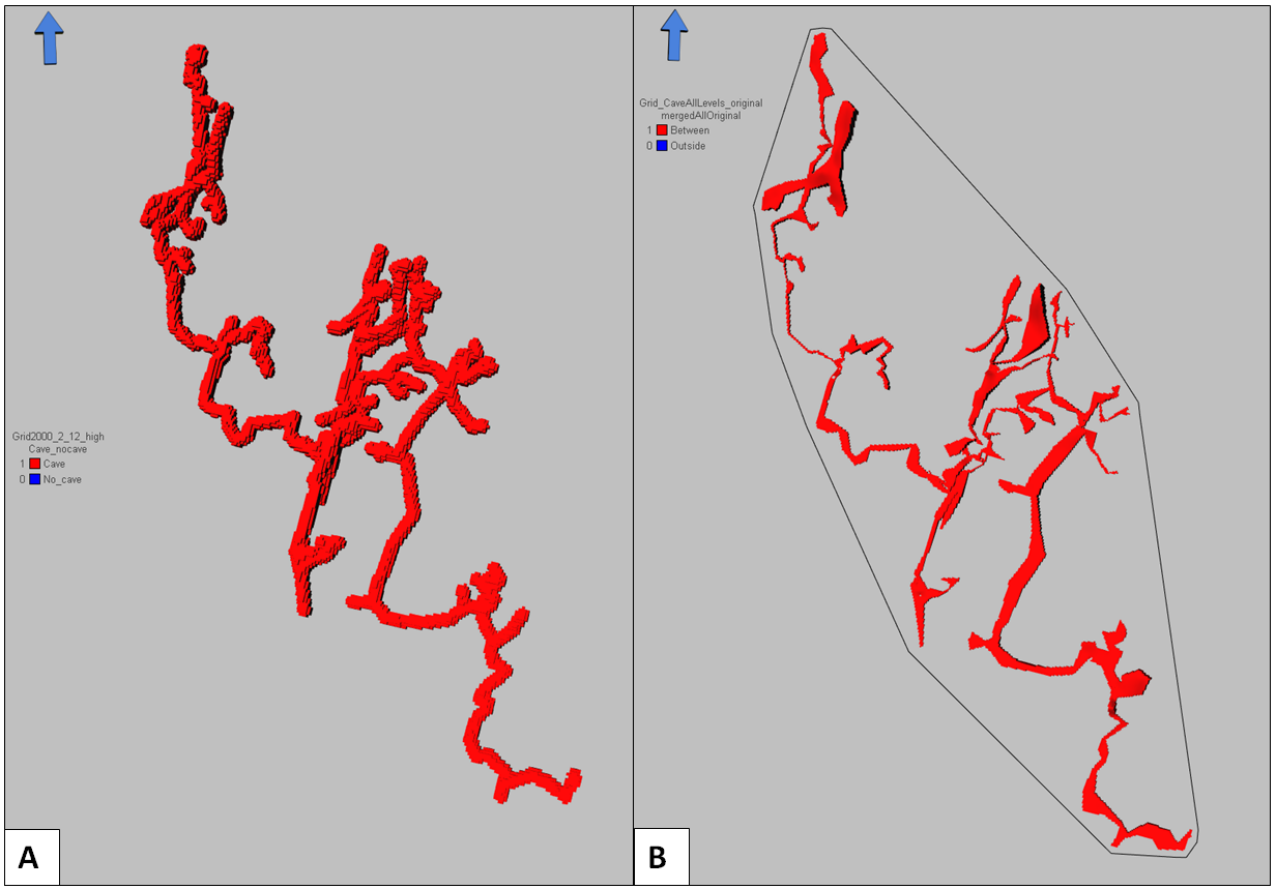

Figure 5.2.1-1: Comparison of cave geometry. Figure A is Furnée's cave geometry, and B is the cave geometry created in this thesis. Notice the varying thickness of the passages in B compared to A.

The cave geometry generated in the present thesis employs the exact wall, floor and roof coordinates from the cave system. The resolution is not uniform and constrained by the

density of survey points, but it reproduces the actual geometry of the Setergrotta cave fairly accurately.

5.2.2 Collapse of the cave

The collapse of a cave system and resulting geometry and infill of the collapsed cave passages is an important part of modelling of paleocave systems (Loucks, 1999). The collapse of caves may lead to an alteration of the fluid flow and behaviour in the reservoir by expanding cavities and filling them with collapse material. There are several ways of modelling the effect of collapse in a cave, this is evident when comparing the methods used in this thesis and the method used by Furnée (2015).

Furnée (2015) captured the effect of a future collapse of the Setergrotta cave by widening the radius of the cave using the geometric modelling tool while keeping the position of the floor constant. With the use of this method, the collapse of the cave will be the same in all directions, and will once more yield a uniform geometric shape for all of the passages. Figure 5.2.2-1 illustrates the collapse of the cave passages modelled by Furnée. This will not be the most natural shape of a collapsed cave, as the collapse will mainly take place in an upward direction, but it may nevertheless potentially be a good approximation for reservoir modelling purposes.

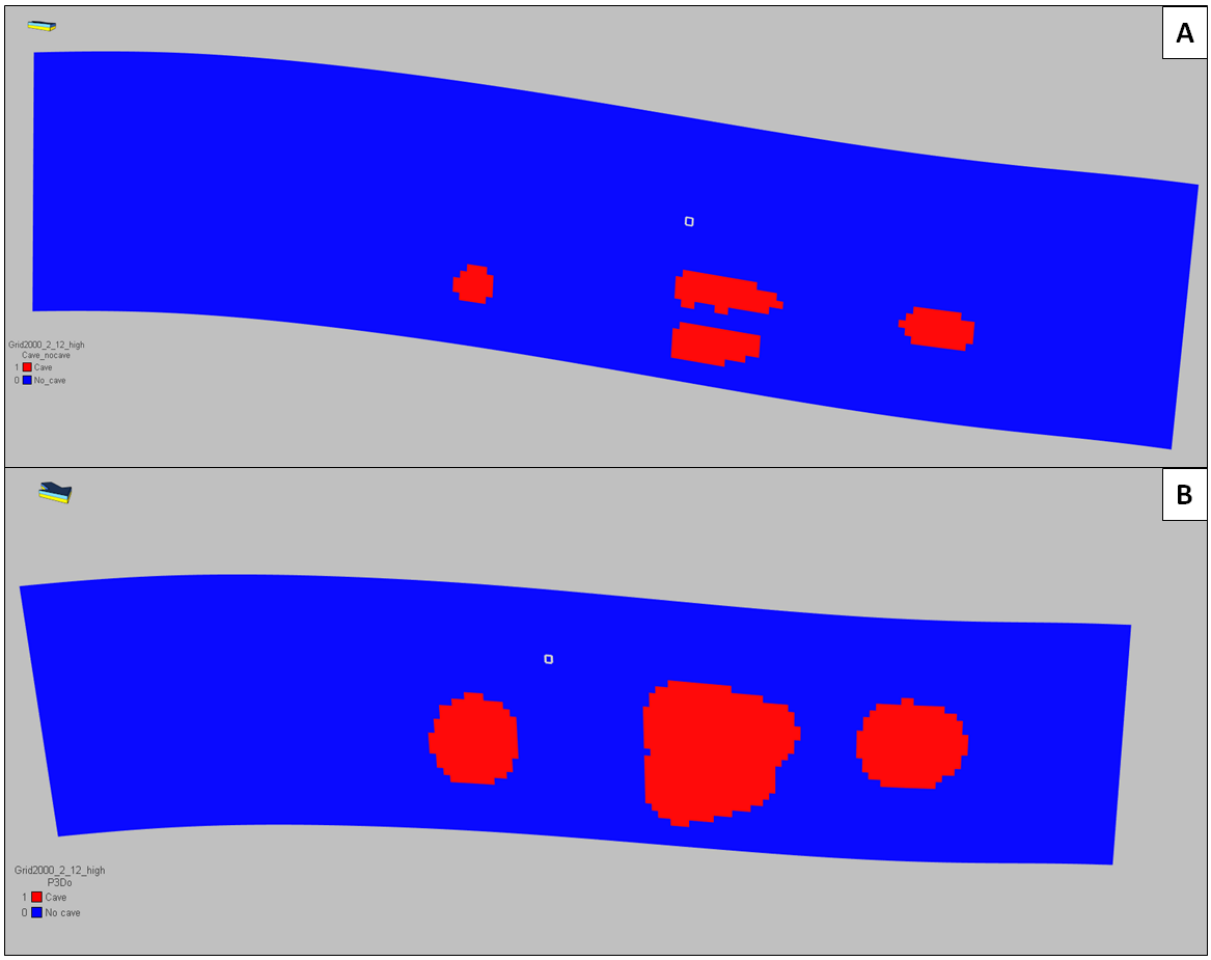

Figure 5.2.2-1: The difference between pre- and post-collapsed cave modelled by Furnée. Figure A is the cave passage pre-collapse, and figure B is the cave post-collapse

The collapse of the cave modelled in this thesis is based on a formula presented by Lauritzen (2015). It is based on the original height of the cave and the density of the surrounding rocks and the resulting collapsed breccias are used to estimate the maximum height of the collapsed cave. We remember from chapter 4.3.1 that this was the formula used for the collapse of the cave:

$$H_t = H_g \left(\frac{p_1}{p_1 - p_2}\right) \quad (1)$$

This formula is based on the density of the surrounding rocks (p_1) and the collapsed brecciated masses (p_2), as well as the original height of the cave passages (H_g), see chapter 4.3.1 for further information. This provides an opportunity to model the collapsed cave with differing heights in different parts of the cave, instead of the continuous and uniform type of collapse found in Furnée's model, see figure 5.2.2-2.

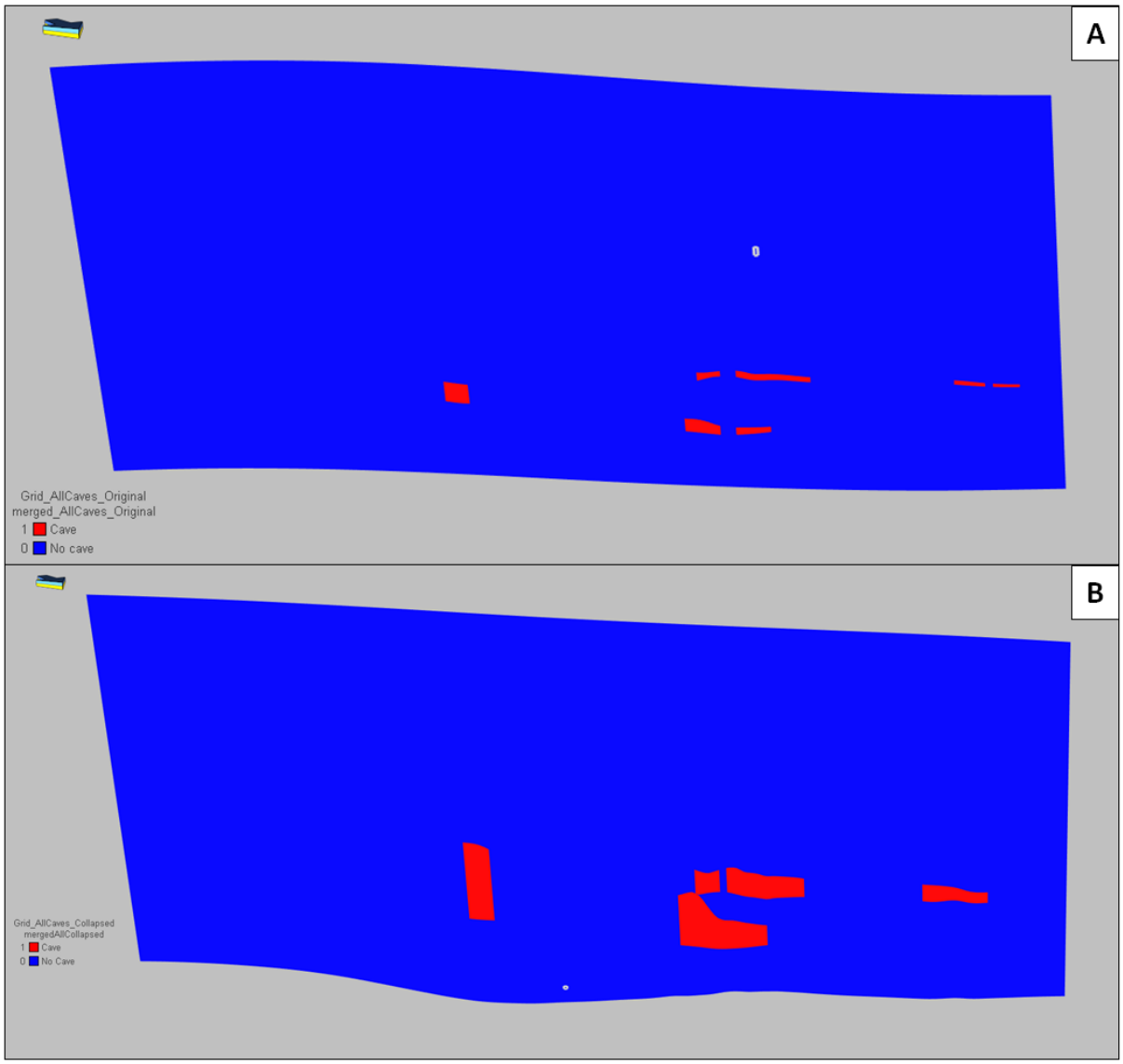

Figure 5.2.2-2: The difference between pre- and post-collapsed cave modelled in this thesis. Figure A is the cave pre-collapse, and B is post-collapse.

The result of the modelling of the collapsed cave can be seen in figure 5.2.2-3. It becomes clear that the areas of the cave that already have some height in the original cave undergo a significantly higher degree of collapse than the parts of the cave with less height. The volume of the cave has increased significantly, which is clear in figure 5.2.2-3.

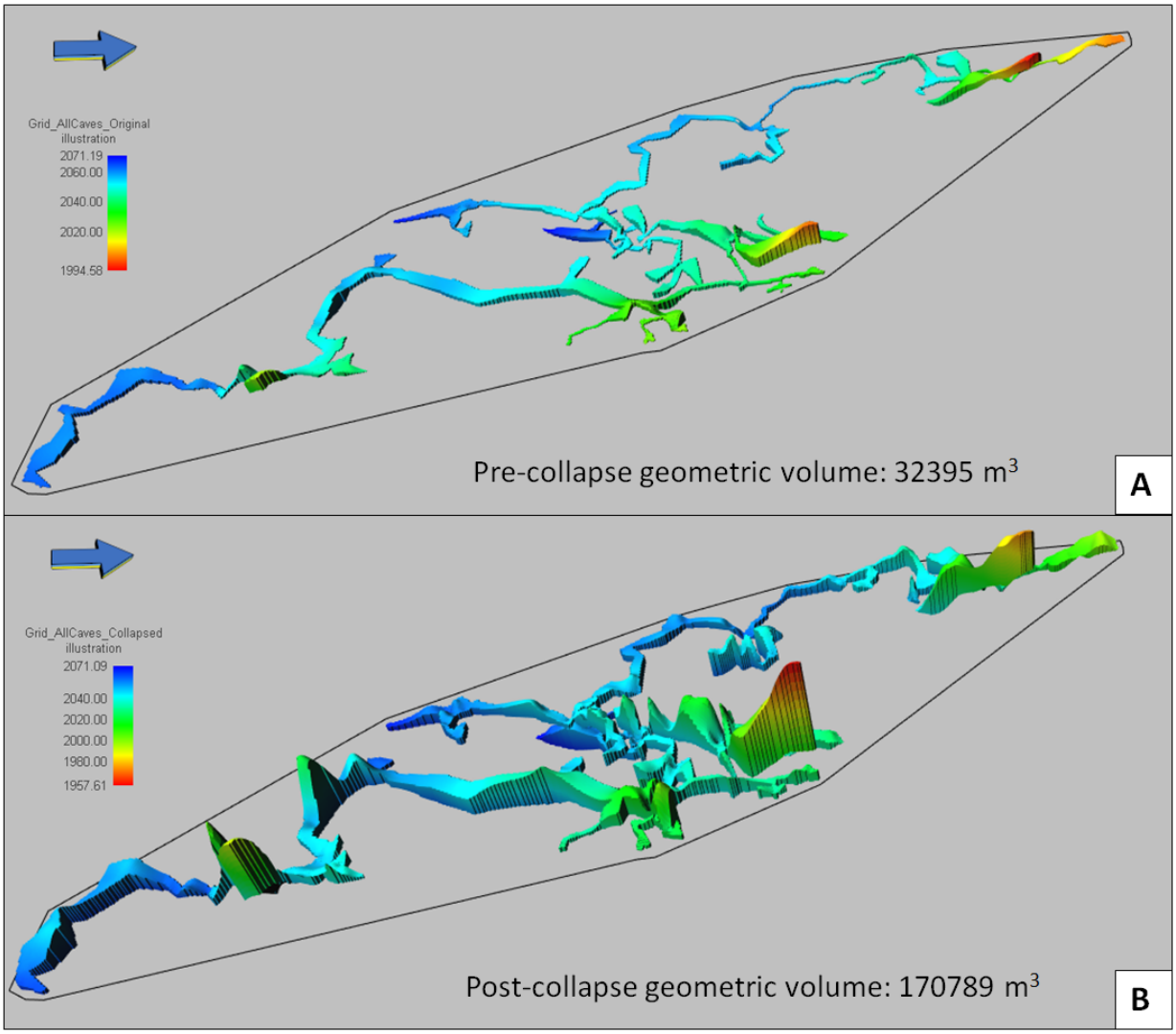

Figure 5.2.2-3: Figure illustrating the difference of the cave geometry pre- and post- collapse. The difference in volume can also be seen. Figure A is pre-collapse and B is post-collapse. The cave height is defined by colour.

Also for the areas where the cave can be found in different levels, the collapse may lead to the formation of one single continuous upwards collapse. This was found in the collapsed cave model between cave 1 and cave 2, see figure 5.2.2-4. This phenomenon can be linked to Loucks (1999) hypothesis of coalescence of collapsing caves; here in the vertical direction. It may also lead to enhanced fluid flow through the cave system and more accommodation space for the fluids.

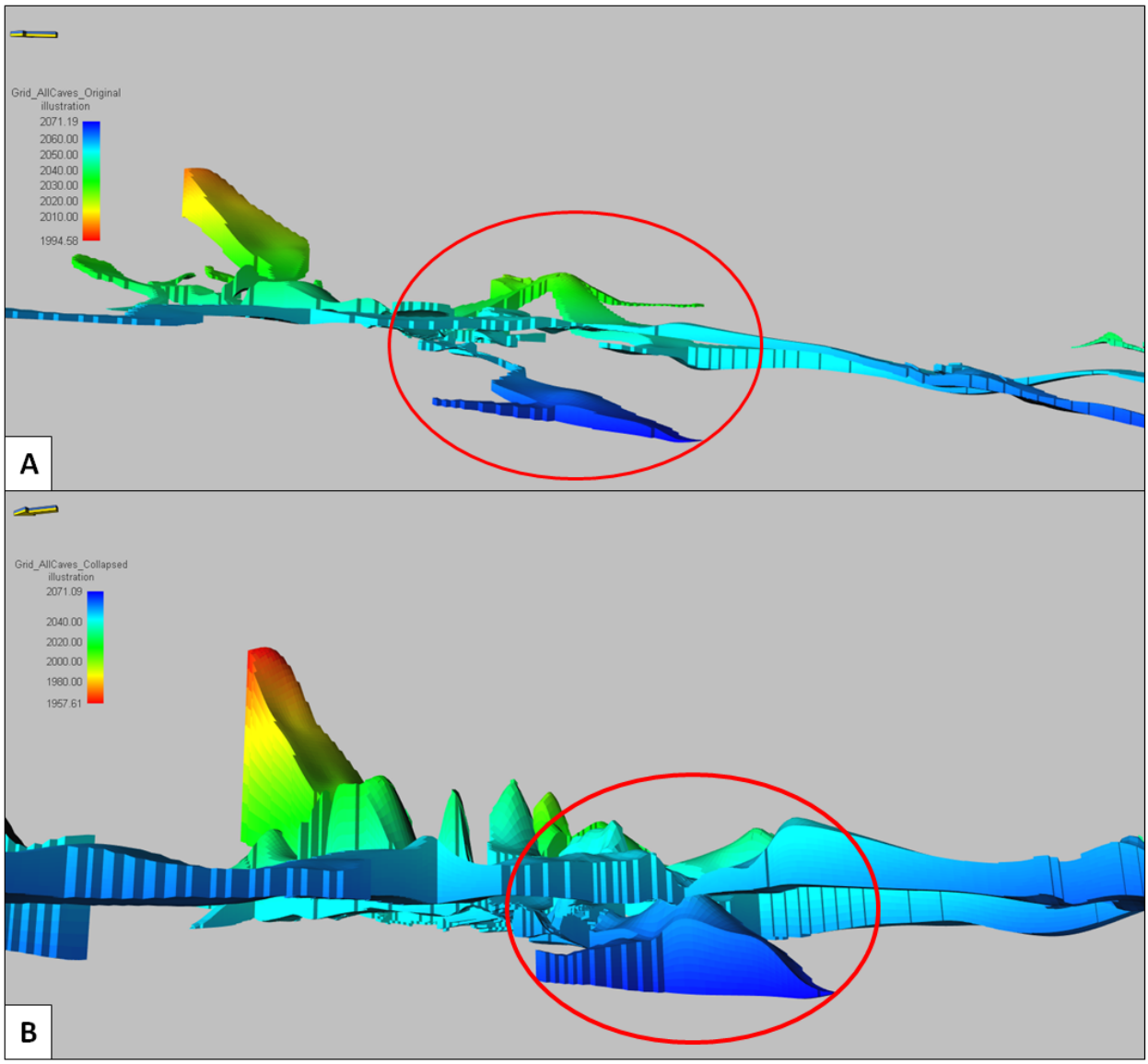

Figure 5.2.2-4: Figure illustrating a previous passage of the cave that is linking up with the above-lying passage post-collapse. Figure A shows the cave pre-collapse, the lower blue passage is cave 2. Figure B shows the cave post-collapse, where cave 2 has linked up with the passage located above.

If the fluids run through the passages, a more accurate definition of the cave and its collapse may reveal a fluid flow through the reservoir that must be considered during production. This may be the case where the passages are significantly narrower than the surrounding passages, or for big collapse rooms.

5.3 Streamline simulations in RMS

Time-constraints resulting from unforeseen challenges while modelling this cave system precluded conducting flow simulations in ECLIPSE and a comparison with simulation results by Furnée (2015) as originally intended. Instead, streamline simulations in RMS was executed, and may provide an indication of the results that may have been achieved from simulations in ECLIPSE.

The streamline simulation tool in RMS provides an opportunity to visualize fluid flow patterns through the reservoir during production. The tool simulates the flow through the reservoir over time, and can be used to evaluate reservoir flow behaviour during production prior to more detailed flow simulations. Simulation in Eclipse would provide more accurate information about the reservoir, and its behaviour during production.

The streamline simulations that were executed on this thesis were all done on the same reservoir, but with different grid resolution. Each simulation had one producing well with 160 bhp and one injection well with 260 bhp. The reference pressure was set to 200 bar, see chapter 4.6.2 for further information about the settings for the streamline simulations.

5.3.1 Upscaling for streamline simulations

The streamline simulations were conducted on three grids (Table 5.3.1-1) with different resolution while employing identical simulation settings. The petrophysical properties were upscaled from the initial grid with 1m*1m XY resolution in the manner described in chapter 4.6.2.

GRID NAME	RESOLUTION (m)	NUMBER OF CELLS
Grid_Upscaled2	2*2	3 061 800
Grid_Upscaled4	4*4	768 852
Grid_Upscaled6	6*6	340 200

Table 5.3.1-1: Grids created for streamline simulations

The purpose of running streamline simulations on grids with different grid size was to investigate the effect the upscaling has on the flow patterns. The goal of upscaling is to keep the grid as coarse as possible to cut CPU cost, while avoiding the loss of important details that could affect simulation outcomes. Figure 5.3.1-2 illustrates the difference on the upscaled grid. The total number of cells for each grid can be seen in table 5.3.1-1.

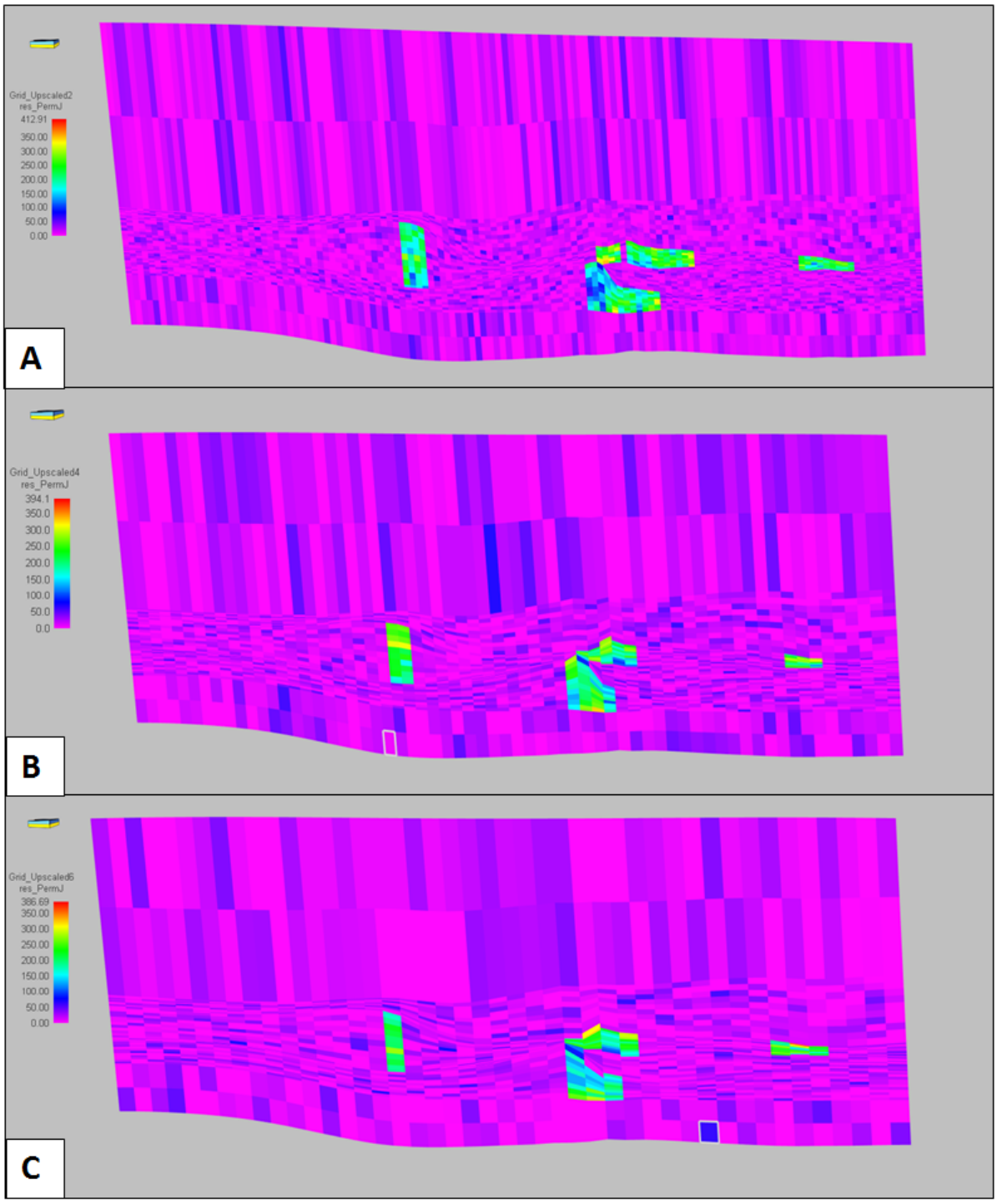

Figure 5.3.1-2: The three different upscaled grids, A is Grid_Upscaled2, B is Grid_Upscaled4 and C is Grid_Upscaled6.

5.3.2 Results of the streamline simulations

The visual results from the streamline simulations of the three upscaled grids are illustrated in figure 5.3.2-1. The figure shows that there will be fluid flow through the whole system according to the streamlines. Two major factors appear to influence the simulation; the degree of upscaling, and the petrophysical values chosen for the background facies.

For the grids *Grid_Upscaled2* and *Grid_Upscaled4*, the streamlines are almost identical, with break-through times on similar scales, and with similar results for the parameters created during streamline simulations, see table 5.3.2-1. *Grid_Upscaled6* differs from the two other grids. The flow shows less preference for passing through the collapsed cave passages, the breakthrough-time is much shorter, and calculated production and injection rates are much lower. Some of these observations can probably be explained by the upscaling process, which "blurs" the narrower cave passages into the background. For the present model this suggests that an upscaling beyond a 4*4 meter resolution will alter simulated flow behaviour significantly. Furnée (2015) concluded that a resolution of 4*4 or 8*8 would provide a sufficiently detailed reservoir for fluid flow purposes.

Grid	Production Rate (m^3/day)	Injection Rate (m^3/day)	Breakthrough-time (days)
Grid_Upscaled2	415	1000	19346
Grid_Upscaled4	405	1000	25185
Grid_Upscaled6	188	317	775

Table 5.3.2-1: Data from the streamline simulations. The data can also be found in the appendix where the streamline run files are located. Notice the significant difference in breakthrough-times between Grid_Upscaled6 and Grid_UpsCaled2 and Grid_Upscaled4.

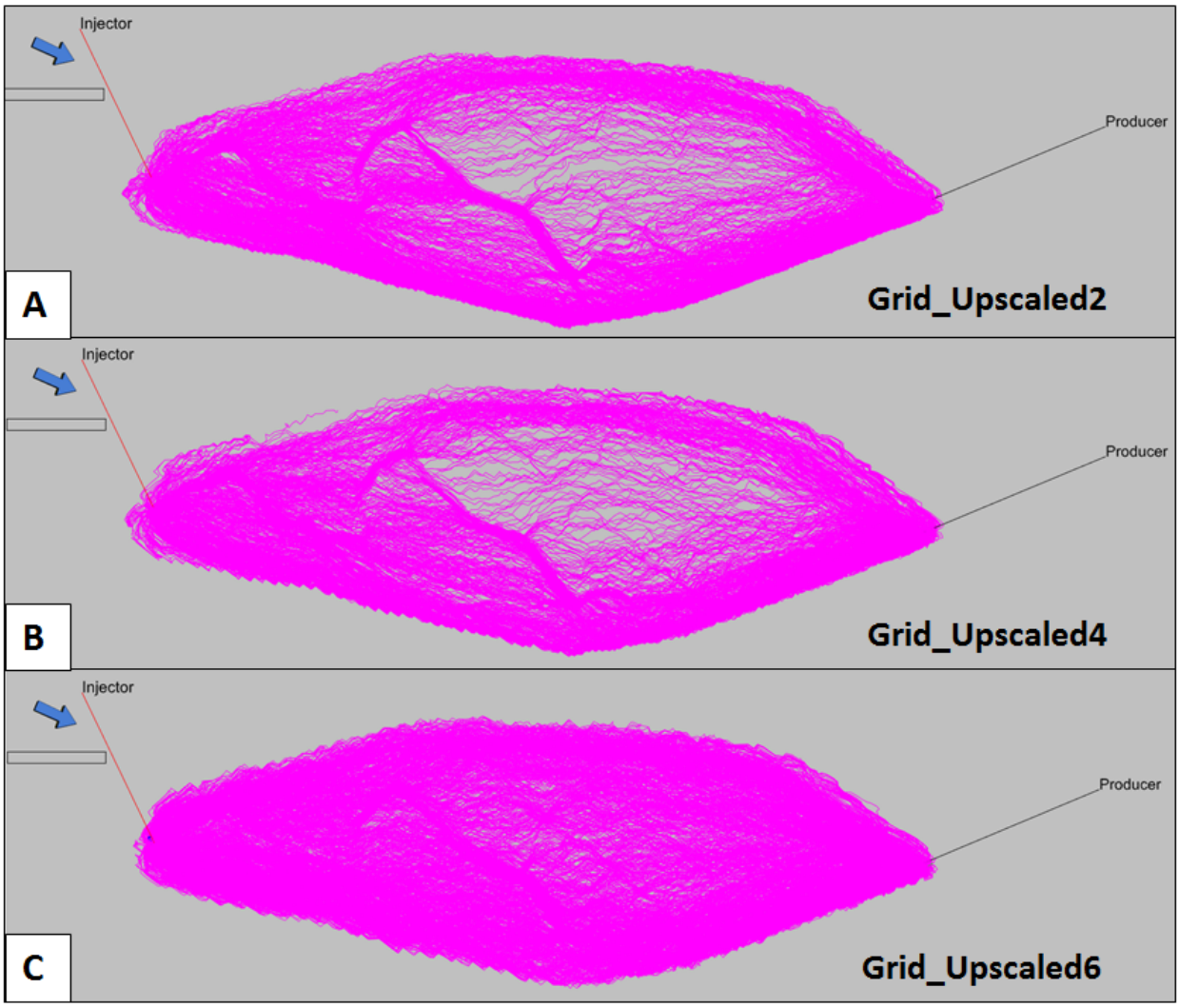

Figure 5.3.2-2: Results of the streamline simulations on the different upscaled grids, not filtered on time. A is the Grid_Upscaled2, B is the Grid_Upscaled4 and C is the Grid_Upscaled6

The petrophysical values chosen for the Cave and the background, No Cave facies have a substantial influence on how the fluids will flow through the reservoir. If the permeability contrasts between Cave and No-Cave facies is small, flow will exhibit a preference for following the former caves, se figure 5.3.2-3. The fluids will in any case find the easiest paths through the reservoir, and will move through the cave passages where it is accessible and the passages have a favourable orientation with respect to pressure gradients. It is worth noticing the significant fluid flow along the edges of the reservoir, especially for *Grid_Upscaled2* and *Grid_Upscaled4*. It seems like the fluids prefer to move along the edges instead of straight through the reservoir where the cave facies are located. This may be caused by the edge-effects that can be seen in figure 5.3.2-4. Edge effects are artefacts that can be found along the edges of a reservoir model after upscaling.

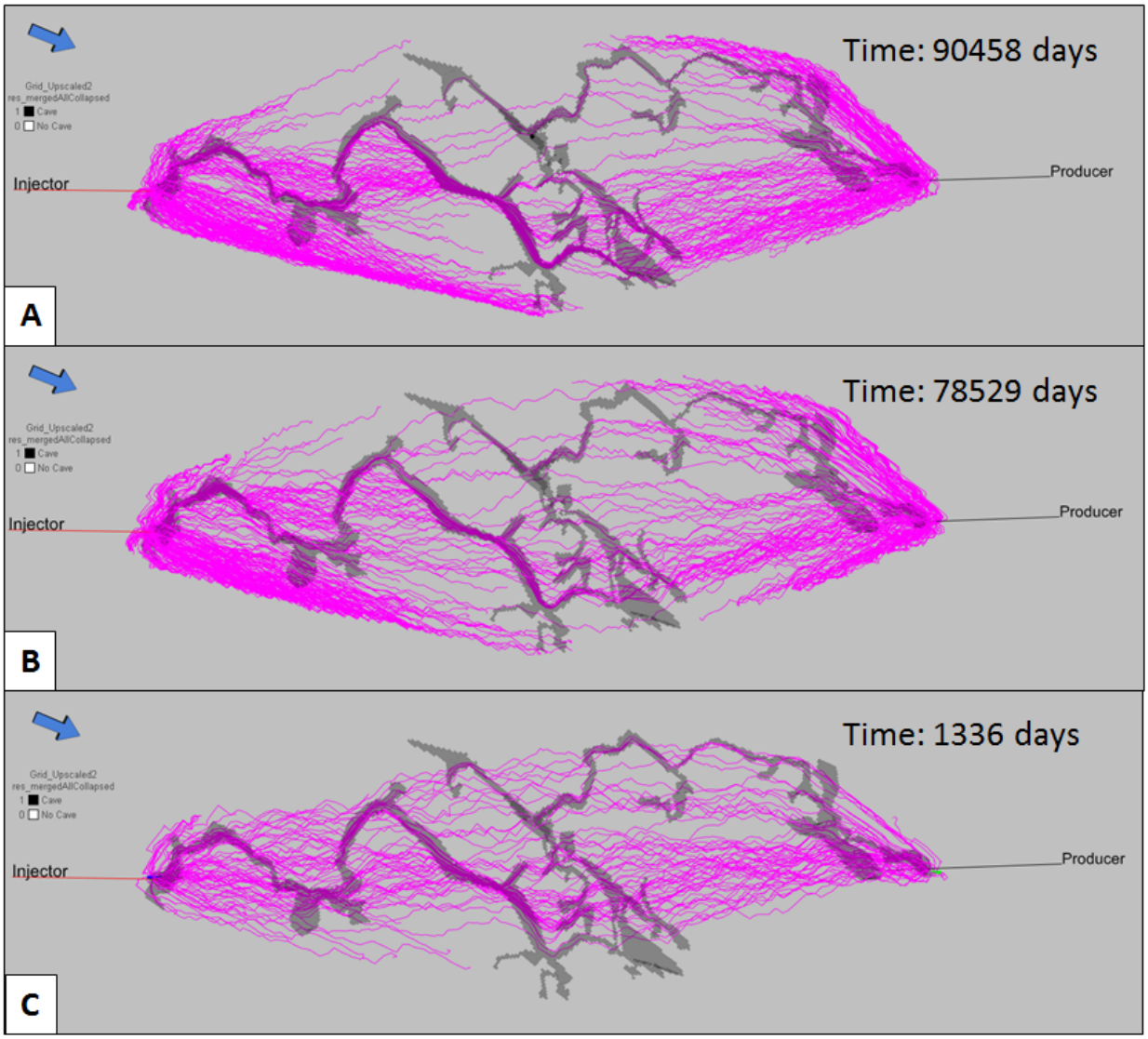

Figure 5.3.2-3: Results of the streamline simulations filtered on time. The cave facies can be seen in the background. A is the Grid_Upscaled2, B is the Grid_Upscaled4 and C is the Grid_Upscaled6. It is clear that the fluid flow will prefer the cave facies where they are available. Note also the time it has taken for the fluid to flow to the current location, it has taken much shorter time in Grid_Upscaled6 than the others. Also note the fluid flow along the edges of reservoir A and B.

The permeability also affects overall drainage of the model domain, which is clearly illustrated with the parameters PRESSURE, INJREG and PRDREG for all the upscaled grids. The amount of non-drained cells is high, but this can be directly correlated to grid cells that have permeability and porosity values of 0, see figure 5.3.2-4. Edge effects are also affecting the drainage of the reservoir, and a high amount of the outer edges of the reservoir are not drained. Permeability and porosity values of 0 are likely to be found in paleokarst reservoirs as a result of diagenetic process like compaction and cementation (Brown, 1997).

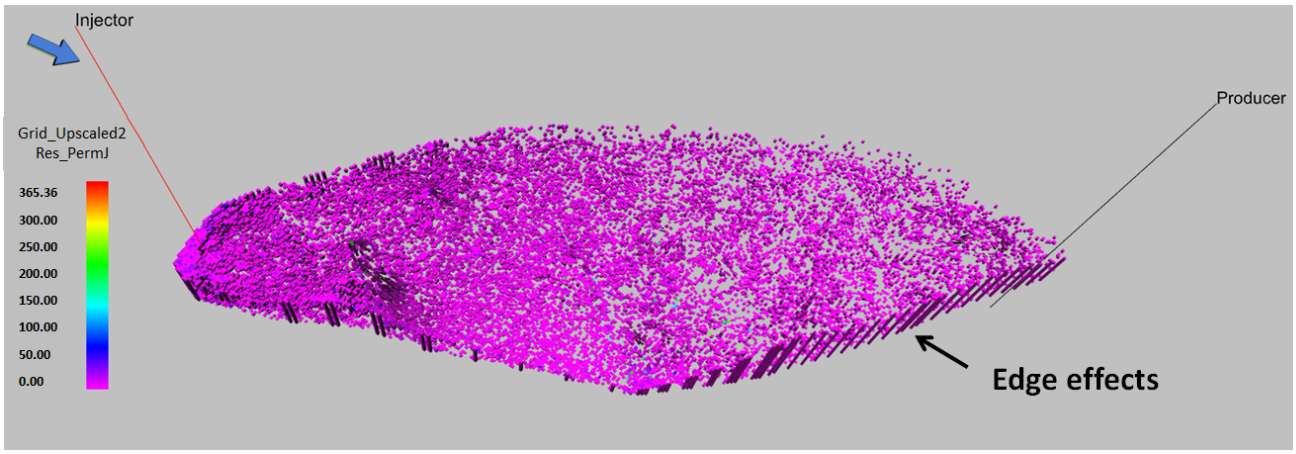

Figure 5.3.2-4: Cells in the grid Grid_Upscaled2 that are not drained. The PermJ parameter is filtered on the parameter PRDREG, which illustrates which cells are drained by the producing well. The figure shows that the cells that are not drained have a permeability of 0.

From the streamline simulations created for the paleokarst reservoir, it becomes clear that the cave facies have an impact on the fluid flow, but chiefly during the earlier phases of the production. The passages serves as fluid pathways where this is preferential, but the fluids will eventually flow through the whole reservoir. There may of course be other results if the model is run using a more advanced reservoir simulation software.

Streamline simulations were done on the reservoir model Furnée (2015) created, and the result can be seen in figure 5.3.2-5. Similar petrophysical values were used. For the No Cave facies the mean permeability was set to 11 mD, and the mean porosity was set to 5 %. For the Cave facies, the petrophysical values chosen by Furnée were lower than what was chosen in this study, with a mean permeability of 24 mD and a mean porosity of 12 %. The rest of the settings for the simulations were set the same way as for the streamline simulations executed on the present model. The grid is upscaled with a 2*2 meter resolution in the XY direction. From the figure it seems like there is no preferential fluid flow through any cave passages in the reservoir. This observation may be linked to the lack of contrast between the petrophysical values for the Cave and No Cave facies. But this is only a theory, and needs to be investigated further in a more advanced reservoir simulation software.

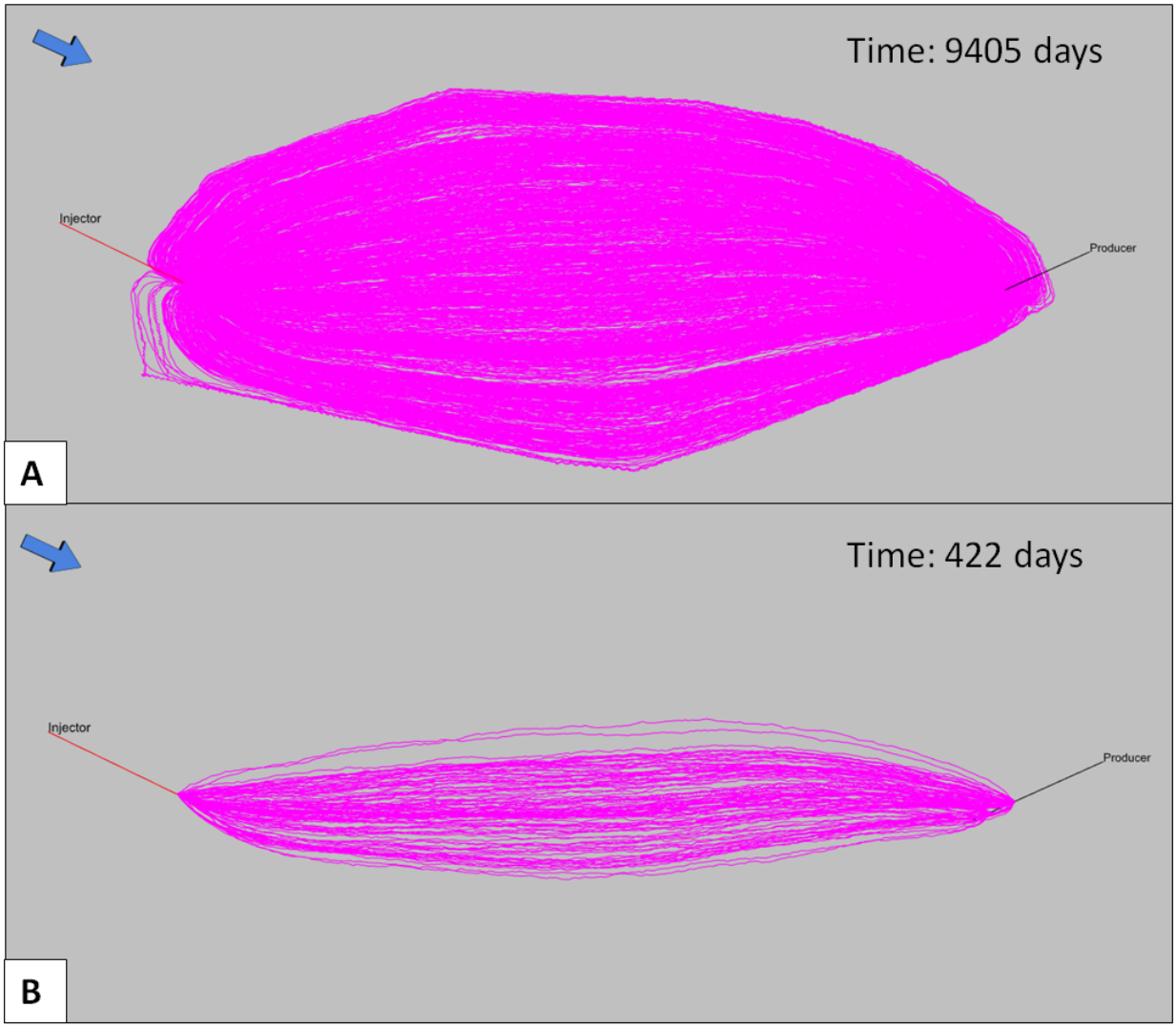

Figure 5.3.2-5: Streamline simulations done on the reservoir model created by Furnée (2015). A shows the streamlines unfiltered, and B shows the streamlines filtered on time. Notice that there are no apparent fluid flow through cave passages.

5.3.3 Drainage functions

The drainage functions can be used to compare behaviour of the three upscaled models. Tables for the drainage functions can be found in Appendix 8.5. Figure 5.3.3-1 illustrates the drainage over 5 years for the three different upscaled grids. Figure 5.3.3-2 illustrates the time of maximum drainage from the reservoir for the different upscaled grids.

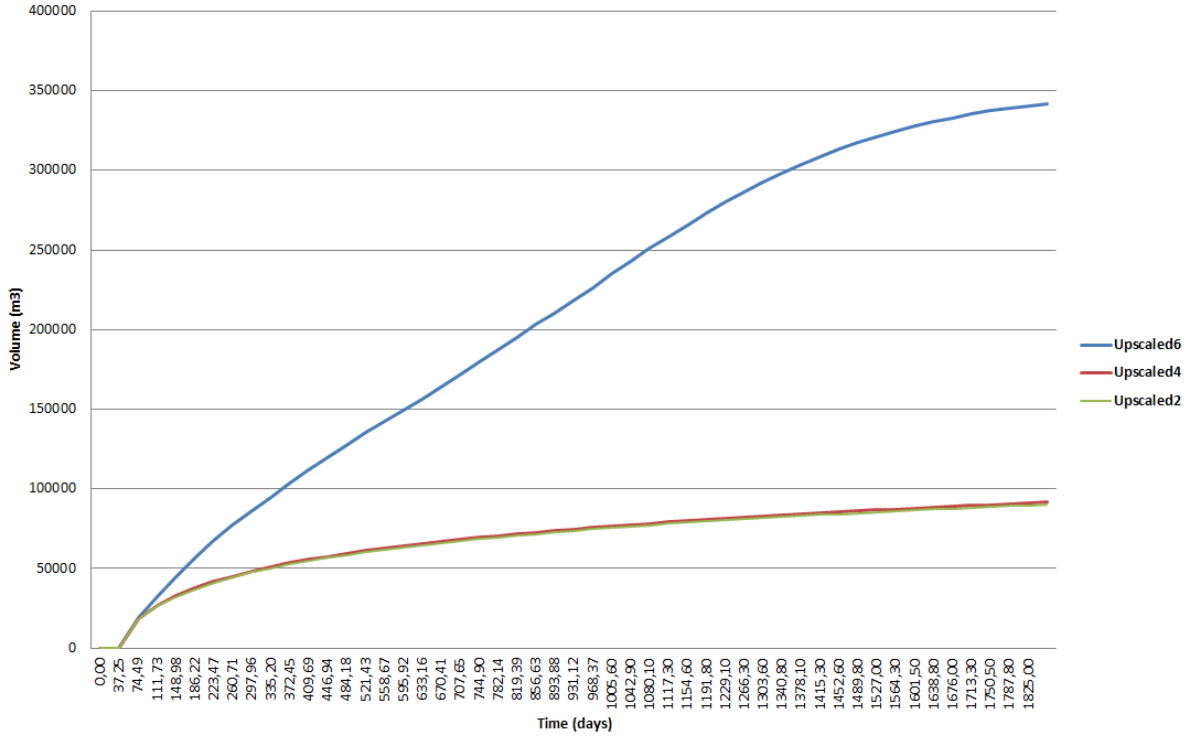

Figure 5.3.3-1: Drainage function illustrating the cumulative production from the producing well over 5 years in the reservoir. The blue line illustrates the drainage pattern for Grid_Upscaled6, the red line illustrates the drainage pattern for Grid_Upscaled4 and the green line illustrates the drainage pattern for Grid_Upscaled2. It is clear from this graph that the drainage pattern for Grid_Upscaled2 and Grid_Upscaled4 is almost identical, but Grid_Upscaled6 differs significantly.

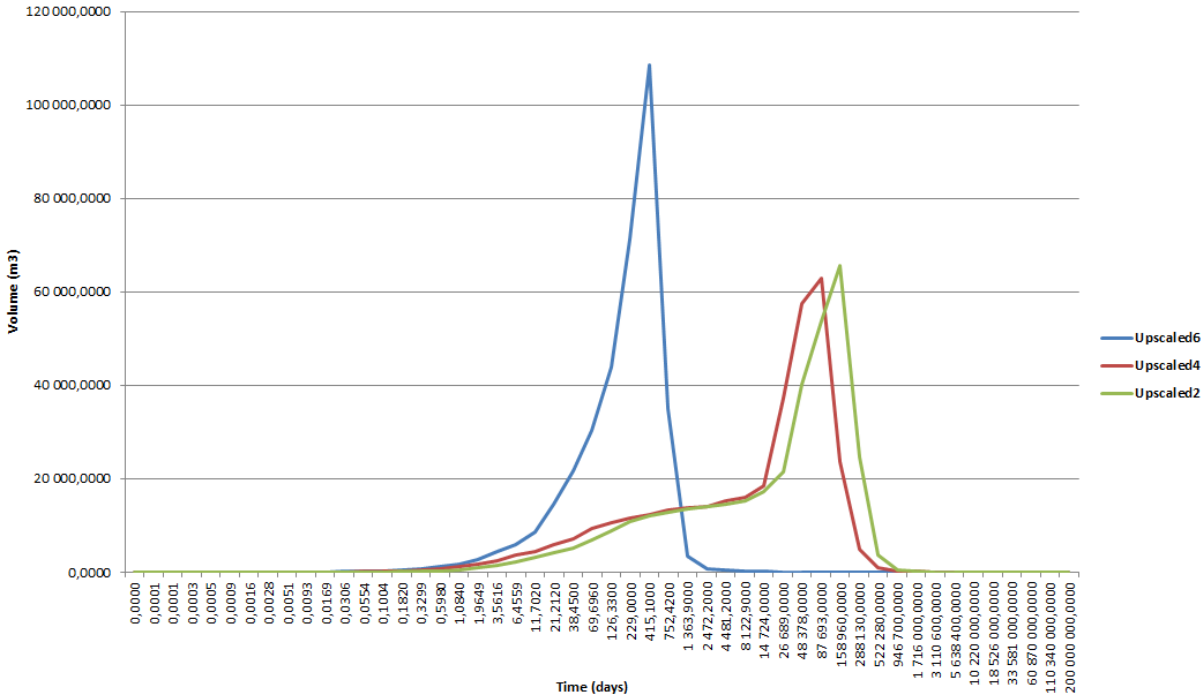

Figure 5.3.3-2: Figure illustrating the time of the maximum production rate of the different grids. . The blue line illustrates the drainage pattern for Grid_Upscaled6, the red line illustrates the drainage pattern for Grid_Upscaled4 and the green line illustrates the drainage pattern for Grid_Upscaled2. It is once again clear that Grid_Upscaled6 differs significantly from the two others.

From the graphs it is clear to see that *Grid_Upscaled6* differs significantly from the two other grids. This is an indication that the simulation outcomes will be influenced if a larger resolution than 4*4 meters is chosen for conducting the simulation. For *Grid_Upscaled6* the cave geometry with its higher porosity and permeability has been effectively "blurred" into the surrounding host rock. This averaging process levels out extreme values, but apparently creates better connectivity in the reservoir, see figure 5.3.3-3.

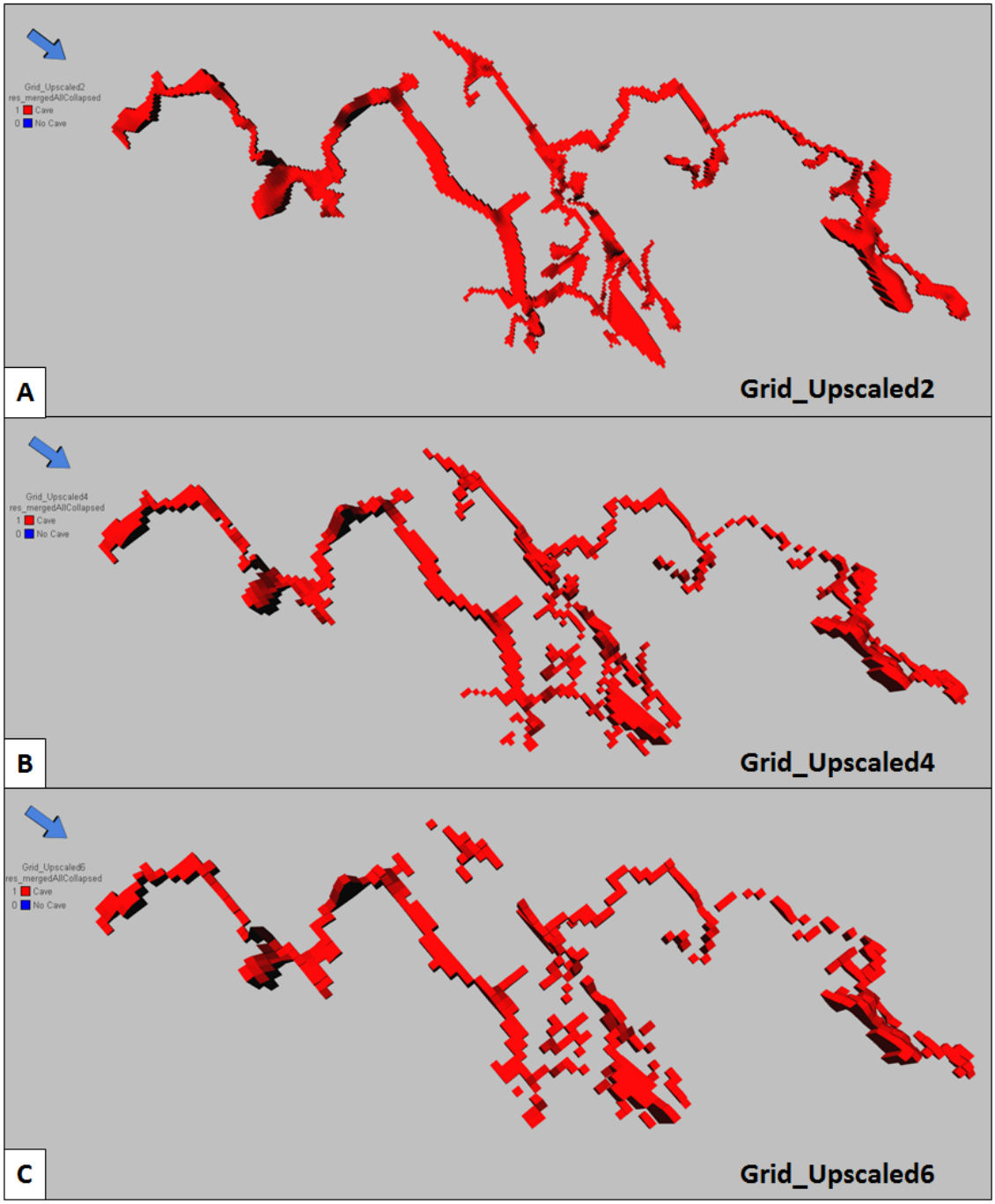

Figure 5.3.3-3: The effect the upscaling of the grids has on the cave geometry. A is the cave in Grid_Upscaled2, B is the cave in Grid_Upscaled4 and C is the cave in Grid_Upscaled6.

The result of the upscaling of the cave geometry may be the reason for the differing results from the streamline simulations and the drainage functions. The cave passages in *Grid_Upscaled6* are rendered discontinuous, and the geometry is ignored. The parameter *MergedAllCollapsed* is a discreet parameter, and the cells are given the values 1 or 0 depending if the cave is present or not. When this parameter is upscaled, the narrowest passages disappear, and the result is loss of connection throughout the cave system, as observed in figure 5.3.3-3.

This behaviour was also observed by Erzeybek Balan (2012). The fluid flow simulations run on her model of the Yates Field in West Texas revealed a drastic response in fluid flow response for the changes in connectivity and description of cave facies. In the simulations run on the models where the cave facies were given less attention, resulting in a poor connectivity of cave facies, some wells reported unrealistically high oil production in some wells, in other wells unrealistically low oil production was reported. Water breakthrough also differed significantly from the more detailed models.

Furnée (2015) concluded in his thesis that an upscaling of more than 8 grid cell diameters will lead to an unwanted effect on the production curves for the reservoir. This level of upscaling is higher than the results found in this thesis. This is probably caused by the difference in the cave radius used in this thesis compared to the radius used by Furnée. Furnée used a diameter of 10 meters for the cave passages, while some of the cave passages in this thesis have a diameter of 2 meters. A grid resolution of more than 4*4 meters will thus lead to grid cells unable to represent the narrowest passages. This was observed by Furnée when the grid resolution was more than 8*8 m. He stated that if the diameter of the cave passage were less then the grid cell diameter, the upscaling would work. This is also the case here. From figure 5.3.3-3 it appears that *Grid_Upscaled4* also has some discontinuous passages as a result of the upscaling, but this is apparently not enough to have any significant effect on the fluid flow through the reservoir.

From the streamline simulations, it is clear that the cave system influences modelled fluid flow if the contrast between petrophysical values chosen for the Cave and No-Cave facies is large enough, and within certain limits of upscaling. The geometry of the cave

passages does not seem to have any significant impact on the fluid flow through the system, if the degree of upscaling is carefully monitored. If the upscaling is too coarse, the connection and coherency of the cave passages is lost, and the fluid flow through the system is affected. This merits a more detailed study using Eclipse or another specialized flow simulation program.

5.4 Volumetric calculations in RMS

Volumetric calculations were performed on all three upscaled grids. In theory results should be identical. The volumetric calculations generate several output parameters describing different volumetric properties. A report file is created, and the results of the volume calculations can be seen in table 5.4-1. The report files can be found in Appendix 8.6. The volumetric calculations are conducted without the upper and lower zones of the reservoir, including only the parts of the reservoir containing the collapsed caves.

GRID	BULK	NET	PORE	HCPV	STOIIP
UPSCALED2	3928309	3928309	362861	326575	326575
UPSCALED4	3927032	3927032	361354	325218	325218
UPSCALED6	3929036	3929036	361887	325698	325698

Table 5.4-1: The results of the volumetric calculations on the three different upscaled grids.

For the streamline simulations the difference between the grids were obvious, probably because of the impact of the cave facies and the effect the upscaling had on the parameter *MergedAllCollapsed*. It is clear from Table 5.4-1 that the upscaling of the grids has close to no impact on the volumetrics of the reservoir. For the volumetric calculations, the only input from the grid was the *PORO_FRAC* parameter, which is a continuous parameter as opposed to the *MergedAllCollapsed* parameter, which is discrete. The upscaling of a discrete parameter can often result in a more “jagged” result,

since the values are only given as 1 and 0. For the PORO_FRAC parameter the upscaling has had limited effect, which is reflected in the results of the volume calculations.

6 CONCLUSIONS

Creating a working method for rendering realistic paleokarst features in reservoir models is very much still a work-in-progress. The present contribution to this effort, in the shape of a new method for capturing initial cave geometries and the products of their eventual collapse, is very time-consuming, and the amount of details in the cave geometry is high. The workflow created can be used for forward modelling cave systems into paleokarst reservoirs which can be used to improve our understanding of such reservoirs, in particular with respect to production behaviour.

Several conclusions can be drawn from the work performed as a part of this thesis:

- Modelling the complexity of the natural paleokarst reservoir is faced by several shortcomings in the software available today. The greatest shortcoming is the lack of algorithms that allow complex shapes like cave systems to be integrated in modelling grids without performing substantial pre-processing of the input data. Also the incompatibility of needing continuous surfaces for capturing cave passage geometries extending over several stories and the requirement for using zones bounded by surfaces complicates the workflow substantially.
- The workflow created by Furnée (2015) produces a cave geometry with uniform passages, and the collapse of the cave is modelled by widening the radius of the cave passages. The cave geometry created by the workflow presented in this thesis is based on actual cave measurements, and results in a more natural looking cave and collapse geometry based on an understanding of how the collapse process operates.
- The degree of upscaling of the grid for simulation purposes is important. Results from the streamline simulations and drainage functions revealed that an upscaling of more than 4*4 meters will have a significant impact on the fluid flow through the reservoir. The upscaling of the cave facies causes this effect. If the grid increment is greater than 4*4 meter, the connection through the cave passages is lost, and the cave is ignored in the system.

- Time constraints precluded a full investigation of the fluid flow behaviour for the model, so only streamline simulation was used to perform a first assessment. The streamline simulations reveal that the fluids will follow the cave passages as long as they are oriented in a preferential direction, most likely with respect to the pressure field, if not they will follow the shortest path. Further simulation studies should be performed in Eclipse or another simulation tool, for more accurate simulation results.

6.1 Suggestions for further work

This study may be used as a basis for further work on the topic. The different challenges met during the modelling of the cave should be further investigated.

Further work on this topic is needed to create a less time-consuming workflow, and to be able to predict the behaviour of the fluids in the reservoir in a more precise way. The workflow presented in this thesis can hopefully be improved to solve some of the zonation issues that were encountered in the process. Several of the challenges met during the work on this thesis are caused by shortcomings in the RMS modelling software. If the improvements suggested in this thesis are dealt with, the workflow presented in the thesis will be much less extensive.

For more realistic reservoir models a range of real petrophysical data from known paleokarst reservoirs could be included in the model. This will make the results from the simulations more accurate, and provide a better understanding of the reservoir by testing flow responses to changes in petrophysical settings.

Simulation in Eclipse will provide a better understanding of the importance of the more detailed cave geometry, and the behaviour of the fluids during production. This will also allow comparison with the cave modelled by Furnée (2015) and establish the actual impact of employing detailed description of cave geometry in paleokarst reservoir models.

Finally, the model offers the opportunity to conduct seismic forward modelling, which could improve our ability to identify and interpret paleokarst features present, not recognized in seismic data.

7 REFERENCES

Bathurst, Robin GC (1976) *Carbonate sediments and their diagenesis*, Elsevier Science B.V.

Blickwede, Jon & Rosenfeld, Josh (2010) The Greatest Oil Well in History? The Story of Cerro Azul# 4. *AAPG bulletin*.

Boggs Jr, S. (2012) *Principles of sedimentology and stratigraphy*, Upper Saddle River, New Jersey, Pearson Education, Ltd.

Borghi, Andrea, Renard, Philippe & Jenni, Sandra (2012) A pseudo-genetic stochastic model to generate karstic networks. *Journal of Hydrology,* 414**,** 516-529.

Botton-Dumay, Roselyne, Manivit, Thierry, Massonnat, Gerard & Gay, Viviane (2002) Karstic high permeability layers: Characterization and Preservation while modeling carbonate reservoirs. *Abu Dhabi International Petroleum Exhibition and Conference.* Society of Petroleum Engineers.

Brigaud, Benjamin, Vincent, Benoît, Durlet, Christophe, Deconinck, Jean-François, Jobard, Emmanuel, Pickard, Neil, Yven, Béatrice & Landrein, Philippe (2014) Characterization and origin of permeability–porosity heterogeneity in shallow-marine carbonates: From core scale to 3D reservoir dimension (Middle Jurassic, Paris Basin, France). *Marine and Petroleum Geology,* 57**,** 631-651.

Brown, Alton (1997) Porosity variation in carbonates as a function of depth: Mississippian Madison Group, Williston Basin. *AAPG bulletin*.

Cartwright, Joe, Huuse, Mads & Aplin, Andrew (2007) Seal bypass systems. *AAPG bulletin,* 91**,** 1141-1166.

Choquette, Philip W. & James, Noel P. (1988) *Paleokarst,* Society of Economic, Paleontologists

Mineralogists. Midyear, Meeting, Springer-Verlag.

Dunham, Robert J (1962) Classification of carbonate rocks according to depositional textures. *AAPG bulletin*.

Erzeybek Balan, Selin (2012) Characterization and modeling of paleokarst reservoirs using multiple-point statistics on a non-gridded basis. *Faculty of the Graduate School.* The University of Texas as Austin.

Esteban, Mateu (1993) Introduction to karst systems and paleokarst reservoirs. *AAPG bulletin*.

Folk, Robert L (1959) Practical petrographic classification of limestones. *AAPG Bulletin,* 43**,** 1-38.

Ford, Derek (1988) Characteristics of dissolutional cave systems in carbonate rocks. *Paleokarst.* Springer.

Ford, Derek & Williams, Paul D. (2013) *Karst hydrogeology and geomorphology*, John Wiley & Sons.

Fournillon, F, Viseur, S, Arfib, B & Borgomano, J (2010) Insights of 3D geological modelling in distributed hydrogeological models of karstic carbonate aquifers. *Advances in Research in Karst Media.* Springer.

Furnée, Jon Petter Bjerkreim (2015) Geo-modeling and fluid flow simulation in paleokarst reservoirs. *Department of Earth Science, University of Bergen.*

Glover, JE (1968) Significance of stylolites in dolomitic limestones. *Nature,* 217**,** 835-836.
Halbouty, Michel T, Meyerhoff, Arthur Augustus, King, Robert E, Dott Sr, Robert H, Klemme, H Douglas & Shabad, Theodore (1970) World's giant oil and gas fields, geologic factors affecting their formation, and basin classification: Part I: Giant oil and gas fields. *AAPG bulletin*.
Ham, William E. & Pray, Lloyd C. (1962) Modern concepts and classifications of carbonate rocks. *AAPG bulletin*.
James, NP (1997) *The cool-water carbonate depositional realm*.
Kaiser, Mark J & Pulsipher, Allan G (2007) A review of the oil and gas sector in Kazakhstan. *Energy Policy,* 35**,** 1300-1314.
Kerans, Charles (1988) Karst-controlled reservoir heterogeneity in Ellenburger Group carbonates of west Texas. *AAPG bulletin,* 72**,** 1160-1183.
Lauritzen, SE (1996) Karst landforms and caves of Nordland, North Norway. *Guide for Excursion2, Climate Change: the Karst Record*.
Lauritzen, SE (2003) Grottolf.
Lauritzen, SE (2015) *Kompendium i Speleologi (Unpublished material),* Department of Earth Science, University of Bergen, Unpublished.
Lauritzen, Stein-Erik, Hestangen, Hilde, Skutlaberg, Sara M & Øvrevik, Rannveig (2005) The Grønli-Seter cave research project, Rana, North Norway. *Proceedings of the 14th International Congress of Speleology, Athen-Kalamos.*
Li, Jian, Zhang, Wenzheng, Luo, Xia & Hu, Guoyi (2008) Paleokarst reservoirs and gas accumulation in the Jingbian field, Ordos Basin. *Marine and Petroleum Geology,* 25**,** 401-415.
Loucks, Robert G. (1999) Paleocave carbonate reservoirs: origins, burial-depth modifications, spatial complexity, and reservoir implications. *AAPG bulletin,* 83**,** 1795-1834.
Loucks, Robert G. & Anderson, James H. (1985) Depositional facies, diagenetic terranes, and porosity development in Lower Ordovician Ellenburger Dolomite, Puckett field, west Texas. *Carbonate petroleum reservoirs.* Springer.
Lucia, F Jerry (1996) Structural and fracture implications of Franklin Mountains collapse brecciation. *PUBLICATIONS-WEST TEXAS GEOLOGICAL SOCIETY***,** 117-124.
Lucia, F Jerry (2007) *Carbonate reservoir characterization: an integrated approach*, Springer Science & Business Media.
Lucia, F. Jerry (1995) Lower Paleozoic cavern development, collapse, and dolomitization, Franklin Mountains, El Paso, Texas. *AAPG bulletin*.
Mazzullo, S. J. & Chilingarian, G. V. (1996) Hydrocarbon reservoirs in karsted carbonate rocks. *Developments in Petroleum Science,* 44**,** 797-865.
Moore, Clyde H. (1989) *Carbonate diagenesis and porosity*, Elsevier.
Murray, Raymond Carl (1960) Origin of porosity in carbonate rocks. *Journal of Sedimentary Research,* 30.
Nelson, Campbell S, Keane, Sandra L & Head, Philip S (1988) Non-tropical carbonate deposits on the modern New Zealand shelf. *Sedimentary geology,* 60**,** 71-94.
Nordeide, Hege Cecilie (2008) Spatial distribution and architecture of breccia pipes features at Wordiekammen, Billefjorden, Svalbard. *Department of Earth Science.* Master's Thesis, Department of Earth Science, University of Bergen.
Palmer, Arthur N. (1991) Origin and morphology of limestone caves. *Geological Society of America Bulletin,* 103**,** 1-21.
R. Ø. Skoglund, S.E Lauritzen (2005) Setergrotta kartleggingsdata.
ROXAR, 2013.1.2a (2016a) Upscaling Parameters.

ROXAR, 2013.1.2b (2016b) Geometric modelling.
ROXAR, 2013.1.2c (2016c) Fracture Modelling.
ROXAR, 2013.1.2d (2016d) Petrophysical modelling.
ROXAR, 2013.1.2e (2016e) Blocking of wells.
ROXAR, 2013.1.2f (2016f) Resampling parameters.
Schmoker, James W, Krystinik, Katherine B & Halley, Robert B (1985) Selected characteristics of limestone and dolomite reservoirs in the United States. *AAPG Bulletin,* 69**,** 733-741.
Schmoker, James W. & Halley, Robert B. (1982) Carbonate porosity versus depth: a predictable relation for south Florida. *AAPG Bulletin,* 66**,** 2561-2570.
Scholle, P. & Scholle D. (2014) Carbonate reservoir geology: Understanding Depositional and diagenetic factors for controlling porosity. *AAPG bulletin,* WEC 2014.
Shen, Feng, Qi, Lixin & Han, Gehua (2007) Characterization and preservation of karst networks in the carbonate reservoir modeling. *SPE Annual Technical Conference and Exhibition.* Society of Petroleum Engineers.
Smart, PL & Whitaker, FF (1991) Karst processes, hydrology, and porosity evolution. *Palaeokarsts and palaeokarstic reservoirs. Reading England, Postgraduate Research Institute for Sedimentology, University of Reading***,** 1-55.
Thrailkill, John (1968) Chemical and hydrologic factors in the excavation of limestone caves. *Geological Society of America Bulletin,* 79**,** 19-46.
Tinker, Scott W (1995) Reservoir characterization of a Permian giant: Yates field, west Texas. *AAPG bulletin*.
Trice, Robert (2005) Challenges And Insights In Optimising Oil Production Form Middle Eastern Karst Reservoirs. *SPE Middle East Oil and Gas Show and Conference.* Society of Petroleum Engineers.
Vacher, H Len & Mylroie, John E (2002) Eogenetic karst from the perspective of an equivalent porous medium. *Carbonates and Evaporites,* 17**,** 182-196.
Walkden, Gordon M. (1974) Palaeokarstic surfaces in upper Visean (Carboniferous) limestones of the Derbyshire Block, England. *Journal of Sedimentary Research,* 44.
Weinrich, Karen J & Sutphin, Hoyt B (1994) Grand Canyon caves, breccia pipes and mineral deposits. *Geology Today,* 10**,** 97-104.
White, Elizabeth L. & White, WIlliam B. (1969) Processes of cavern breakdown. *Nat. Spel. Soc. Bull,* 31**,** 83-96.
White, William Blaine (1988) *Geomorphology and hydrology of karst terrains*, Oxford university press New York.
Wilson, JL (1975) *Carbonate facies In geologic history*, New York, Springer-Verlag.
Xu, Kang, Yu, Bingsong, Gong, Hanning, Ruan, Zhuang, Pan, Yinglu & Ren, Yan (2015) Carbonate reservoirs modified by magmatic intrusions in the Bachu area, Tarim Basin, NW China. *Geoscience Frontiers,* 6**,** 779-790.
Øvrevik, Rannveig (2002) Hydrogeologi og karstkorrosjon i Grønli-Seterakviferen, Mo i Rana. *Department of Earth Science.* University of Bergen.

8 APPENDICES

8.1 Explanation of objects in RMS

CLIPBOARD

FOLDER	OBJECT	EXPLANATION
	Skeletonlines2000Points	Skeletonlines defining the middle of the cave shown as points
	XYZwallsImport	Imported wall coordinates from cave survey
	XYZfloorImport	Imported floor coordinates from cave survey
	XYZroofImport	Imported roof coordinates from cave survey
	XYZoctaImport	Imported octahedral coordinates from cave survey
	Boundary	Project boundary
	Boundary43up	Project boundary moved 43 meters up
	Boundary27down	Project boundary moved 27 meters down
	Skeletonlines	Skeletonlines of cave shown as lines
	Boundary73up	Project boundary moved 73 meters up
Polygons	Polygons_1-24	Polygons defining the walls of the cave passages, a total of 24 polygons were made
	AllPolygons	All polygons gathered
	PolygonsCave1	Polygons defining the walls of cave 1
	PolygonsCave2	Polygons defining the walls of cave 2
	PolygonsCave3	Polygons defining the walls of cave 3
MappedSurfaces	MappedSurfacesP1-24	Mapped surfaces made from the polygons, a total of 24 surfaces
	MappedSurfaces_Cave1	Mapped surfaces defining cave 1

	MappedSurfaces_Cave2	Mapped surfaces defining cave 2
	MappedSurfaces_Cave3	Mapped surfaces defining cave 3
Points_Cave1	PointsXYZ_Cave1_Roof	Filtered points defining the roof for cave 1
	PointsXYZ_Cave1_Floor	Filtered points defining the floor for cave 1
Points_Cave2	PointsXYZ_Cave2_roof	Filtered points defining the roof for cave 2
	PointsXYZ_Cave2_floor	Filtered points defining the floor for cave 2
Points_Cave3	PointsXYZ_Cave3_roof	Filtered points defining the roof for cave 3
	PointsXYZ_Cave3_floor	Filtered points defining the floor for cave 3
FolderIsochores		
Iso_Cave1	InterpolatedSurface_Cave1	Surface defining the new collapsed floor of cave 1, made from interpolation operation
	BoundaryInterpolated_Cave1	Boundary made around the interpolated surface for cave 1
	Below_Cave1_roof	Isochore made between cave 1 roof and floor and cut by the interpolated boundary
	isoCave1export	Isochore points imported from Excel after editing the points to match the collapse of the cave
Iso_Cave3	InterpolatedSurface_Cave3	Surface defining the new collapsed floor of cave 3, made from interpolation operation
	BoundaryInterpolated_Cave3	Boundary made around the interpolated surface for cave 3
	Below_Cave3_roof	Isochore made between cave 3 roof and floor and cut by the interpolated boundary
	isoCave3export	Isochore points imported from Excel after editing the points to match the collapse of the cave
Iso_Cave2	interpolatedSurface_Cave2	Surface defining the new collapsed floor of cave 2, made from interpolation operation
	BoundaryInterpolated_Cave2	Boundary made around the interpolated surface for cave 2
	Below_Cave2_roof	Isochore made between cave 2 roof and floor and cut by the interpolated boundary
	Iso_Cave2export	Isochore points imported from Excel after editing the points to

		match the collapse of the cave
PointsAndHorizonsOriginal	PointsXYZ_Cave1_RoofOriginal	Original points from cave 1, these had to be edited to avoid that the roof cut the floor
	Cave1_roof_OriginalSurface	Original cave 1 roof surface

GRID MODELS

FOLDER	OBJECT	EXPLANATION
Grid_Cave3_Original	Grid	
	GeometricAVBS_Cave3_Original	Geometric model for original cave 3, AVBS = Assign Values Between Surfaces
Grid_Cave1_Original	Grid	
	GeometricAVBS_Cave1_Original	Geometric model for original cave 1, AVBS = Assign Values Between Surfaces
Grid_Cave2_Original	Grid	
	GeometricAVBS_Cave2_Original	Geometric model for original cave 2, AVBS = Assign Values Between Surfaces
Grid_AllCaves_Original	Grid	
	Res_GeometricAVBS_Cave3_Original	Resampled geometric model for cave 3
	Res_GeometricAVBS_Cave1_Original	Resampled geometric model for cave 1
	Res_GeometricAVBS_Cave2_Original	Resampled geometric model for cave 2
	Merged_Cave1andCave3	Merged parameter containing geometric models from cave 1 and cave 3
	Merged_AllCaves_Original	Discrete Merged parameter containing the whole original cave with the facies Cave and No cave
	Zone	Discrete parameter defining the different zones in the grid.
Grid_Cave1_Collapsed	Grid	
	GeometricAVBS_Cave1_Collapsed	Geometric model for collapsed cave 1, AVBS = Assign Values Between Surfaces

Grid_Cave3_Collapsed	Grid	
	GeometricAVBS_Cave3_ Collapsed	Geometric model for collapsed cave 3, AVBS = Assign Values Between Surfaces
Grid_Cave2_Collapsed	Grid	
	GeometricAVBS_Cave2_ Collapsed	Geometric model for collapsed cave 2, AVBS = Assign Values Between Surfaces
Grid_AllCaves_ Collapsed	Grid	
	BW	Blocked wells for streamline simulations
	Zone	Discrete parameter defining the different zones in the grid.
	Res_GeometricAVBS_ Cave1_Collapsed	Resampled geometric model for cave 1, collapsed
	Res_GeometricAVBS_ Cave3_Collapsed	Resampled geometric model for cave 3, collapsed
	Res_GeometricAVBS_Cav e2_Collapsed	Resampled geometric model for cave 2, collapsed
	MergedCave1andCave3_ Collapsed	Merged parameter containing geometric models from cave 1 and cave 3, collapsed
	MergedAllCollapsed	Discrete Merged parameter containing the whole collapsed cave with the facies Cave and No cave
	Job1_PORO	Porosity created by the petrophysical modelling tool
	Job1_PERMX	Permeability in the X and Y direction created by the petrophysical modelling tool
	Job1_PERMZ	Permeability in the Z direction created by the petrophysical modelling tool
	SimboxLayer_Zone4	Simbox layer parameter filtered on zone 4
	Cave1Trend	Trend parameter for cave 1 created with the use of the simboxLayer_Zone4 parameter. Used as input for the petrophysical modelling
	SimboxLayer_Zone6	Simbox layer parameter filtered on zone 6
	Cave2Trend	Trend parameter for cave 2 created with the use of the simboxLayer_Zone6 parameter. Used as input for the petrophysical modelling

	SimboxLayer_Zone2	Simbox layer parameter filtered on zone 2
	Cave3Trend	Trend parameter for cave 3 created with the use of the simboxLayer_Zone2 parameter. Used as input for the petrophysical modelling
	Density1	Density parameter used as input for fracture model
	FRAC_15	Fracture 15 parameter used as input for fracture model
	FRAC_90	Fracture 90 parameter used as input for fracture model
	FRAC_170	Fracture 170 parameter used as input for fracture model
	FracturePorosity	Fracture porosity created from the dual- porosity modelling tool
	PermI	Permeability parameter containing fracture permeability created by the single-porosity modelling tool. Used as input for streamline simulations
	PermJ	Permeability parameter containing fracture permeability created by the single-porosity modelling tool. Used as input for streamline simulations
	PORO_FRAC	Porosity parameter combined with the FracturePorosity parameter. Used as input for streamline simulations
	illustration	Parameter used for illustration purposes
	Oil_bulk	Parameter created by the volumetric calculations
	Oil_Net	Parameter created by the volumetric calculations
	Oil_pore	Parameter created by the volumetric calculations
	Oil_HCPV	Parameter created by the volumetric calculations
	STOIIP	Parameter created by the volumetric calculations
	Discrete_fluid	Parameter created by the volumetric calculations

For the upscaled grids, the same parameters are resampled, and streamline simulations and volumetric calculations are produced for the grids.

8.2 Detailed workflow from RMS

8.2.1 Workflow for Original cave

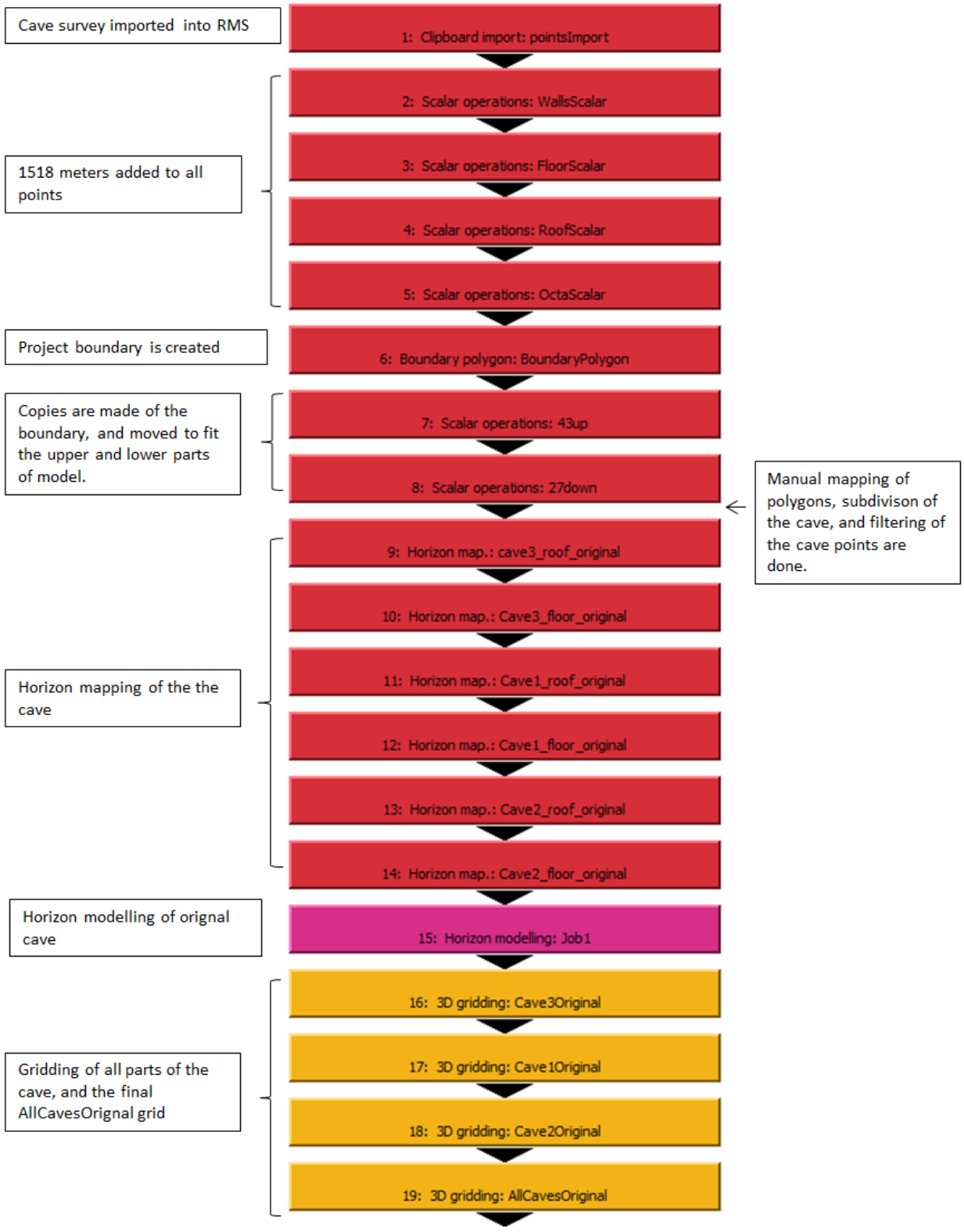

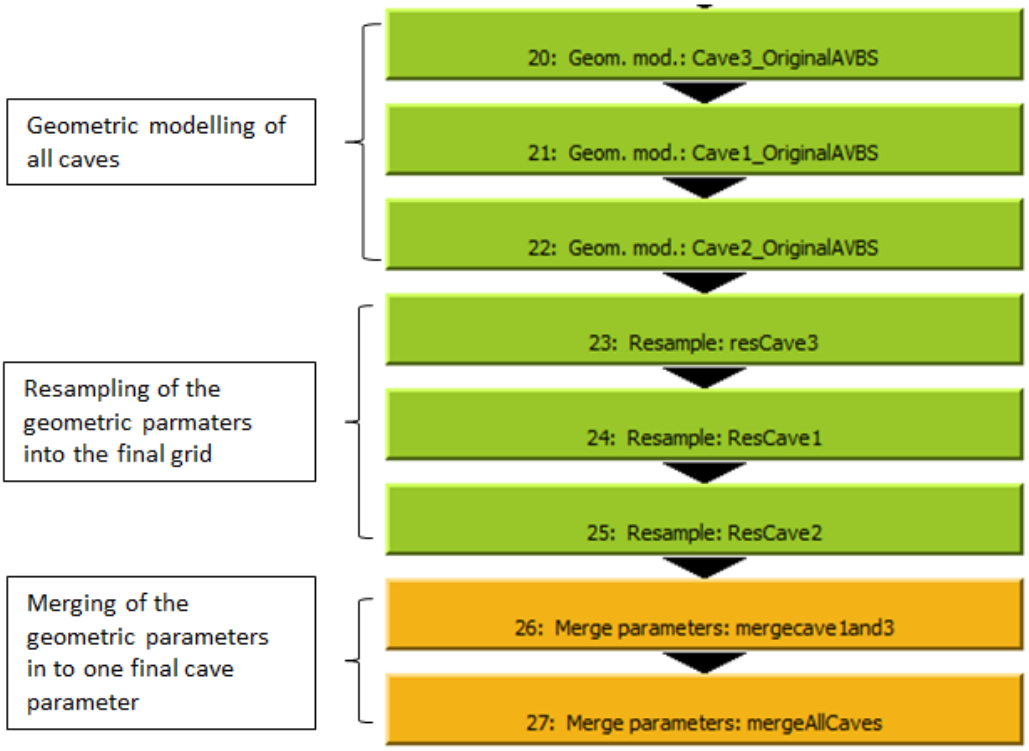
Geometric modelling of all caves
20: Geom. mod.: Cave3_OriginalAVBS
21: Geom. mod.: Cave1_OriginalAVBS
22: Geom. mod.: Cave2_OriginalAVBS
Resampling of the geometric parmaters into the final grid
23: Resample: resCave3
24: Resample: ResCave1
25: Resample: ResCave2
Merging of the geometric parameters in to one final cave parameter
26: Merge parameters: mergecave1and3
27: Merge parameters: mergeAllCaves

8.2.2 Workflow for Collapsed cave

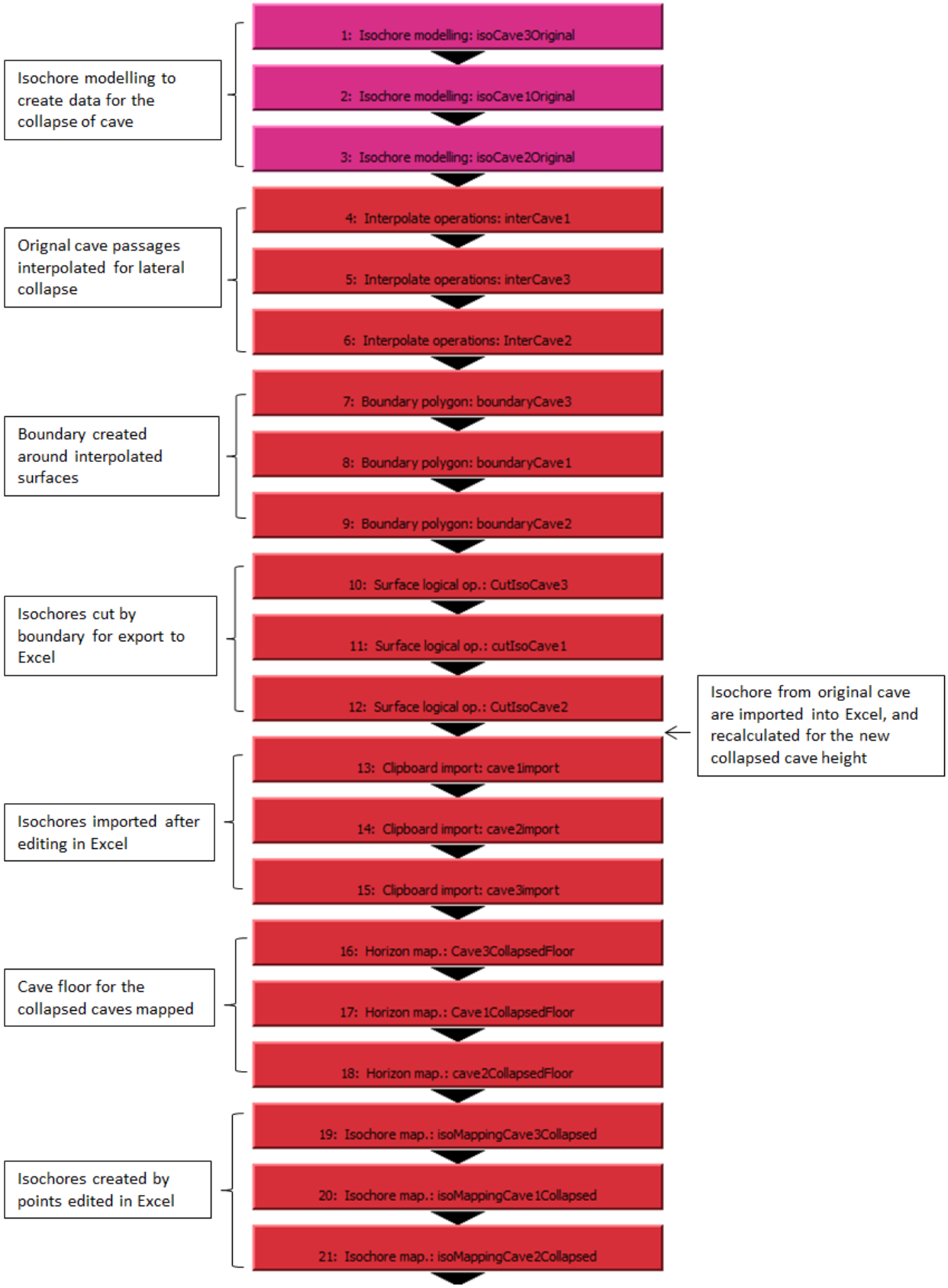

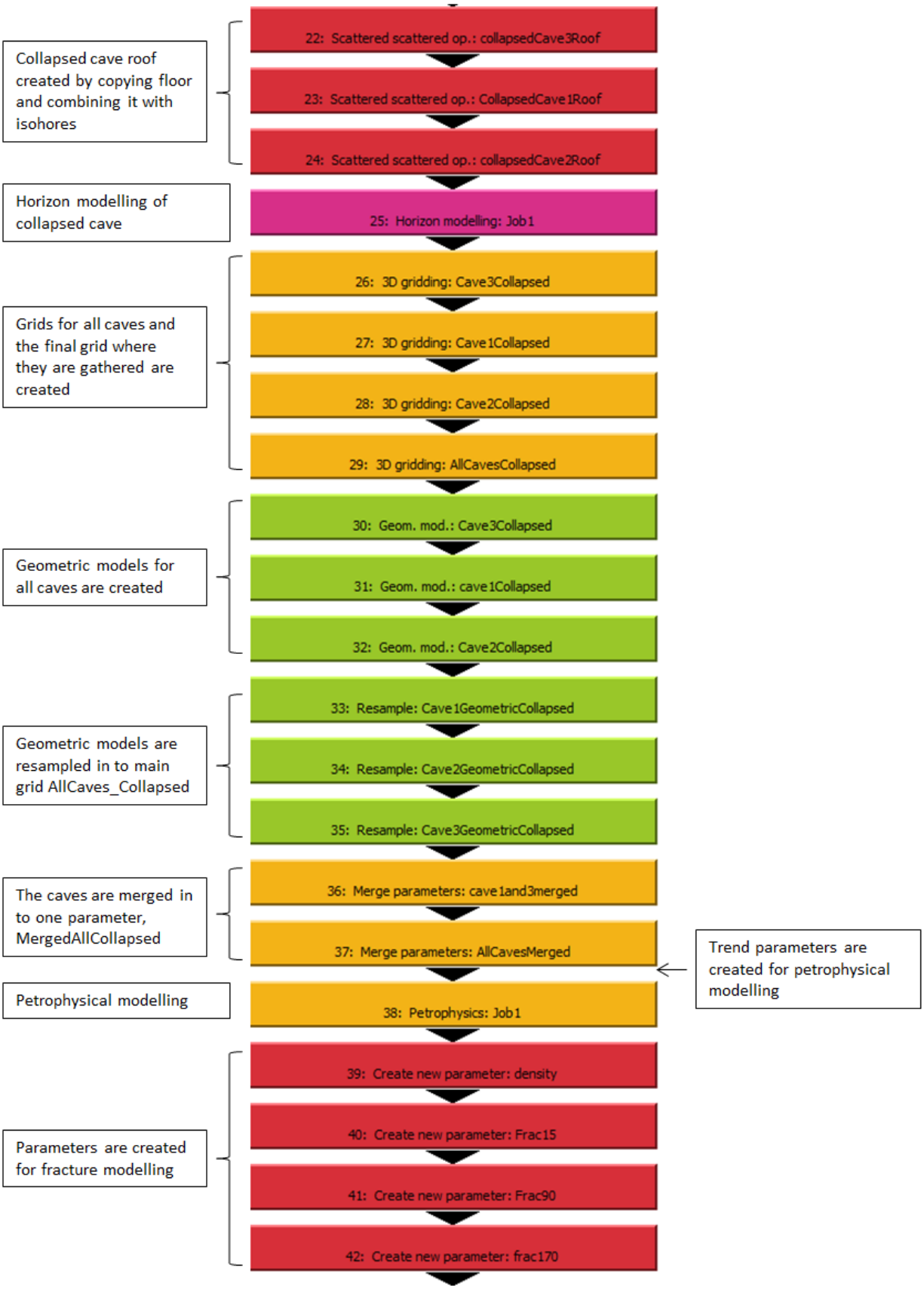
Collapsed cave roof created by copying floor and combining it with isohores
22: Scattered scattered op.: collapsedCave3Roof
23: Scattered scattered op.: CollapsedCave1Roof
24: Scattered scattered op.: collapsedCave2Roof
Horizon modelling of collapsed cave
25: Horizon modelling: Job1
Grids for all caves and the final grid where they are gathered are created
26: 3D gridding: Cave3Collapsed
27: 3D gridding: Cave1Collapsed
28: 3D gridding: Cave2Collapsed
29: 3D gridding: AllCavesCollapsed
Geometric models for all caves are created
30: Geom. mod.: Cave3Collapsed
31: Geom. mod.: cave1Collapsed
32: Geom. mod.: Cave2Collapsed
Geometric models are resampled in to main grid AllCaves_Collapsed
33: Resample: Cave1GeometricCollapsed
34: Resample: Cave2GeometricCollapsed
35: Resample: Cave3GeometricCollapsed
The caves are merged in to one parameter, MergedAllCollapsed
36: Merge parameters: cave1and3merged
37: Merge parameters: AllCavesMerged
Trend parameters are created for petrophysical modelling
Petrophysical modelling
38: Petrophysics: Job1
Parameters are created for fracture modelling
39: Create new parameter: density
40: Create new parameter: Frac15
41: Create new parameter: Frac90
42: Create new parameter: frac170

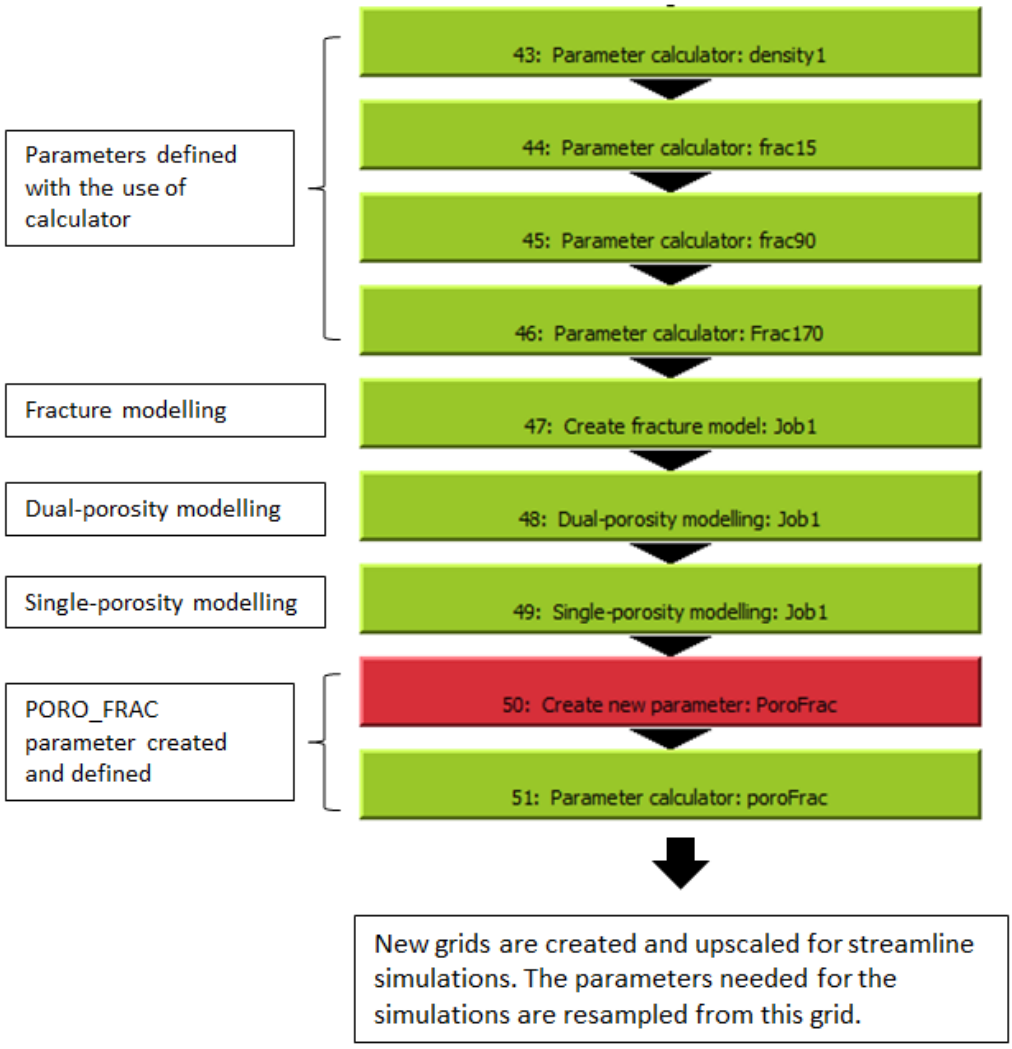
43: Parameter calculator: density1
44: Parameter calculator: frac15
45: Parameter calculator: frac90
46: Parameter calculator: Frac170
Parameters defined with the use of calculator
47: Create fracture model: Job1
Fracture modelling
48: Dual-porosity modelling: Job1
Dual-porosity modelling
49: Single-porosity modelling: Job1
Single-porosity modelling
50: Create new parameter: PoroFrac
51: Parameter calculator: poroFrac
PORO_FRAC parameter created and defined
New grids are created and upscaled for streamline simulations. The parameters needed for the simulations are resampled from this grid.

8.3 Screenshots from petrophysical modelling

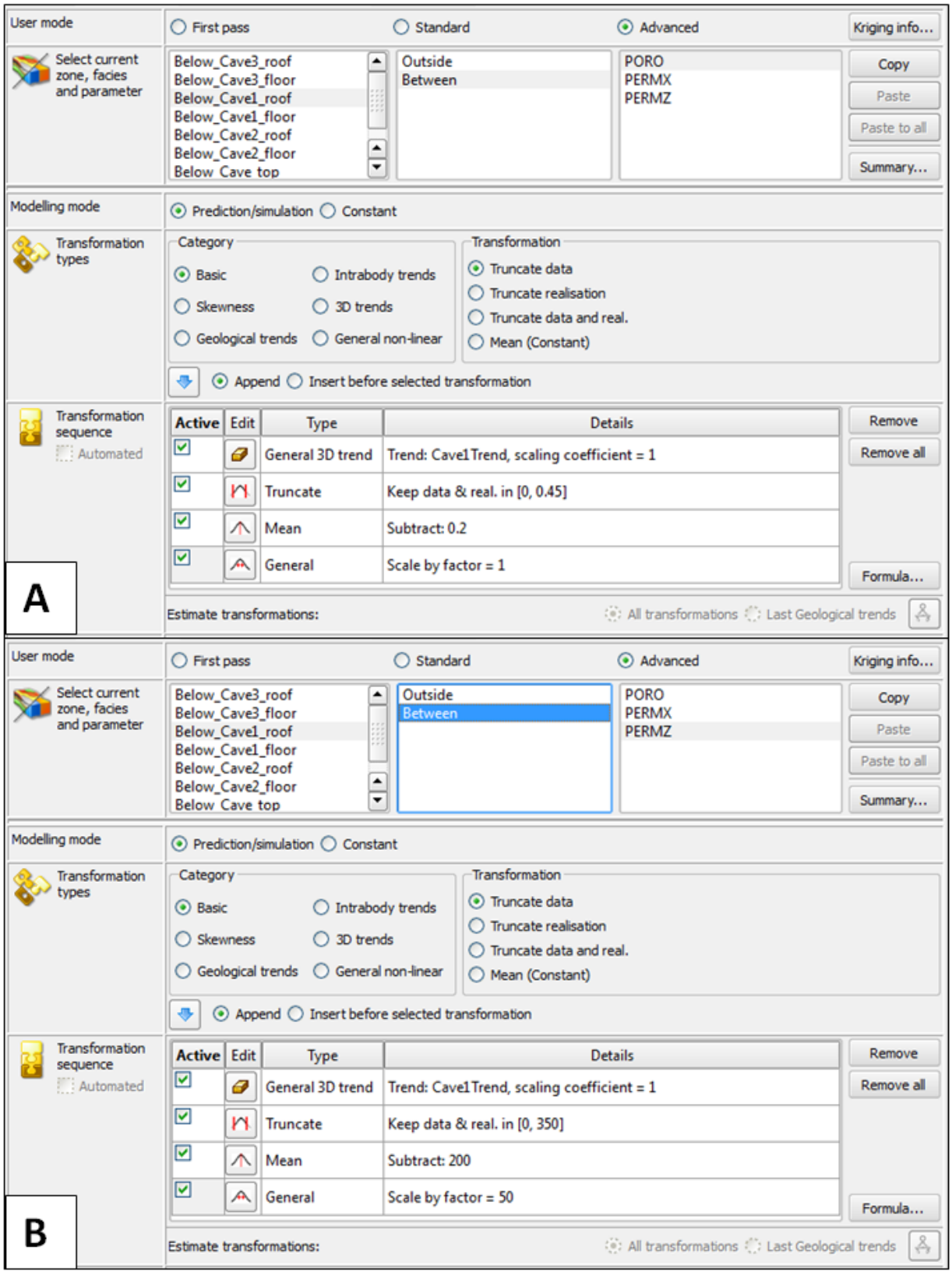

Figure 8.3-1: The distribution set-up for the petrophysical modelling fro Cave facies in the zone containing cave 1. A is the set-up for the porosity (PORO) and B is the set-up for the permeability in Z direction (PERMZ)

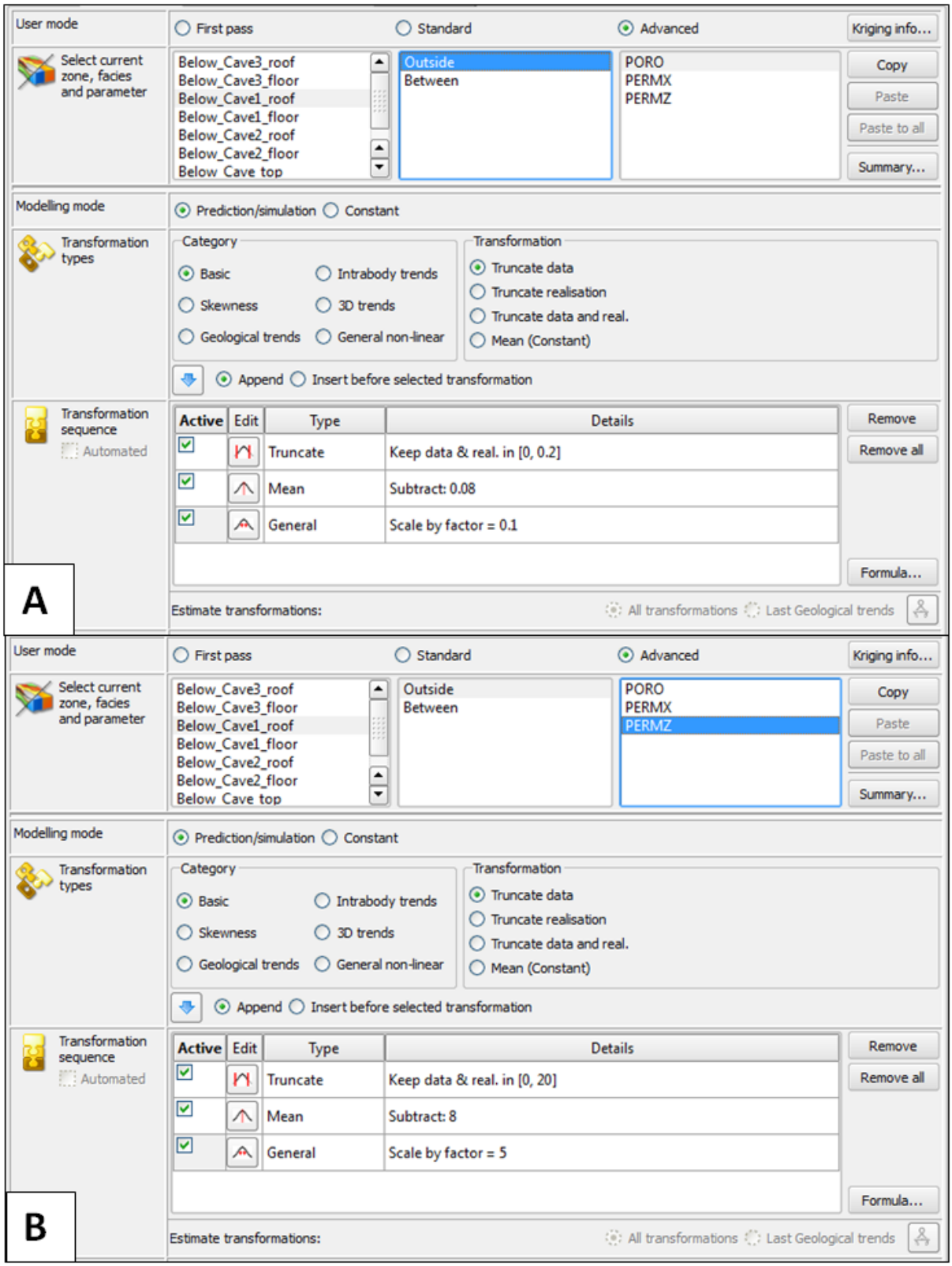

Figure 8.3-2: The distribution set-up for the petrophysical modelling for No Cave facies in the zone containing cave 1. A is the set-up for the porosity (PORO) and B is the set-up for the permeability in Z direction (PERMZ)

8.4 Streamline report files

8.4.1 Streamline report files for Grid_Upscaled2

```
******************************************************
Report File for Streamline Job: Job1
******************************************************

***************** Model Parameters *********************
Reference pressure:    200 bar
Reference depth   :    2000 m
Fluid viscosity   :    0.25 cP
Fluid compressibility: 0.0001 /bar
Rock compressibility:  1e-05 /bar
Solution time:         1 d

Porosity:        res_PORO_FRAC
Net/Gross:               1
Permeability X:          res_PermI
Permeability Y:          res_PermJ
Permeability Z:          res_Job1_PERMZ

********************** Well input ********************

--      Well       Type    State  Rate (m3/d) Bhp (bar)
     Producer    PRODUCER   OPEN    1000       160
-- Completions:
--         I      J      K    Direction
        13    247      1      K
        13    247      2      K
        13    247      3      K
        13    247      4      K
        13    247      5      K
        13    247      6      K
        13    247      7      K
        13    247      8      K
        13    247      9      K
        13    247     10      K
        13    247     11      K
        13    247     12      K
        13    247     23      K
        13    247     24      K
        13    247     25      K
        13    247     26      K
        13    247     27      K
        13    247     28      K
```

```
      13   247   29    K
      13   247   30    K
      13   247   31    K
      13   247   32    K
      13   247   33    K
      13   247   34    K
      13   247   35    K
      13   247   36    K
      13   247   37    K
      13   247   38    K
      13   247   39    K
      13   247   40    K
      13   247   41    K
      13   247   42    K
      13   247   43    K
      13   247   44    K
      13   247   45    K
      13   247   46    K
      13   247   47    K
      13   247   48    K
      13   247   49    K
      13   247   50    K
      13   247   51    K
      13   247   52    K
      13   247   53    K
      13   247   54    K

--    Well      Type    State  Rate (m3/d) Bhp (bar)
    Injector   INJECTOR  OPEN    1000       260
-- Completions:
--       I     J     K   Direction
      212     9     1     K
      212     9     2     K
      212     9     3     K
      212     9     4     K
      212     9     5     K
      212     9     6     K
      212     9     7     K
      212     9     8     K
      212     9     9     K
      212     9    10     K
      212     9    11     K
      212     9    12     K
      212     9    23     K
      212     9    24     K
      212     9    25     K
      212     9    26     K
      212     9    27     K
      212     9    28     K
```

```
      212    9    29    K
      212    9    30    K
      212    9    31    K
      212    9    32    K
      212    9    33    K
      212    9    34    K
      212    9    35    K
      212    9    36    K
      212    9    37    K
      212    9    38    K
      212    9    39    K
      212    9    40    K
      212    9    41    K
      212    9    42    K
      212    9    43    K
      212    9    44    K
      212    9    45    K
      212    9    46    K
      212    9    47    K
      212    9    48    K
      212    9    49    K
      212    9    50    K
      212    9    51    K
      212    9    52    K
      212    9    53    K
      212    9    54    K


********** Results **********
Number of open injectors: 1
Total injection rate    : 1000 rm3/d

Number of open producers: 1
Total production rate   : 415.078 rm3/d

********** Well status **********

--      Well       Type    State  Rate (m3/d) Bhp (bar)
     Producer    PRODUCER   OPEN  415.078       160
     Injector    INJECTOR   OPEN    1000     257.68


********** Table of Break through times  **********

Producer: Producer      Injector        BT-time
                        Injector        19346.2

**************************************************
```

8.4.2 Streamline report files for Grid_Upscaled4

```
**************************************************
Report File for Streamline Job: Job1
**************************************************

********** Model Parameters **********
Reference pressure:    200 bar
Reference depth   :    2000 m
Fluid viscosity   :    0.25 cP
Fluid compressibility: 0.0001 /bar
Rock compressibility:  1e-05 /bar
Solution time:         1 d

Porosity:        res_PORO_FRAC
Net/Gross:               1
Permeability X:          res_PermI
Permeability Y:          res_PermJ
Permeability Z:          res_Job1_PERMZ

********** Well input **********

--      Well       Type    State  Rate (m3/d) Bhp (bar)
      Producer   PRODUCER   OPEN    1000       160
-- Completions:
--        I     J     K    Direction
          7   124     1      K
          7   124     2      K
          7   124     3      K
          7   124     4      K
          7   124     5      K
          7   124     6      K
          7   124     7      K
          7   124     8      K
          7   124     9      K
          7   124    10      K
          7   124    11      K
          7   124    12      K
          7   124    23      K
          7   124    24      K
          7   124    25      K
          7   124    26      K
          7   124    27      K
          7   124    28      K
          7   124    29      K
          7   124    30      K
          7   124    31      K
          7   124    32      K
          7   124    33      K
```

```
      7   124    34    K
      7   124    35    K
      7   124    36    K
      7   124    37    K
      7   124    38    K
      7   124    39    K
      7   124    40    K
      7   124    41    K
      7   124    42    K
      7   124    43    K
      7   124    44    K
      7   124    45    K
      7   124    46    K
      7   124    47    K
      7   124    48    K
      7   124    49    K
      7   124    50    K
      7   124    51    K
      7   124    52    K
      7   124    53    K
      7   124    54    K

--     Well      Type    State  Rate (m3/d) Bhp (bar)
    Injector   INJECTOR  OPEN    1000       260
-- Completions:
--       I     J     K   Direction
      107     5     1     K
      107     5     2     K
      107     5     3     K
      107     5     4     K
      107     5     5     K
      107     5     6     K
      107     5     7     K
      107     5     8     K
      107     5     9     K
      107     5     10    K
      107     5     11    K
      107     5     12    K
      107     5     23    K
      107     5     24    K
      107     5     25    K
      107     5     26    K
      107     5     27    K
      107     5     28    K
      107     5     29    K
      107     5     30    K
      107     5     31    K
      107     5     32    K
      107     5     33    K
```

```
      107     5    34     K
      107     5    35     K
      107     5    36     K
      107     5    37     K
      107     5    38     K
      107     5    39     K
      107     5    40     K
      107     5    41     K
      107     5    42     K
      107     5    43     K
      107     5    44     K
      107     5    45     K
      107     5    46     K
      107     5    47     K
      107     5    48     K
      107     5    49     K
      107     5    50     K
      107     5    51     K
      107     5    52     K
      107     5    53     K
      107     5    54     K


********** Results **********
Number of open injectors: 1
Total injection rate    : 1000 rm3/d

Number of open producers: 1
Total production rate   : 405.588 rm3/d

********** Well status **********

--     Well       Type    State  Rate (m3/d) Bhp (bar)
     Producer    PRODUCER   OPEN  405.588       160
     Injector    INJECTOR   OPEN    1000    257.706


********** Table of Break through times  **********

Producer: Producer      Injector        BT-time
                Injector        25185.7

**************************************************
```

8.4.3 Streamline report files for Grid_Upscaled6

```
**************************************************
Report File for Streamline Job: Job1
**************************************************
```

********** Model Parameters **********
Reference pressure: 200 bar
Reference depth : 2000 m
Fluid viscosity : 0.25 cP
Fluid compressibility: 0.0001 /bar
Rock compressibility: 1e-05 /bar
Solution time: 1 d

Porosity: res_PORO_FRAC
Net/Gross: 1
Permeability X: res_PermI
Permeability Y: res_PermJ
Permeability Z: res_Job1_PERMZ

********** Well input **********

-- Well Type State Rate (m^3/d) Bhp (bar)
Producer PRODUCER OPEN 1000 160
-- Completions:
-- I J K Direction
5 83 1 K
5 83 2 K
5 83 3 K
5 83 4 K
5 83 5 K
5 83 6 K
5 83 7 K
5 83 8 K
5 83 9 K
5 83 10 K
5 83 11 K
5 83 12 K
5 83 23 K
5 83 24 K
5 83 25 K
5 83 26 K
5 83 27 K
5 83 28 K
5 83 29 K
5 83 30 K
5 83 31 K
5 83 32 K
5 83 33 K
5 83 34 K
5 83 35 K
5 83 36 K
5 83 37 K
5 83 38 K

```
      5    83    39    K
      5    83    40    K
      5    83    41    K
      5    83    42    K
      5    83    43    K
      5    83    44    K
      5    83    45    K
      5    83    46    K
      5    83    47    K
      5    83    48    K
      5    83    49    K
      5    83    50    K
      5    83    51    K
      5    83    52    K
      5    83    53    K
      5    83    54    K

--    Well      Type    State  Rate (m3/d) Bhp (bar)
    Injector  INJECTOR  OPEN    1000       260
-- Completions:
--      I     J     K   Direction
      71    3     1     K
      71    3     2     K
      71    3     3     K
      71    3     4     K
      71    3     5     K
      71    3     6     K
      71    3     7     K
      71    3     8     K
      71    3     9     K
      71    3     10    K
      71    3     11    K
      71    3     12    K
      71    3     23    K
      71    3     24    K
      71    3     25    K
      71    3     26    K
      71    3     27    K
      71    3     28    K
      71    3     29    K
      71    3     30    K
      71    3     31    K
      71    3     32    K
      71    3     33    K
      71    3     34    K
      71    3     35    K
      71    3     36    K
      71    3     37    K
      71    3     38    K
```

```
      71    3    39    K
      71    3    40    K
      71    3    41    K
      71    3    42    K
      71    3    43    K
      71    3    44    K
      71    3    45    K
      71    3    46    K
      71    3    47    K
      71    3    48    K
      71    3    49    K
      71    3    50    K
      71    3    51    K
      71    3    52    K
      71    3    53    K
      71    3    54    K


********** Results **********
Number of open injectors: 1
Total injection rate    : 317.078 rm3/d

Number of open producers: 1
Total production rate   : 188.147 rm3/d

********** Well status **********

--     Well      Type    State  Rate (m3/d) Bhp (bar)
     Producer    PRODUCER   OPEN  188.147       160
     Injector    INJECTOR   OPEN  317.078       260


********** Table of Break through times  **********

Producer: Producer      Injector        BT-time
                Injector        775.369

**************************************************
```

8.5 Tables for drainage functions

UPSC2	Time	Producer	UPSC4	Time	Producer	UPSC6	Time	Producer
	4,40E-05	0,00030633		0,00	0,00		0,00	0,01
	37,245	18091		37,25	18473,00		37,25	19043,00
	74,49	26096		74,49	26697,00		74,49	32464,00
	111,73	32077		111,73	32784,00		111,74	44952,00
	148,98	36991		148,98	37716,00		148,98	56862,00
	186,22	41035		186,22	41762,00		186,23	67433,00
	223,47	44515		223,47	45104,00		223,47	77219,00
	260,71	47568		260,71	48222,00		260,71	86194,00
	297,96	50265		297,96	50950,00		297,96	94842,00
	335,2	52663		335,20	53496,00		335,20	103400,00
	372,45	54917		372,45	55546,00		372,45	111620,00
	409,69	56842		409,69	57532,00		409,69	119650,00
	446,94	58594		446,94	59269,00		446,94	127420,00
	484,18	60321		484,18	61141,00		484,18	135210,00
	521,43	61860		521,43	62847,00		521,43	142440,00
	558,67	63307		558,67	64425,00		558,67	149330,00
	595,92	64697		595,92	65714,00		595,92	156390,00
	633,16	66057		633,16	67067,00		633,16	163980,00
	670,41	67343		670,41	68191,00		670,41	171620,00
	707,65	68526		707,65	69437,00		707,65	179580,00
	744,9	69667		744,90	70483,00		744,90	187150,00
	782,14	70780		782,14	71548,00		782,14	195340,00
	819,39	71762		819,39	72547,00		819,39	203090,00
	856,63	72786		856,63	73558,00		856,63	210520,00
	893,88	73717		893,88	74514,00		893,88	218600,00
	931,12	74645		931,12	75594,00		931,12	226430,00
	968,37	75569		968,37	76465,00		968,37	234980,00
	1005,6	76400		1005,60	77392,00		1005,60	242740,00
	1042,9	77255		1042,90	78277,00		1042,90	250860,00
	1080,1	78046		1080,10	79107,00		1080,10	258190,00
	1117,3	78789		1117,30	79933,00		1117,30	265730,00
	1154,6	79557		1154,60	80685,00		1154,60	273170,00
	1191,8	80276		1191,80	81454,00		1191,80	280080,00
	1229,1	80963		1229,10	82088,00		1229,10	286750,00
	1266,3	81659		1266,30	82825,00		1266,30	292820,00
	1303,6	82274		1303,60	83527,00		1303,60	298400,00
	1340,8	82947		1340,80	84147,00		1340,80	303690,00
	1378,1	83614		1378,10	84819,00		1378,10	308620,00
	1415,3	84229		1415,30	85406,00		1415,30	313520,00
	1452,6	84837		1452,60	86052,00		1452,60	317270,00
	1489,8	85447		1489,80	86726,00		1489,80	321090,00
	1527	85996		1527,00	87272,00		1527,00	324510,00
	1564,3	86561		1564,30	87853,00		1564,30	327620,00
	1601,5	87093		1601,50	88374,00		1601,50	330540,00
	1638,8	87642		1638,80	88976,00		1638,80	333020,00
	1676	88168		1676,00	89530,00		1676,00	335310,00
	1713,3	88699		1713,30	90072,00		1713,30	337320,00
	1750,5	89199		1750,50	90579,00		1750,50	339210,00
	1787,8	89678		1787,80	91131,00		1787,80	340610,00
	1825	90135		1825,00	91612,00		1825,00	341890,00

Table for drainage of the reservoir for each grid after 5 years. Function can be found in chapter 5.3.3.

UPSC2	Time	Producer	UPSC4	Time	Producer	UPSC6	Time	Producer
	0,0000	0,0003		0,0002	0,0022		0,0007	0,0115
	0,0001	0,0000		0,0003	0,0000		0,0012	0,0000
	0,0001	0,0010		0,0006	0,0029		0,0021	0,0000
	0,0003	0,0003		0,0010	0,0026		0,0035	0,0000
	0,0005	0,0013		0,0018	0,0026		0,0061	0,4259
	0,0009	0,0011		0,0032	4,5560		0,0104	4,0364
	0,0016	0,2040		0,0057	1,2019		0,0178	4,8796
	0,0028	0,5501		0,0100	2,9083		0,0305	10,3010
	0,0051	3,4680		0,0175	16,9640		0,0523	23,4710
	0,0093	6,3191		0,0308	26,3340		0,0896	50,9900
	0,0169	14,2300		0,0542	36,8440		0,1535	46,8530
	0,0306	16,2330		0,0954	71,7290		0,2629	93,4240
	0,0554	43,8840		0,1678	132,1400		0,4503	120,4700
	0,1004	61,7250		0,2952	139,3900		0,7713	249,1700
	0,1820	112,5400		0,5192	270,4500		1,3212	378,4600
	0,3299	166,1000		0,9134	433,3000		2,2630	621,2000
	0,5980	277,2300		1,6068	733,0900		3,8761	1 110,8000
	1,0840	535,3100		2,8266	1 086,0000		6,6392	1 684,1000
	1,9649	906,9300		4,9724	1 787,9000		11,3720	2 750,1000
	3,5616	1 418,0000		8,7473	2 555,8000		19,4780	4 379,3000
	6,4559	2 255,1000		15,3880	3 629,5000		33,3630	5 955,4000
	11,7020	3 173,8000		27,0700	4 365,3000		57,1450	8 633,8000
	21,2120	4 193,4000		47,6200	5 804,3000		97,8800	14 504,0000
	38,4500	5 204,6000		83,7710	7 179,1000		167,6500	21 612,0000
	69,6960	6 854,4000		147,3700	9 261,1000		287,1600	30 405,0000
	126,3300	8 893,9000		259,2400	10 547,0000		491,8600	43 997,0000
	229,0000	10 855,0000		456,0500	11 651,0000		842,4800	71 192,0000
	415,1000	12 109,0000		802,2600	12 350,0000		1 443,0000	108 470,0000
	752,4200	12 801,0000		1 411,3000	13 264,0000		2 471,7000	35 102,0000
	1 363,9000	13 461,0000		2 482,7000	13 904,0000		4 233,6000	3 490,7000
	2 472,2000	13 986,0000		4 367,5000	14 105,0000		7 251,4000	736,3400
	4 481,2000	14 512,0000		7 683,1000	15 290,0000		12 421,0000	380,0100
	8 122,9000	15 368,0000		13 516,0000	15 953,0000		21 274,0000	148,1500
	14 724,0000	17 126,0000		23 776,0000	18 476,0000		36 439,0000	184,5000
	26 689,0000	21 491,0000		41 827,0000	37 214,0000		62 415,0000	88,6130
	48 378,0000	40 226,0000		73 580,0000	57 522,0000		106 910,0000	42,5370
	87 693,0000	53 761,0000		129 440,0000	62 998,0000		183 110,0000	34,4840
	158 960,0000	65 597,0000		227 700,0000	23 683,0000		313 640,0000	5,2513
	288 130,0000	24 601,0000		400 570,0000	4 945,6000		537 220,0000	30,3570
	522 280,0000	3 696,3000		704 660,0000	1 009,3000		920 170,0000	14,4850
	946 700,0000	574,1300		1 239 600,0000	261,8100		1 576 100,0000	10,2770
	1 716 000,0000	148,2700		2 180 700,0000	142,1200		2 699 600,0000	29,7010
	3 110 600,0000	53,7990		3 836 100,0000	74,5950		4 624 000,0000	15,4900
	5 638 400,0000	53,4590		6 748 400,0000	60,5620		7 920 200,0000	4,2044
	10 220 000,0000	26,6450		11 871 000,0000	39,3480		13 566 000,0000	47,4950
	18 526 000,0000	20,8820		20 884 000,0000	33,1160		23 236 000,0000	26,0840
	33 581 000,0000	21,2890		36 738 000,0000	26,6010		39 800 000,0000	35,7830
	60 870 000,0000	15,2910		64 628 000,0000	10,1420		68 171 000,0000	42,2870
	110 340 000,0000	0,0001		113 690 000,0000	13,1800		116 770 000,0000	43,5630
	200 000 000,0000	1,8711		200 000 000,0000	7,3582		200 000 000,0000	38,2480

Table for maximum drainage of reservoir for each grid, function can be found in chapter 5.3.3

8.6 Volumetrics report files

8.6.1 Volumetric report files for Grid_Upscaled2

VOLUME CALCULATION FOR : Masterprosjekt20.10preworkflow

Date : 2016.10.22 13:57:38

CALCULATED WITH RMS VOLUMETRIC

User : kle069

Platform :

Project file name : E:\KARINA\Masterprosjekt20.10preworkflow

Report file name : E:\KARINA\Volumetrics files\volumeCalculationsUpscaled2_1.txt

Volume name : Grid_Upscaled2

No. of licences : 0

No. of zones : 5

No. of facies codes : 0

No. of regions : 0

Grouped by : Zone/

UNITS:

Input unit (XY) : metre

Input unit (Z) : metre

Output unit, reservoir : cubic metre

Output unit, surface oil : st. cubic metre

FORMATION PARAMETER VALUES:

Net/Gross : See PARAMETER TABLE below.

Porosity : res_PORO_FRAC Min = 0 Max = 0.454954

PARAMETER VALUES OIL:

Sw oil : See PARAMETER TABLE below.

Bo : See PARAMETER TABLE below.

PARAMETER TABLE:

Below_Cave3_roof:

Net/Gross	Sw oil	Bo
1.0000	0.1000	1.0000

Below_Cave3_floor:

Net/Gross	Sw oil	Bo
1.0000	0.1000	1.0000

Below_Cave1_roof:

Net/Gross	Sw oil	Bo
1.0000	0.1000	1.0000

Below_Cave1_floor:

Net/Gross	Sw oil	Bo
1.0000	0.1000	1.0000

Below_Cave2_roof:

Net/Gross	Sw oil	Bo
1.0000	0.1000	1.0000

OWC TABLE:

Below_Cave3_roofBelow_Cave3_floor Below_Cave1_roof Below_Cave1_floor Below_Cave2_roof

2100.0 2100.0 2100.0 2100.0 2100.0

OIL ZONE:

Below_Cave3_roof:

Bulk	Net	Pore	Hcpv	Stoiip
1779007.60	1779007.60	157394.16	141654.74	141654.74

Below_Cave3_floor:

Bulk	Net	Pore	Hcpv	Stoiip
65881.91	65881.91	5335.31	4801.78	4801.78

Below_Cave1_roof:

Bulk	Net	Pore	Hcpv	Stoiip
926353.81	926353.81	99687.54	89718.79	89718.79

Below_Cave1_floor:

Bulk	Net	Pore	Hcpv	Stoiip
414699.98	414699.98	35929.71	32336.74	32336.74

Below_Cave2_roof:

Bulk	Net	Pore	Hcpv	Stoiip
742366.50	742366.50	64514.67	58063.20	58063.20

E:\KARINA\Masterprosjekt20.10preworkflow

Total:

3928309.81	3928309.81	362861.40	326575.25	326575.25

==========

8.6.2 Volumetric report files for Grid_Upscaled4

VOLUME CALCULATION FOR : Masterprosjekt20.10preworkflow

Date : 2016.10.22 13:58:41

CALCULATED WITH RMS VOLUMETRIC

User : kle069

Platform :

Project file name : E:\KARINA\Masterprosjekt20.10preworkflow

Report file name : E:\KARINA\Volumetrics files\volumeCalculationsUpscaled4_1.txt

Volume name : Grid_Upscaled4

No. of licences : 0

No. of zones : 5

No. of facies codes : 0

No. of regions : 0

Grouped by : Zone/

UNITS:

Input unit (XY) : metre

Input unit (Z) : metre

Output unit, reservoir : cubic metre

Output unit, surface oil : st. cubic metre

FORMATION PARAMETER VALUES:

Net/Gross : See PARAMETER TABLE below.

Porosity : res_PORO_FRAC Min = 0 Max = 0.45499

PARAMETER VALUES OIL:

Sw oil : See PARAMETER TABLE below.

Bo : See PARAMETER TABLE below.

PARAMETER TABLE:

Below_Cave3_roof:

Net/Gross	Sw oil	Bo
1.0000	0.1000	1.0000

Below_Cave3_floor:

Net/Gross	Sw oil	Bo
1.0000	0.1000	1.0000

Below_Cave1_roof:

Net/Gross	Sw oil	Bo

1.0000 0.1000 1.0000

Below_Cave1_floor:

Net/Gross Sw oil Bo

1.0000 0.1000 1.0000

Below_Cave2_roof:

Net/Gross Sw oil Bo

1.0000 0.1000 1.0000

OWC TABLE:

Below_Cave3_roofBelow_Cave3_floor Below_Cave1_roof Below_Cave1_floor Below_Cave2_roof

2100.0 2100.0 2100.0 2100.0 2100.0

OIL ZONE:

Below_Cave3_roof:

Bulk Net Pore Hcpv Stoiip 1778676.59 1778676.59 156651.03 140985.93 140985.93

Below_Cave3_floor:

Bulk Net Pore Hcpv Stoiip

65890.47 65890.47 5205.30 4684.77 4684.77

Below_Cave1_roof:

Bulk Net Pore Hcpv Stoiip

925823.85 925823.85 98868.23 88981.40 88981.40

Below_Cave1_floor:

Bulk Net Pore Hcpv Stoiip

414465.78 414465.78 36097.80 32488.02 32488.02

Below_Cave2_roof:

Bulk	Net	Pore	Hcpv	Stoiip
742175.63	742175.63	64532.05	58078.84	58078.84

E:\KARINA\Masterprosjekt20.10preworkflow

Total:

3927032.31	3927032.31	361354.41	325218.96	325218.96

==========

8.6.3 Volumetric report files for Grid_Upscaled6

VOLUME CALCULATION FOR : Masterprosjekt20.10preworkflow

Date : 2016.10.22 13:59:55

CALCULATED WITH RMS VOLUMETRIC

User : kle069

Platform :

Project file name : E:\KARINA\Masterprosjekt20.10preworkflow

Report file name : E:\KARINA\Volumetrics files\volumeCalculationsUpscaled6_1.txt

Volume name : Grid_Upscaled6

No. of licences : 0

No. of zones : 5

No. of facies codes : 0

No. of regions : 0

Grouped by : Zone/

UNITS:

Input unit (XY) : metre

Input unit (Z) : metre

Output unit, reservoir : cubic metre

Output unit, surface oil : st. cubic metre

FORMATION PARAMETER VALUES:

Net/Gross : See PARAMETER TABLE below.

Porosity : res_PORO_FRAC Min = 0 Max = 0.454905

PARAMETER VALUES OIL:

Sw oil : See PARAMETER TABLE below.

Bo : See PARAMETER TABLE below.

PARAMETER TABLE:

Below_Cave3_roof:

Net/Gross	Sw oil	Bo
1.0000	0.1000	1.0000

Below_Cave3_floor:

Net/Gross	Sw oil	Bo
1.0000	0.1000	1.0000

Below_Cave1_roof:

Net/Gross	Sw oil	Bo
1.0000	0.1000	1.0000

Below_Cave1_floor:

Net/Gross	Sw oil	Bo
1.0000	0.1000	1.0000

Below_Cave2_roof:

Net/Gross Sw oil Bo

1.0000 0.1000 1.0000

OWC TABLE:

Below_Cave3_roofBelow_Cave3_floor Below_Cave1_roof Below_Cave1_floor Below_Cave2_roof

2100.0 2100.0 2100.0 2100.0 2100.0

OIL ZONE:

Below_Cave3_roof:

Bulk Net Pore Hcpv Stoiip

1779310.50 1779310.50 156980.58 141282.52 141282.52

Below_Cave3_floor:

Bulk	Net	Pore	Hcpv	Stoiip
65550.12	65550.12	5364.19	4827.77	4827.77

Below_Cave1_roof:

Bulk	Net	Pore	Hcpv	Stoiip
926987.16	926987.16	98787.24	88908.51	88908.51

Below_Cave1_floor:

Bulk	Net	Pore	Hcpv	Stoiip
414567.55	414567.55	36320.54	32688.49	32688.49

Below_Cave2_roof:

Bulk	Net	Pore	Hcpv	Stoiip
742621.44	742621.44	64434.72	57991.24	57991.24

E:\KARINA\Masterprosjekt20.10preworkflow

Total:

3929036.77 3929036.77 361887.27 325698.54 325698.54

==========
==========